High resolution, in-situ studies of seawater carbonate chemistry and carbon cycling in coastal systems using CHANnelized Optical System II

By

Mallory Ringham

B.S., Syracuse University, 2013
M.S., Syracuse University, 2015

Submitted to the Department of Earth, Atmospheric and Planetary Sciences
in partial fulfillment of the requirements for the degree of

Doctor of Philosophy

at the

MASSACHUSETTS INSTITUTE OF TECHNOLOGY

and the

WOODS HOLE OCEANOGRAPHIC INSTITUTION

May 2022

Author

_____

Joint Program in Oceanography/Applied Ocean Science and Engineering
Massachusetts Institute of Technology
and Woods Hole Oceanographic Institution
March 25, 2022

Certified by

_____

Dr. Zhaohui 'Aleck' Wang
Associate Scientist
Woods Hole Oceanographic Institution
Thesis Supervisor

Accepted by

_____

Dr. Colleen Hansel
Chair, Joint Committee for Chemical Oceanography
Massachusetts Institute of Technology
& Woods Hole Oceanographic Institution

High resolution, in-situ studies of seawater carbonate chemistry and carbon cycling in coastal systems using CHANnelized Optical System II

By

Mallory Ringham

Submitted to the Department of Earth, Atmospheric and Planetary Sciences
Massachusetts Institute of Technology & Woods Hole Oceanographic Institution
on March 25, 2022, in partial fulfillment of the
requirements for the degree of
Doctor of Philosophy
in Chemical Oceanography

Abstract

Study of the marine CO_2 system is critical for understanding global carbon cycling and the impacts of changing ocean chemistry on marine ecosystems. This thesis describes the development of a near-continuous, in-situ dissolved inorganic carbon (DIC) sensor, CHANnelized Optical System (CHANOS) II, suitable for deployment from both mobile and stationary platforms. The system delivers DIC measurements with an accuracy of 2.9 (laboratory) or 9.0 (field) µmol kg^{-1}, at a precision of ~4.9-5.5 µmol kg^{-1}. Time-series field deployments in the Pocasset River, MA, revealed seasonal and episodic biogeochemical shifts in DIC, including two different responses to tropical storm and nor'easter systems. Towed surface mapping deployments across Waquoit Bay, MA, highlighted the export of DIC from salt marshes through tidal water. High resolution (<100 m) data collected during ROV deployments over deep coral mounds on the West Florida Slope revealed a much wider DIC range (~1900 – 2900 µmol kg^{-1}) across seafloor and coral habitats than was observed through the few bottle samples collected during the dives (n = 5, 2190.9 ± 1.0 µmol kg^{-1}). These deployments highlight the need to investigate deep sea biogeochemistry at high spatial scales in order to understand the range of environmental variation encountered by benthic communities.

Thesis Supervisor: Dr. Zhaohui 'Aleck' Wang

Title: Associate Scientist with Tenure, Woods Hole Oceanographic Institution

Acknowledgements

First and foremost, I owe everything I've accomplished to my family and their unending love and support: Mom, Dad, Rob, Luke, Dale, Casey, Addie, Uncle Brett, and the rest of the Ringham clan. I love you all and could not have made it through this program without you. Many thanks to Kendra Sadler for all her support. And Dylan—I certainly would not have made it to writing this without you. I am thankful for you every day.

"The power of water is its ability to take any shape"- Rhodeia of Loch

I want to thank my chemistry cohort—Jule Middleton, Jen Kenyon, Lydia Babcock-Adams, Sheron Luk, and Craig McLean. I guess we're no longer MIT students (for God's sake), and I still can't believe they're letting us graduate.

I've had an incredible variety of housemates throughout this PhD program, and I thank every one of them for supporting and putting up with me over the past 5.5 years: from the Concord apartment, Rose Palermo and Patrick Varin, Makayla Betts, Genevieve Flaspohler and Nick Kalweit. In the OP days, Rose again, Joleen Heiderich, Laura Fleming, & Lauren Dykman. From Reed Street, Dylan, Wes, and Brian. And at Woods Hole Road, Jule Middleton, Rachel Housego, Astrid Pacini, Danielle Freeman, Chloe Smith, Hazelnut, Paddy, and Georgie. You have all helped me build a home away from home, and I will smile every time I think back about these strange little families.

I'm lucky to have the love of friends back home: Alex Smith, Autumn Mercadante, Briana Heldt, Julie Green, and Meghan Ryan, thank you all for supporting me for more than a decade now.

I am grateful for the support of caring and inspiring educators and mentors who encouraged me to follow my dreams and my interests, wherever they take me. I'm not sure any of them would have predicted I would end up in oceanography, let alone that I'd spend so many days at sea throwing expensive sensors overboard. I have to thank my Master's advisor, Greg Hoke, and the rest of the Syracuse University Earth Sciences, Physics, and Chemical Engineering departments for starting me down this path. WHOI has been an incredible place to live, work, and grow, and I'm grateful for all of the time I have spent here, from my undergraduate summer working with Chip Breier to my entire PhD with Aleck Wang. Aleck has enabled me to do some incredible field work around the world on land and at sea, and I'm grateful for all that I have learned and will continue to learn through his lab.

I thank my lab mates, particularly Kate Morkeski, Jennie Rheuban, and Dylan Titmuss, for their endless emotional support, let alone the scientific help. Many thanks go out to the CHANOS team-- Fritz Sonnichsen, Steve Lerner, Glenn McDonald, Jonathan Pfeifer—without whom this thesis would have drowned long ago. Many thanks to my committee—Dan McCorkle, Matt Long, Ryan Woosley, and Harry Hemond—and all their encouraging words. And I thank the many incredible crews I have worked with over the years, spanning the R/Vs *Armstrong, Pelican, Point Sur,* Oceaneering's ROV *Global Explorer*, Vitalii Sheremet of the *Trifly*, Dan Ward and Matty Paquette of Scallop Bay Marina, Spohr Gardens, and the many welcoming members of the IUI in Eilat. Special thanks go out to Boaz Lazar, Eyal Wurgaft, and Jim Churchill—while our carbonate work didn't make it into this thesis, I'm excited to continue it in the future. Finally, I thank all aboard the E/V *Nautilus*—you helped me cruise between my Master's and PhD programs, and I owe the success of Chapter 3 to the incredible learning experiences I had on this ship.

Financial Support

Funding for this work was provided by the National Science Foundation (OCE Award No. 1233654, OCE 1635388, OCE 1841092), National Oceanic and Atmospheric Administration Office of Ocean Exploration and Research (NA18OAR0110352), MIT Seagrant (2017-R/RCM-51), and Woods Hole Oceanographic Institution (Ocean Ventures Fund, Grassle Fellowship).

TABLE OF CONTENTS

LIST OF FIGURES

LIST OF TABLES

Chapter 1

Introduction

1.1 Understanding the marine inorganic carbon system

Study of the marine CO_2 system is critical for understanding global carbon cycling and the impacts of changing ocean chemistry on marine ecosystems. The global carbon cycle links carbon reservoirs by exchanges and fluxes of varying magnitudes and rates, as illustrated in the schematic below from the Intergovernmental Panel on Climate Change (2013). In this figure, carbon reservoirs and fluxes listed in black represent pre-Industrial estimates ~1750 A.D. Red arrows and numbers represent the anthropogenic perturbation in this cycle averaged between 2000 and 2009. While many of these estimates are well constrained, improving carbon parameter measurement capabilities is a major priority for both the global and regional carbon cycling communities. Higher resolution measurements in both space and time are needed to understand and extrapolate the impacts of anthropogenic CO_2 pollution on the oceans, especially in the dynamic coastal regions where nutrient and other chemical pollution factors perturb the marine carbon cycle and interact with ocean acidification (OA).

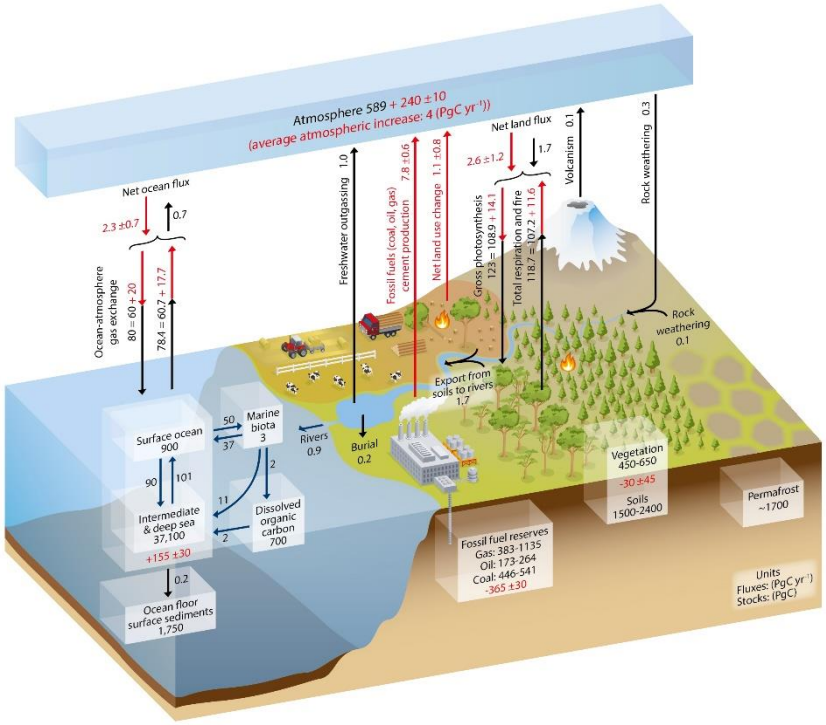

Figure 1.1: Schematic of the global carbon cycle (IPCC AR5, 2013). Reservoir masses are represented in PgC (10^{15} gC) and fluxes are in PgC yr^{-1} (*black*). Anthropogenic fluxes are averaged between 2000 and 2009 (*red*).

Ocean acidification (OA) is a major focus in ocean research that requires large quantities of data to establish baseline carbon system dynamics and to evaluate shifts in the changing oceans. OA is the absorption of anthropogenic CO_2 by the oceans that drives a decrease in both $CaCO_3$ saturation states and pH (Doney et al., 2009; Orr et al., 2015). Globally, CO_2 uptake has led to a rapid ~31% increase in average surface ocean acidity since the beginning of the Industrial Revolution, with regional OA hotspots linked to areas of upwelling, rivers and estuaries, and other low pH sources (Feely et al., 2009). Measurements of CO_2 parameters coupled with other relevant biogeochemical, physical, and ecological measurements are necessary to understand the complex impacts of OA and to constrain rates of biogeochemical and ecological changes that may impact a broad spectrum of marine life. The dynamic nature of ocean environments requires high-resolution measurements to realistically assess major carbon pools and fluxes, particularly in biogeochemically active settings and at the water-sediment, terrestrial-coast, air-sea, and shelf-ocean interfaces (Bauer et al. 2013; Wang et al. 2016). As the OA signal is small, with average ocean surface pH already declining from 8.2 to below 8.1 over the industrial era, there is a great need for new technology to monitor seawater inorganic carbon chemistry at high resolution in dynamic environments.

Full characterization of the marine inorganic carbonate system requires simultaneous measurement of at least 2 out of 4 primary inorganic carbon parameters, along with physical temperature, salinity, and pressure measurements. These parameters include pH, partial pressure (pCO_2) or fugacity (fCO_2) of CO_2, Total Alkalinity (TA), and Dissolved Inorganic Carbon (DIC). pH, determined on the total scale in this work (e.g. Millero, 1986), is a measure of the hydrogen ion concentration in solution, as defined by:

$$pH_T = -\log[H^+] \tag{1.1}$$

The partial pressure of CO_2 in equilibrium with seawater, pCO_2, is defined as:

$$pCO_2 = x_{CO2} \cdot P \tag{1.2}$$

where x_{CO2} is the mole fraction of CO_2 and P is the total absolute pressure (Takahashi and Sutherland, 2017). An experimentally derived or modeled fugacity of CO_2 (fCO_2), is typically used in seawater carbon chemistry calculations, adjusting for the deviation from ideal gas behavior, such that:

$$fCO_2 = K_0 \cdot ([CO_{2,\,aq}] + [H_2CO_3]) \tag{1.3}$$

where K_0 is a solubility constant (Dickson, 2007).

Total alkalinity or TA is defined by the moles of hydrogen ion equivalent to the excess of proton acceptors over donors in solution (Dickson and Riley, 1978). It is largely dominated by carbonate alkalinity, with smaller contributions from borate and nutrients, and may be complicated by organic contributions in coastal areas (Cai et al., 1998).

$$TA = 2\,[CO_3^{2-}] + [HCO_3^-] + [OH^-] - [H^+] + [B(OH)_4^-] + [HS^-] + 2\,[S_2^{2-}] + [NH_3] + [HPO_4^{2-}] + \ldots \quad (1.4)$$

DIC is defined as the sum of aqueous inorganic carbon species in solution, and is often referred to as total carbon or TCO_2:

$$[DIC] = ([CO_{2,\,aq}] + [H_2CO_3]) + [HCO_3^-] + [CO_3^{2-}] \quad (1.5)$$

The inorganic carbon species in seawater may interchange rapidly between carbonic acid (H_2CO_3), bicarbonate (HCO_3^-), and carbonate ion (CO_3^{2-}), to maintain chemical equilibrium as below:

$$(CO_2)_{aq} + H_2O \quad \leftrightarrow \quad H_2CO_3 \quad \leftrightarrow \quad HCO_3^- + H^+ \quad \leftrightarrow \quad CO_3^{2-} + 2H^+ \quad (1.6)$$

More than 98% of carbon in the oceans is stored in DIC, primarily as the bicarbonate anion (HCO_3^-; ~90%) (Dickson, 2007).

Measurement of 2 of these parameters allows for calculation of the others, though overdetermination of the system can be useful for quality control or for confidence in systems with uniquely complicated chemistry, such as in anoxic pore waters (Millero, 2007; Wolf-Gladrow et al., 2007; Bryne, 2014). Currently, only pH and pCO_2 sensors are widely commercially available for autonomous measurements, though some TA units are beginning to appear on the market. However, the strong covariance of the pH–pCO_2 pair typically results in greater calculation uncertainties than are predicted for pairings including DIC (Dickson and Riley, 1978; Millero et al., 2007; Fassbender et al., 2015; Orr et al., 2017). The DIC-pH pair reduces probable error for derived TA and pCO_2, while DIC-pCO_2 reduces probable error in pH calculations. Overdetermination of the inorganic carbon system is useful to reduce calculated carbon system uncertainties from a less-ideal pair of parameters.

A full resolution of the inorganic carbon system allows for calculation of other values that aid understanding of carbon cycling. Carbonate saturation state, Ω_{CaCO3}, is a thermodynamic indicator of the degree to which carbonate minerals will form or dissolve, defined as:

$$\Omega_{CaCO3} = (Ca^{2+})(CO_3^{2-}) / K_{sp} \quad (1.7)$$

where (Ca^{2+}) is the activity of dissolved calcium ions in seawater, and K_{sp} is the solubility product (Carter et al., 2014). Ω_{CaCO3} values are usually designated separately for calcite and aragonite minerals, polymorphs of calcium carbonate with solubility differences arising from the difference in their crystalline structure, using different K_{sp} values for each mineral. Low or undersaturated ($\Omega_{CaCO3} < 1$) conditions favor calcium carbonate dissolution. The presence of undersaturated conditions may have important implications for inorganic carbon cycling and biogeochemistry, particularly in environments supporting calcium carbonate shell building organisms (Waldbusser et al., 2015).

Practically, the choice of inorganic carbon parameters measured by sensors must include an evaluation of relevant sensor applicability to specific deployments, depending on their strengths and weaknesses, which may include measuring under conditions of high turbidity, low salinity, and vibration or other sources of noise that can obstruct data collection. When it is not possible to measure two simultaneous parameters to fully resolve the inorganic carbon system, it may often be valuable to measure DIC alone. DIC is an important parameter that allows assessment of a range of biogeochemical processes, including photosynthesis and respiration, dissolution and precipitation of $CaCO_3$, carbon storage and transport, and air-sea and sediment-water interactions. DIC varies with depth and latitude in open oceans and is influenced by both biological processes and the solubility of carbon dioxide in seawater. It can vary strongly along coasts, where tidal fluxes, complex biological communities, and complicated bathymetry produce highly dynamic environments (Dickson, 2007). For these reasons, there is a great interest in the development of high resolution autonomous DIC sensors for deployment from a variety of platforms in a range of environments.

1.2 Overview of traditional bottle sampling and laboratory analysis methods

DIC measurements produced through traditional bottle sampling and laboratory analysis aim for a high accuracy and precision of ~± 2 µmol kg^{-1} DIC, or ~0.1% of typical surface seawater values. However, the number of discrete samples are limited by both cost and effort for studies that require high sample frequency or sustained time series and site access. Seawater bottle samples for DIC, TA, and pH analysis are collected in borosilicate glass bottles and are poisoned with mercuric chloride following standard operating procedures (Dickson et al., 2007). DIC laboratory measurements typically involve a CO_2 extraction step, such as acidification, purging the extracted CO_2 with an inert gas, and detection of aqueous or gaseous CO_2 by infrared, gas chromatographic, or spectrophotometric methods (e.g., coulometry (Johnson et al., 1993),

potentiometry (Choi et al., 2002; Xie et al., 2013), nondispersive infrared (NDIR) (Hales et al., 2004; Kaltin et al., 2005; Bandstra et al., 2006), conductimetry (Sayles and Eck, 2009), and spectrophotometry (Byrne et al., 2002; Wang et al., 2007; Wang et al., 2013). The standard Certified Reference Material (CRM) used in this field is produced by the Dickson lab at Scripps Institute of Oceanography (e.g., Dickson 2010).

A sample precision of ~10 μmol kg^{-1} DIC, or ~0.5% of typical surface seawater, is required in order to resolve relative spatial patterns and short-term time-series variation in DIC. According to recommendations from the Global Ocean Acidification Observing Network (GOA-ON), resolution of long-term trends requires a precision of better than 2 μmol kg^{-1} DIC (Dickson, 2007; Newton et al., 2014). It is important to note that interlaboratory analyses for DIC have found that highly trained staff are required to produce consistent seawater inorganic carbon measurements across laboratories, with some seawater CO_2 labs falling short of the 2 μmol kg^{-1} precision benchmark (Bockmon and Dickson, 2015).

These factors are pushing the field towards a preference for automated sensors in order to reduce the cost of sample collection and measurement, and to increase the volume and resolution of seawater inorganic carbon data generated. Specifically, development of automated sensors must balance the need for precise and accurate high-frequency measurements (e.g., ± 2 μmol kg^{-1} DIC), ideally with in-situ self-calibration during deployment, with the ability to operate at depth and on small platforms with low demands for power, reagents, maintenance, and waste. However, the cost of developing climate-quality DIC and other inorganic carbon parameter sensors is high and may limit access to and deployment of such sensors. In many circumstances, deploying several less expensive, lower quality (± 5-10 μmol kg^{-1} DIC) sensors to increase spatial-temporal data coverage may suitably detect OA and other biogeochemical signals (Newton et al., 2014). As such, when developing and deploying sensors, it is necessary to consider the spatial-temporal scales required to capture inorganic carbon signals in a given environment.

1.3 Overview of Chapter 2: CHANOS II development and deployment in the Pocasset River and Waquoit Bay, MA

In Chapter 2, we discuss the development of the CHANnelized Optical System (CHANOS) II, an in-situ DIC sensor that is targeted for near-continuous measurements covering the dynamic range of DIC in marine systems. An assessment of existing and upcoming in-situ DIC sensors is provided this chapter, followed by a description of the development and testing of the CHANOS II. This sensor applies the spectrophotometric

method used in CHANOS I (Wang et al., 2013; 2015), with a miniaturized, modular design to allow for deployment from a variety of stationary and mobile platforms as well as various time scales and resolutions.

We deployed this system dockside at the Scallop Bay Marina in Pocasset, MA, for testing and ground-truthing in continuous and intermittent time-series modes. This field site, located ~500 m from the mouth of the Pocasset River emptying into Buzzards Bay, experiences tidal flooding from the downstream bay and upstream salt marshes. CHANOS II collected 59 days of high resolution DIC measurements at this location and achieved a laboratory accuracy and precision of ±2.9 and ±5.5 μmol kg^{-1}, and field accuracy of ±9.0 μmol kg^{-1}. The time-series data at this site spans late August through mid-November, 2021, and reveals tidal and seasonal variations in DIC. We describe biogeochemical responses to two contrasting storm systems at this site that were not captured by bottle samples due to inaccessibility in poor weather. During an August tropical storm, strong winds stirred up the bottom sediment, releasing high DIC and low oxygen water into the river. During an October nor'easter, heavy rains diluted the DIC signal through the input of fresh rainwater. These cases highlight the importance of autonomous sensor use in capturing signals for which bottle samples are not available.

In this chapter, we also demonstrate the use of the CHANOS II in towed applications. A series of high spatial resolution DIC surface maps were generated as the CHANOS II package was towed through Waquoit Bay, MA, via small boat, during two high and two low tides in September 2021. These surface maps show the impact of tidal export from salt marshes into the bay. Taken together, these in-situ time-series and mobile deployments demonstrate the capabilities of the CHANOS II as a new tool for high-resolution, near-continuous DIC sensing, and allow for fine-scale characterization of carbon cycling in dynamic coastal environments including salt marshes and tidal rivers.

1.4 Overview of Chapter 3: Inorganic carbon chemistry across deep coral mounds on the West Florida Slope

The CHANOS II sensor is particularly valuable in characterizing inorganic carbon chemistry in poorly accessible regions that limit sampling by traditional bottle methods. Sampling at deep coral reefs is constrained to the low volumes of seawater that may be collected during Autonomous Underwater Vehicles (AUVs), Remotely Operated Vehicles (ROVs), and human operated vehicles. Since these vehicles can operate over many hours and kilometers on a single dive and tend to be equipped with collectors for only a few seawater bottle samples, seafloor carbonate coverage is typically sparse. Missions seeking to

understand the range of inorganic carbon chemistry in these environments, including current baseline conditions experienced by deep sea corals and changing ocean conditions in the future, should cover both the spatial variations that may occur across the reef systems and temporal resolution over days, seasons, and years.

In Chapter 3, we present the first observations of high-resolution seafloor DIC across deep coral reef mounds during four ROV dives on the West Florida Slope between 400 and 850 m depth. The ROV *Global Explorer* only carried two Niskin samplers per dive, resulting in at best one water sample per 650 m (along track) for bottle DIC and TA analysis. The CHANOS II measurements are far more frequent and represent better than 20 m along track resolution of in-situ DIC measurements. CHANOS II data agreed well with bottle samples and in-situ calibration materials, and showed large (hundreds of μmol kg^{-1}) variations across seafloor dives as the ROV progressed upslope and over coral mounds during each dive. These DIC variations may be caused by a combination of factors, including depth-dependence of carbonate solubility, calcium carbonate dissolution and calcification, and benthic sediment processes. Since two carbonate parameters are required to fully resolve the marine CO_2 system, we conservatively estimate seafloor TA using multilinear regressions trained on historical water column TA:DIC data in the region. Using CO2SYS (e.g., Pierrot et al., 2006; Van Heuven et al., 2011), CHANOS II DIC data, and seafloor TA model outputs, we estimate seafloor pH and $\Omega_{Aragonite}$, which may vary significantly at the seafloor. This work illuminates the need to sample deep coral sites in greater resolution to understand how frequently deep corals already experience variable carbonate conditions, which may have important ecological implications as these systems face environmental changes in the future.

1.5 Summary

This thesis advances our ability to capture high resolution DIC dynamics from a variety of stationary and mobile platforms using the CHANOS II sensor. This research encompasses the fieldwork, laboratory analysis, and modeling necessary to measure in-situ coastal biogeochemical processes through dockside, small boat tows, and ROV sensor deployments.

1.6 References

Anisfeld, S.C., and Benoit, G., 1997. Impacts of flow restrictions on salt marshes: An instance of acidification. Environmental Science and Technology, v. 31, pp. 1650-1657.

Bandstra, L., Hales, B., and Takahashi, T., 2006. High-frequency measurements of total CO_2: Method development and first oceanographic observations. Marine Chemistry, v. 100, pp. 24-38.

Bauer, J.E., Cai, W.J., Raymond, P.A., Bianchi, T.S., Hopkinson, C.S., and Regnier, P.A.G., 2013. The changing carbon cycle of the coastal ocean. Nature, v. 504, pp. 61-70.

Baumann, H., Wallace, R.B., Tagliaferri, T., and Gobler, C.J., 2014. Large natural pH, CO2 and O2 fluctuations in a temperate tidal salt marsh on diel, seasonal, and interannual time scales. Estuaries and Coasts, v. 38, pp. 220-231.

Bockmon, E.E., and Dickson, A.G., 2016. An inter-laboratory comparison assessing the quality of seawater carbon dioxide measurements. Marine Chemistry, v. 171, pp. 36-43.

Boulais, M., Chenevert, K.J., Demey, A.T., Darrow, E.S., Robison, M.R., Roberts, J.P., and Volety, A., 2017. Oyster reproduction is compromised by acidification experienced seasonally in coastal regions. Nature: Scientific Reports. v. 7., a 13276.

Bryne, R.H., 2014. Measuring ocean acidification: new technology for a new era of ocean chemistry. Environmental Science & Technology, v. 48, pp. 5352-5360.

Byrne, R.H., Liu, X.W., Kaltenbacher, E.A., and Sell, K., 2002. Spectrophotometric measurement of total inorganic carbon in aqueous solutions using a liquid core waveguide. Analytica Chimica Acta, v. 451, pp. 221-229.

Cai, W.J., Wang, Y., and Hodson, R.E., 1998. Acid-base properties of dissolved organic matter in the estuarine waters of Georgia, USA. Geochemica et Cosmochemica Acta, v. 62, pp. 473-483.

Carter, B.R., Toggweiler, J.R., Key, R.M., and Sarmiento, J.L., 2014. Processes determining the marine alkalinity and calcium carbonate saturation state distributions. Biogeosciences, v. 11, pp. 7349-7362.

Choi, Y.S., Lvova, L., Shin, J.H., Oh, S.H., Lee, C.S., Kim, B.H., Cha, G.S., and Nam, H., 2002. Determination of oceanic carbon dioxide using a carbonate-selective electrode. Analytical Chemistry, v. 85, pp. 1332-1336.

Chu, S.N., Wang, Z.A., Gonneea, M.E., Kroeger, K.D., and Ganji, N.K., 2018. Deciphering the dynamics of inorganic carbon export from intertidal salt marshes using high-frequency measurements. Marine Chemistry, v. 206, pp. 7-18.

Dickson, A.G., 2010. "The carbon dioxide system in seawater: equilibrium chemistry and measurements." *Guide to best practices for ocean acidification research and data reporting*, v. 1, pp. 17-40.

Dickson, A.G., Riley, J., 1978. The effect of analytical error on the evaluation of the components of the aquatic carbon-dioxide system. Marine Chemistry, v. 6, pp. 77-85.

Dickson, A.G., Sabine, C.L., and Christian, J.R., 2007. Guide to best practices for ocean CO_2 measurements. North Pacific Marine Science Organization.

Doney, S.C., Balch, W.M., Fabry, V.J., and Feely, R.A., 2009. Ocean Acidification: A critical emerging problem for the ocean sciences. Oceanography, v. 22.

Fassbender, A.J., Sabine, C.L., Lawrence-Slavas, N., De Carlo, E.H., Meinig, C., and Jones, S.M., 2015. Robust sensor for extended autonomous measurements of surface ocean dissolved inorganic carbon. Environmental Science and Technology, v. 49, pp. 3628-3635.

Feely, R.A., Doney, S.C., and Cooley, S.R., 2009. Ocean acidification: Present conditions and future changes in a high-CO_2 world. Oceanography, v. 22, pp. 36-47.

Gledhill, D.K., White, M.M., Salisbury, J., Thomas, H., Mlsna, I., Liebman, M., Mook, B., Grear, J., Candelmo, A.C., Chambers, R.C., Gobler, C.J., Hunt, C.W., King, A.L., Price, N.N., Signorini, S.R., Stancioff, E., Stymiest, C., Wahle, R.A., Waller, J.D., Rebuck, N.D., Wang, Z.A., Capson, T.L., Morrison, J.R., Cooley, S.R., and Doney, S.C., 2015. Ocean and coastal acidification off New England and Nova Scotia. Oceanography, v. 28, pp. 182-197.

Hales, B., Chipman, D., and Takahashi, T., 2004. High-frequency measurement of partial pressure and total concentration of carbon dioxide in seawater using microporous hydrophobic membrane contactors. Limnology and Oceanography: Methods, v. 2, pp. 356-364.

IPCC, 2013. Climate change 2013: They physical science basis. Contribution of working group I to the Fifth Assessment Report of the Intergovernmental Panel on Climate Change. Stocker, T.F., Qin, D., Plattner, G.K., Tignor, M., Allen, S.K., Boschung, J., Nauels, A., Xia, Y., Bex, V., and Midgley, PM. (eds.) Cambridge University Press, Cambridge, United Kingdom and New York, NY, USA. 1595 pp.

Johnson, K.M., Wills, K.D., Butler, D.B., Johnson, W.K., and Wong, C.S., 1993. Coulometric total carbon-dioxide analysis for marine studies: Maximizing the performance of an automated gas extraction system and coulometric detector. Marine Chemistry, v. 44, pp. 167-187.

Kaltin, S., Haraldsson, C., and Anderson, L.G., 2005. A rapid method for determination of total dissolved inorganic carbon in seawater with high accuracy and precision. Marine Chemistry, v. 96, pp. 53-60.

Liu, X., Byrne, R.H., Adornato, L., Yates ,K.K., Kaltenbacher, E., Ding, X., and Yang, B., 2013. In situ spectrophotometric measurement of dissolved inorganic carbon in seawater. Environmental Science & Technology, v. 27, pp. 11106-11114.

Millero, F.J., 1986. The pH of estuarine waters. Limnology & Oceanography, v. 31, pp. 839-847.

Millero, F.J., 2007. The Marine Inorganic Carbon Cycle. Chemical Reviews, v. 107, pp. 308-341.

Moseman-Valtierra, S., Abdul-Aziz, O.I., Tang, J., Ishtiaq, K.S., Morkeski, K., Mora, J., Quinn, R.K., Martin, R.M., Egan, K., Brannon, E.Q., Carey, J., and Kroeger, K.D., 2016. Carbon dioxide fluxes reflect plant zonation and belowground biomass in a coastal marsh. Ecosphere, v. 7, article e01560.

Newton, J.A., Feely, R.A., Jewett, E.B., Williamson, P., and Mathis, J., 2014. Global ocean acidification observing network: Requirements and governance plan. GOA-ON, 57.

Orr, J.C., Fabry, V.J., Aumont, O., Bopp, L., Doney, S.C., Feely, R.A., et al., 2005. Anthropogenic ocean acidification over the twenty-first century and its impact on calcifying organisms. Nature, v. 437, pp. 681-686.

Orr, J.C., Najjar, R.G., Aumont, O., et al., 2017. Biogeochemical protocols and diagnostics for the CMIP6 Ocean Model Intercomparison Project (OMIP). Geoscientific Model Development, v. 10, pp. 2169-2199.

Pierrot, D., Lewis, E., and Wallace, D.W.R., 2006. MS Excel program developed for CO2 system calculations. ORNL/CDIAC-105a. Carbon Dioxide Information Analysis Center, Oak Ridge National Laboratory, U.S. Department of Energy, Oak Ridge, Tennessee.

Sayles, F.L., and Eck, C., 2009. An autonomous instrument for time series analysis of TCO_2 from oceanographic moorings. Deep Sea Research, Part I, v. 56, pp. 1590-1603.

Spivak, A.C., Gosselin, K., Howard, E., Mariotti, G., Forbrich, I., Stanley, R., and Sylva, S.P., 2017. Shallow ponds are heterogenous habitats within a temperate salt marsh ecosystem. Journal of Geophysical Research: Biogeosciences, v. 122, pp. 1371-1384.

Takahashi and Sutherland, 2017. Global ocean surface water partial pressure of CO_2 database: Measurements performed during 1957-2016. NOAA/NCEI/ OCADS NDP-088 (V2016).

Van Heuven, S., Pierrot, D., Rae, J.W.B., Lewis, E., and Wallace, D.W.R., 2011. MATLAB program developed for CO2 system calculations.ORNL/CDIAC-105b.

Waldbusser, G.G., and Salisbury, J.E., 2014. Ocean acidification in the coastal zone from an organism's perspective: Multiple system parameters, frequency domains, and habitats. Annual Review of Marine Science, v. 6, pp. 221-247.

Waldbusser, G.G., Hales, B., Langdon, C.J., et al., 2015. Saturation-state sensitivity of marine bivalve larvae to ocean acidification. Nature Climate Change, v. 5, pp. 273-280.

Wang, Z.A., Chu, S.N., and Hoering, K.A., 2013. High-frequency spectrophotometric measurements of total dissolved inorganic carbon in seawater. Environmental Science & Technology, v. 47, pp. 7840-7847.

Wang, A.Z., Kroeger, K.D., Ganju, N.K., Gonneea, M.E., and Chu, S.N., 2017. Intertidal salt marshes as an important source of inorganic carbon to the coastal ocean. Limnology and Oceanography, v. 61, pp. 1916-1931.

Wang, Z.H.A., Liu, X.W., Byrne, R.H., Wanninkhof, R., Bernstein, R.E., Kaltenbacher, E.A., and Patten, J., 2007. Simultaneous spectrophotometric flow-through measurements of pH, carbon dioxide, fugacity, and total inorganic carbon in seawater. Analytica Chimica Acta, v. 596, pp. 23-36.

Wang, Z.A., Sonnichsen, F.N., Bradley, A.M., Hoering, K.A., Lanagan, T.M., Chu, S.N., Hammar, T.R., and Camilli, R., 2015. In-situ sensor technology for simultaneous spectrophotometric measurements of seawater total dissolved inorganic carbon and pH. Environmental Science & Technology, v. 49, pp. 4441-4449.

Wolf-Gladrow, D.A., Zeebe, R.E., Klaas, C., Körtzinger, A., and Dickson, A.G., 2007. Total Alkalinity: The explicit conservative expression and its application to biogeochemical processes. Marine Chemistry, v. 106, pp. 287-300.

Xie, X.J., and Bakker, E., 2013. Non-Severinghaus potentiometric dissolved CO_2 sensor with improved characteristics. Analytical Chemistry, v. 85, pp. 1332-1336.

Chapter 2

Developing an In-situ Sensor for High-frequency Measurements of Dissolved Inorganic Carbon to Enable Fine-scale Studies of Seawater Carbonate Chemistry

Abstract

An understanding of marine carbon cycling and the impacts of changing ocean chemistry on marine ecosystems requires resolution of two out of the four primary parameters in the marine CO_2 system: partial pressure (pCO_2) or fugacity of CO_2 (fCO_2), dissolved inorganic carbon (DIC), total alkalinity (TA), and pH. The CHANnelized Optical System II (CHANOS II) is an autonomous, near-continuous in-situ sensor developed to measure seawater DIC to depths of 1200 m. This enables measurements at high temporal and spatial resolution from both stationary (docks, buoys, moorings) and mobile (ROVs, AUVs, CTD rosettes) platforms. The sensor can be calibrated and/or monitored in-situ using Certified Reference Materials (CRMs) to ensure measurement quality throughout a deployment. We present ground-truthed field measurements displaying the sensor's capabilities for time-series and spatial mapping deployment strategies including: 1) time-series measurements from the Scallop Bay Marina in Pocasset, MA (July – October 2021), and 2) high frequency surface mapping of Waquoit Bay, MA, across tidal cycles (September 2021). We report both continuous and intermittent (hourly) DIC measurements with a laboratory accuracy and precision of ±2.9 and ±5.5 μmol kg^{-1}, respectively. The mean difference between sensor and bottle samples collected during 59 days of time-series measurements was -3.8 ± 9.0 μmol kg^{-1}, suggesting a field accuracy of ~ 9.0 μmol kg^{-1}. Our time-series measurements highlight seasonal and episodic biogeochemical shifts, including two different DIC responses to tropical storm and nor'easter systems. Surface DIC mapping shows bay and river endmembers in Waquoit Bay and highlights the export of DIC from salt marshes through tidal water.

Chapter 2

2.1 Introduction

Study of the marine CO_2 system is critical for understanding global carbon cycling and the impacts of changing ocean chemistry on marine ecosystems. A complete resolution of the marine CO_2 system requires measurement of at least two out of four primary parameters: partial pressure (pCO_2) or fugacity of CO_2 (fCO_2), dissolved inorganic carbon (DIC), total alkalinity (TA), and pH. Traditional bottle sample titrations for DIC and TA are slow, constraining studies by speed and cost of both sample collection and laboratory methods. Commercial pH and pCO_2 sensors are widely available for autonomous, in-situ deployments, and while TA sensors are beginning to appear, there are no commercial in-situ DIC sensors on the market. The strong covariance of the pH-pCO_2 pair can result in large CO_2 system calculation errors (Millero et al., 2007). Simultaneous measurement of the DIC-pCO_2 or DIC-pH pair instead is valuable due to reduced calculation errors, especially for carbonate alkalinity and $CaCO_3$ saturation states, which are highly relevant to Ocean Acidification (OA) studies (Dickson and Riley, 1978). High quality, high resolution DIC measurements on their own are also valuable for many marine carbon studies and beyond, including anthropogenic carbon invasion in the ocean, changes in the marine biological carbon pump, and understanding the marine $CaCO_3$ cycle (Fassbender et al., 2015).

2.1.1 Review of in-situ DIC sensors

All measurements for inorganic carbon parameters require temperature, pressure, and salinity measurements in order to fully resolve the marine CO_2 system. Most commercial sensors carry at least a thermistor, and most sensor deployments benefit from additional Conductivity/ Temperature/ Depth (CTD) and dissolved oxygen sensor readings. pH sensors are available from multiple vendors, with the most popular methods including potentiometric, ion-sensitive field effect transistor (ISFET), and spectrophotometric technologies (Clayton and Bryne,1993; Martz et al., 2015). These systems can operate autonomously and near-continuously, but may struggle during some types of deployments, such as if they are towed or deployed in turbid or high bubble density conditions. More sensor systems are available for pCO_2 analysis in both submerged autonomous and shipboard underway modes, but in-situ calibration for pCO_2 can be complicated, typically requiring access to gas tanks of varying CO_2 concentration (Clark et al., 2017).

TA sensors are far less developed than pH and pCO_2. Some laboratory-built systems are in use (e.g., Briggs et al., 2017; 2020, using a solid state ISFET TA and associated pH sensor), but few commercial options are available. Typical TA measurement involves gran titration, adding precise quantities of acid to a seawater sample and calculating TA from the observed change in pH, which is difficult to adapt to in-situ settings. The CONTROS HydroFIA system, based on CO_2 degassing into an open cell titration followed by spectrophotometrically determined pH, is available commercially for underway flow-through benchtop measurements (e.g., Hunt et al., 2021). The first in-situ submersible SAMI-Alk units are in early use, based on the determination of pH and dilution factor between an indicator solution and sample in a tracer monitored titration (Shangguan et al., 2021).

No in-situ or flow-through DIC sensors are commercially available, but there have been various developments for autonomous DIC sensing by individual groups (i.e., Schuster et al., 2009; Martz et al., 2015; Bushinsky et al., 2019; Colson and Michel, 2022). Published DIC systems are based on the following methods:

The coulometric method is based on the stripping of CO_2 from acidified seawater samples by N_2 gas into a coulometer where it is reacted and titrated with OH^- ions. The titration endpoint may be determined photometrically with a pH sensitive sulfonephthalein indicator, and the change in current is correlated to DIC. The coulometric method is used in the Standard Operating Procedure described by Dickson et al., (2007), and was modified into an autonomous benchtop DIC unit by Amornthammarong et al., (2014). However, due to its large size, large sample volume, potential for hazardous waste production, and requirement for a stable working environment, it has not yet been adapted to in-situ measurements.

In the conductometric method, CO_2 is diffused through a semipermeable membrane from acidified seawater into a sodium hydroxide or DI water acceptor solution. This causes the solution conductivity to decrease proportionally to DIC concentration as CO_2 reacts quantitatively with OH^-. An advantage of this method is that it requires very small sample volumes (~100 μL) at a high sample rate, allowing for small sensor size, such as the early stage Lab-on-Chip as described in Nightingale et al. (2015). Sayles and Eck (2009) adapted this method into an in-situ, autonomous DIC sensor, Robotic Analyzer for the TCO_2 System (RATS). However, this method is particularly sensitive to temperature changes that can impact cell volume, complicating DIC calculations.

In the non-dispersive infrared absorption (NDIR) method, CO_2 is purged from an acidified sample with an inert carrier gas and is quantified via an infrared spectrophotometer. NDIR spectrophotometry is widely

used in laboratory measurements of DIC and for commercial pCO_2 measurement on buoy and mooring systems. It has been developed into a promising in-situ Moored Autonomous DIC (MADIC) system by Fassbender et al., (2015). However, this method is strongly temperature dependent and reliant on a gas stream which can be complicated to adapt to in-situ methods under pressure at depth.

Dual isotope dilution cavity ring-down spectroscopy measures both DIC and $^{13}C/^{12}C$ by mixing seawater with an enriched $NaH^{13}CO_3$ solution. The isotopic composition of CO_2 is measured by spectroscopy, and a mixing ratio of the sample and spike is determined by the $D/^1H$ ratio in the mixture. DIC is calculated from the mixing ratio and ^{13}C concentration of the original spike and mixed sample. This method produces fast (~4 min) and precise measurements. However, while it has been tested as a benchtop underway device at sea, it has not yet been adapted to in-situ deployment (Huang et al., 2015).

In membrane introduction mass spectrometry (MIMS), acidified seawater samples are equilibrated with calibrated gas mixtures, which are then diffused across a gas-permeable membrane into a vacuum chamber where a specified mass to charge ratio is recorded as ion current. This current is related to fCO_2, which is used with a potentiometric pH measurement of seawater to calculate DIC (Bell et al., 2011). MIMS units have been developed for underwater measurements of other dissolved gasses, such as CH_4, N_2, O_2, Ar, VOCs, and hydrocarbons (Chua et al, 2016). MIMS units for DIC may be able to provide contemporaneous measurements for such gases along with pCO_2 and DIC. However, this method is dependent on salinity and requires precise temperature regulation. It requires high flow rates and may experience in-situ complications by requiring a gas stream. One DIC MIMS unit has been tested as a benchtop measurement system, but has not yet been adapted for in-situ measurements (Bell et al., 2011).

In the spectrophotometric method, CO_2 in an acidified seawater sample is equilibrated with a pH sensitive sulfonephthalein indicator across a semipermeable membrane. The absorbance change in the indicator is measured by a spectrometer and correlated to the change in DIC. A major advantage of this method is that it is highly sensitive and can provide near-continuous measurements. This method requires less calibration than other approaches, and can be 'calibration free' provided there is no change in the indicator solution or optical system. Various dyes may be chosen for optimization, and such a system can be easily modified to measure other parameters such as pH or pCO_2. However, temperature must be carefully monitored as a major factor in the equilibration step in this method, and as a wet chemistry method, an in-situ spectrophotometric system relies on multiple pumps, valves, and reagents (see Bryne et al., 2002; Liu et al., 2013; Tue-Ngeun et al., 2005; and Wang et al., 2007; 2013; 2015). This method was first published by Bryne et al. (2002), using discrete acidification of seawater samples via syringe pump and a liquid core

waveguide equilibration cell to determine DIC in river water samples. This system was adapted for simultaneous flow-through measurements of pH, fCO_2, and DIC using a liquid core waveguide via a tube-in-tube Teflon AF 2400 semipermeable membrane tubing in PEEK design (e.g., Multiparameter Inorganic Carbon Analyzer (MICA), Wang et al., 2007). This system could make ~7 measurements per hour as a shipboard underway sensor. The first in-situ spectrophotometric DIC system, SEAS-DIC, integrated the MICA and Spectrophotometric Elemental Analysis System (SEAS) system for autonomous, submersible measurements (Liu et al., 2013). A major improvement to this method was published in Wang et al. (2013), using a dynamic equilibration of countercurrent seawater and indicator flow through the Teflon equilibration cell to achieve a faster response time (~22 s) and near continuous measurement of DIC. This improvement resulted in the CHANnelized Optical System (CHANOS), a simultaneous, autonomous, in-situ DIC-pH sensor described in Wang et al., (2015). A summary of published in-situ DIC sensing systems is given in Table 2.1.

Table 2.1: Summary of published in-situ DIC sensing systems

Measurement principle	**Publication**	**In-situ precision and accuracy (µmol kg^{-1})**	**Measurement cycle time**	**Reported time-series deployment time**
Spectrophotometry	Liu et al., 2015 (SEAS-DIC)	± 2, ± 2	Every ~50 s after ~9 min preparation cycle for 50 min, repeated	~8 day dock deployment
Spectrophotometry	Wang et al., 2015 (CHANOS)	± 2.5, ± 5.2 (DIC), ± 0.0010, ± 0.0024 (pH)	Every ~12 s after ~ 6 min preparation cycle for ~8 min, repeated	~ 3 week dock deployment
Conductometry	Sayles and Eck, 2009 (RATS)	± 2.7, ± 3.6	Hourly	~8 weeks dock deployment
Non-Dispersive Infrared Absorption (NDIR)	Fassbender et al., 2015 (MADIC)	± 5, ± 6 - 7	~12 min	~7 month surface mooring deployment

Because the spectrophotometric method measures only in the aqueous phase, it is well suited for in-situ underwater applications, particularly under high pressures at depth. The original CHANOS I sensor described by Wang et al., (2013, 2015) simultaneously measured DIC and pH via two independent channels, allowing for a complete characterization of the inorganic carbon system when given simultaneous CTD measurements. CHANOS I achieved an accuracy of 0.0024 and 4.1 µmol kg^{-1} for pH and DIC, respectively,

with a corresponding precision of 0.001 and 2.5 µmol kg^{-1}. The sensor could also perform calibrations in the field using Certified Reference Materials (CRMs, obtained from A.G. Dickson at Scripps Institution of Oceanography) to ensure measurement quality (Wang et al., 2015). However, the use of syringe pumps discretized measurements as reagent pumps were refilled frequently, limiting the sensor's ability for continuous measurements. This, along with the large size and power requirements, limited the applications of this system to time-series surface deployments from fixed platforms.

2.1.2 Inorganic carbon chemistry measurements for biogeochemical studies

In order to resolve relative spatial patterns and short-term time-series variation in DIC, we require a sample precision of ~10 µmol kg^{-1} DIC, or ~0.5% of typical surface seawater ("weather quality"). According to Global Ocean Acidification Observing Network (GOA-ON) recommendations, resolution of long-term trends requires a precision of better than 2 µmol kg^{-1} DIC ("climate quality") (Newton et al., 2014). Attempts to develop in-situ automated DIC sensors may address the need for very precise and accurate measurements (e.g., ± 2 µmol kg^{-1} DIC), as targeted by CHANOS I. However, the cost of developing climate-quality DIC and other inorganic carbon parameter sensors is high and may limit the access to and deployment of such sensors. In many circumstances, deploying several less expensive, lower quality (5-10 µmol kg^{-1} DIC) sensors to increase spatial data coverage in different environments over time may suitably detect many biogeochemical signals (Newton et al., 2014).

Salt marshes include high- and low-zones populated by grasses that experience tidal flooding of varying frequency depending on their elevation. They have some of the highest rates of organic matter production and storage in coastal environments and support a great diversity of algaes, shellfish, fishes, and other fauna (Spivak et al., 2017). These highly dynamic systems are impacted by ocean acidification (OA), sea level rise, deoxygenation, and other environmental changes. Marsh environments already experience strong coastal acidification, due to natural and human-driven land-sea interactions. While OA is driven by the ocean's uptake of CO_2, resulting in a decrease in seawater pH, coastal acidification is more localized. An example of this is when run-off introduces excess nutrients to a coastal system, resulting in algal blooms that respire CO_2 into the seawater, impacting local pH (Wallace et al., 2014). In addition to rapid physical changes, such as large temperature swings and storm surges, complex dynamic systems with varying daily, seasonal, and interannual biogeochemical conditions may be produced by river and groundwater inputs, hypoxia, high productivity and respiration, and tidal outwelling of DIC, nutrients, and alkalinity (Baumann et al., 2015; Gledhill et al., 2015; Wang et al., 2016). For example, some studies have found changes of up to 2 pH units in a day during the summer season when larval shellfish are in the process of early shell

building (Anisfeld and Benoit, 1997; Baumann et al. 2015). Many studies have shown the need for higher resolution of carbonate chemistry (i.e., compared to traditional bottle sampling methods of hourly to two-hourly measurements during a single tidal cycle, or long-term monthly schedules) in order to capture representative temporal and spatial variability in marsh environments (Chu et al., 2018, Gledhill et al., 2015, Liu et al., 2017, Moseman-Valtierra et al., 2016, Wang et al., 2016). This need to capture the dynamics of biogeochemical conditions becomes particularly important when considering coastal systems, where strong, shorter-term coastal acidification may obscure the OA signals driven by the relatively small and gradual increase of atmospheric carbon dioxide.

OA may have detrimental effects on carbonate shell and skeleton forming organisms as a result of decreasing pH and carbonate saturation state (Ω_{CaCO3}). Ω_{CaCO3} is a thermodynamic indicator of the degree to which carbonate minerals will form or dissolve (i.e., the product of the activities of dissolved calcium and carbonate ions in seawater divided by the solubility product of aragonite, K_{sp}). Low or undersaturated ($\Omega_{CaCO3} < 1$) conditions favor carbonate dissolution. Undersaturation may disrupt development of vulnerable salt marsh species including larval oysters and other shellfish, which may in turn impact other diverse species and fisheries that rely on the marsh ecosystem (Boulais et al., 2017, Doney et al., 2009, Waldbusser et al., 2014). Therefore, key questions in marsh carbonate chemistry include: what fine-scale heterogeneities of carbonate parameters and saturation states exist in representative salt marsh sites? What are their spatial variabilities across marsh habitats? How frequent and persistent are conditions of low or undersaturated Ω_{CaCO3}, and when do these corrosive conditions impact the life cycle and distribution of marsh bivalves and other organisms?

2.1.3 Chapter overview

In this chapter, we describe the development and testing of the CHANnelized Optical System (CHANOS) II sensor for in-situ near-continuous or intermittent DIC measurement with 'weather' quality precision (~10 µmol kg^{-1}) (Newton et al., 2014). This sensor is designed to be adaptable for high resolution profile or mapping missions on mobile platforms, such as CTD Rosettes, towed vehicles, ROVs, and AUV. It may also be applied to fixed location time-series deployments. Major improvements have been made since the CHANOS I sensor (e.g., Wang et al., 2013), by reducing size, cost, power consumption, and CO_2 exchange mechanism. A full redesign of the sensor components, fluidic pathways, and software of the system allows for in-situ, submerged autonomous deployments. The sensor design relies on inexpensive off the shelf components wherever possible to reduce the overall cost of the sensor package and to allow for easy replacement of spare parts in the field. The CHANOS II was deployed in the tidal Pocasset River, MA to

measure DIC over time between August and November 2021, and during surface mapping missions in Waquoit Bay, MA, in September 2021, from which we report sensor characteristics and tidal, seasonal, and episodic biogeochemical responses.

2.2 Methods

2.2.1 Measurement Principle

The continuous spectrophotometric DIC method operates by acidifying seawater to convert all inorganic carbon species to dissolved CO_2, then equilibrating fCO_2 across a semipermeable membrane between the acidified seawater stream and a pH sensitive indicating dye solution of known alkalinity. Spectrophotometric measurements of the dye solution allow for calculation of the total CO_2 concentration of the original sample (Byrne et al., 2002; Wang et al., 2007; 2013). After full equilibration, DIC of the acidified sample is proportional to the fCO_2 of the indicator such that:

$$\log(fCO_2)_{ASW} = \log\left(p \cdot \frac{[DIC]}{(K_0)_{ASW}}\right) = \log(fCO_2)_{ind} \quad (2.1)$$

where subscript *ASW* designates the acidified seawater sample, *ind* designates the indicator, $(K_0)_{ASW}$ is the Henry's Law constant for the acidified sample, and p is the exchange efficiency for CO_2 equilibration. The indicator solution is further described by the expression:

$$\log\ (fCO_2)_{ind} = B(T) - \log(K_0)_{ind} - \log\left(\frac{R - e_1}{1 - R\cdot\frac{e_3}{e_2}}\right) \quad (2.2)$$

where e_1, e_2, and e_3 are experimentally determined constants representing molar absorbance ratios at wavelengths λ_1 and λ_2, the absorbance maxima for the indicator acid (HI^-) and base (I^{2-}).

CHANOS I used a fast, dynamic equilibration process to improve the DIC measurement frequency. If the indicator is pumped slow enough through the equilibration cell, CO_2 can reach 100% equilibration across the Teflon tubing. However, if the indicator flow rate is increased, we can calculate the exchange efficiency for the partial CO_2 equilibration, p (0 – 1). This is a function of flow rate, temperature, indicator properties, and fCO_2 gradient and can be experimentally calibrated. However, the available Teflon tubing used in this iteration of the sensor was thin, and to avoid damage to the equilibration cell, the indicator flow rate was slowed enough that a correction for partial equilibration was not necessary and p was ~1 in deployments described herein.

A bromocresol purple sulfophthalein pH indicator was used with λ_1 = 432 nm and λ_2 = 589 nm. A third non-absorbing reference wavelength λ_{ref} or λ_3 = 700 nm was used to correct for baseline drift and optical obstructions. Constant molar absorbance ratios ($e_1 \approx 0.00387$ and $e_3/e_2 \approx 0.00633$) for this indicator have been previously described by Bryne et al. (2002) and Wang et al. (2007; 2013). In this expression, B(T) is an experimentally determined constant describing the chemical and optical properties of the indicator at a given temperature such that:

$$B(T) = \log(\, TA + [H^+] - [I^{2-}]_i + \log(\frac{K_I \cdot e_1}{K_1'})_i \,) \tag{2.3}$$

where K_I is the indicator dissociation constant and K_1' is the carbonic acid first dissociation constant. An absorbance ratio R can be defined as:

$$R = \frac{A(\lambda_2) - A(\lambda_3)}{A(\lambda_1) - A(\lambda_3)} \tag{2.4}$$

where A is the absorbance at a given wavelength λ_i, calculated from the intensities between the sample (I_i) and reference (I_0) spectrum at that given wavelength by:

$$A(\lambda_i) = -\log(\frac{I_i(\lambda_i)}{I_0(\lambda_i)}) \tag{2.5}$$

In this way, absorbances measured at the indicator acid and base peaks are used to calculate R, which can be converted into DIC concentration after calibration with CRMs.

2.2.2 Sensor System

The CHANOS II sensor (Figure 2.1) uses an array of 4 peristaltic pumps (OEM-B02, Baoding Shenchen Precision Pump Co., Ltd, Baoding, China) and 2 switch valves (T225PK031, NResearch, Inc., West Caldwell, NJ, USA) to move seawater, CRMs, acid, reference, and indicator solutions through the system. These components are packed in custom pressure housings filled with electronic liquid (FC-770, 3M, St. Paul, MN, USA), with a custom membrane to compensate for pressure. Seawater is filtered through nylon and copper mesh, passively mixed with acid, and directed into the outer shell of a custom 3 m fluid manifold equilibration cell, mimicking the tube-in-tube design used in CHANOS I (Figure 2.2, 2.3, 7 mL internal volume). Indicator is pumped through the inner shell of a Teflon AF 2400 semi-permeable tubing inside

the fluid manifold channel (Biogeneral Inc., San Diego, CA, USA). After passing through the equilibration cell, indicator is directed into a 10 mm optical "Z" cell (SMA-Z-10mm, 26 µL internal volume, FIALab, Seattle, WA, USA) where its spectra are continually monitored by an Ocean Optics USB4000 spectrophotometer. A custom pressure housing contains the optical cell, the controlling electronics and light source (Cool White (6500K) LUXEON Rebel LED, MR-WC120-20S, Quadica Developments, Inc., Lethbridge, Alberta, Canada). Temperature is monitored by an independent CTD sensor at the intake to the seawater line (SBE FastCAT 49 CTD, Seabird Scientific, Bellevue, WA, USA), and by thermistors at the equilibration and optical cells (Smartec, Breda, Netherlands). The custom controlling boards include one main board for overall sensor operation, a second board controlling the peristaltic pumps, and a third that monitors environmental conditions inside the pressure housing, including temperature, relative humidity, and leak detection. Custom controlling software runs on a TERN microprocessor (TS7600, Technologic Systems, Fountain Hills, AZ, USA). Spectra and absorbance data are measured and recorded with a custom web browser-based software. Data are stored on an internal micro-USB card or transferred via Ethernet to a shore computer. The system runs on 12V DC power through an external power source or rechargeable battery pack.

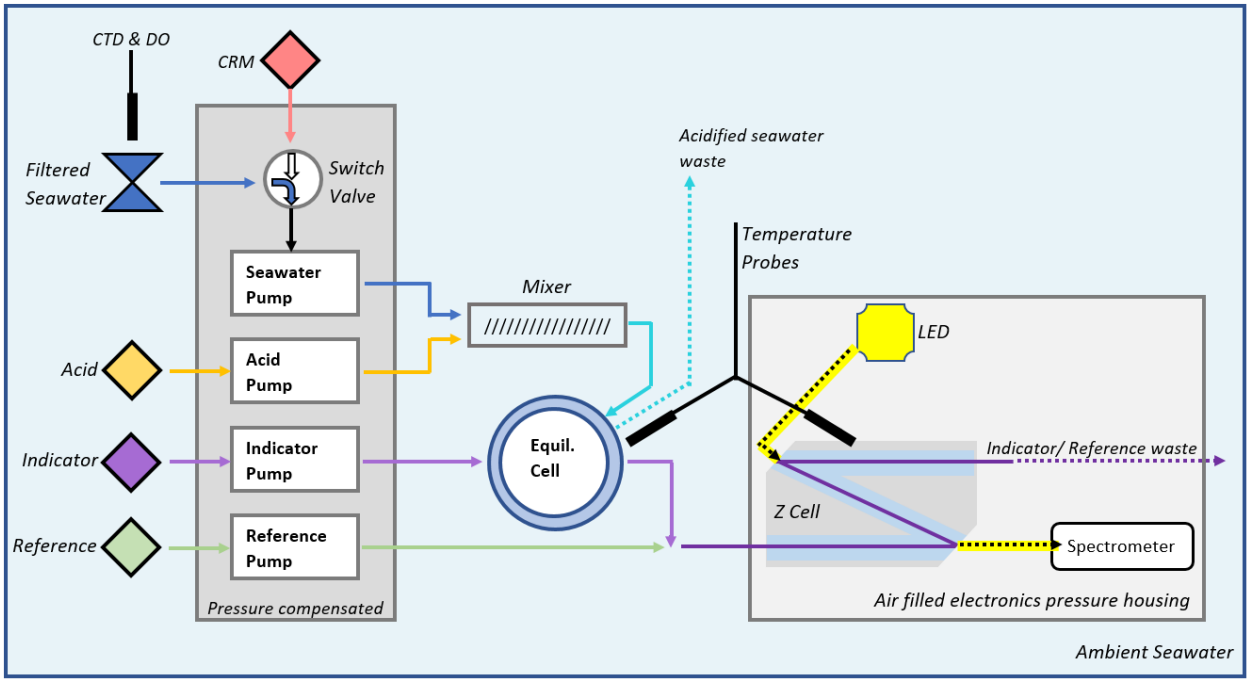

Figure 2.1: Schematic of the CHANOS II DIC channel. Seawater is continually acidified and pumped through the outer shell of CO_2 equilibration cell. Indicator is continually pumped countercurrent to the acidified seawater through the inner shell of the CO_2 equilibration cell. Reference or indicator are pumped through the optical "Z" cell for measurement via spectrometer.

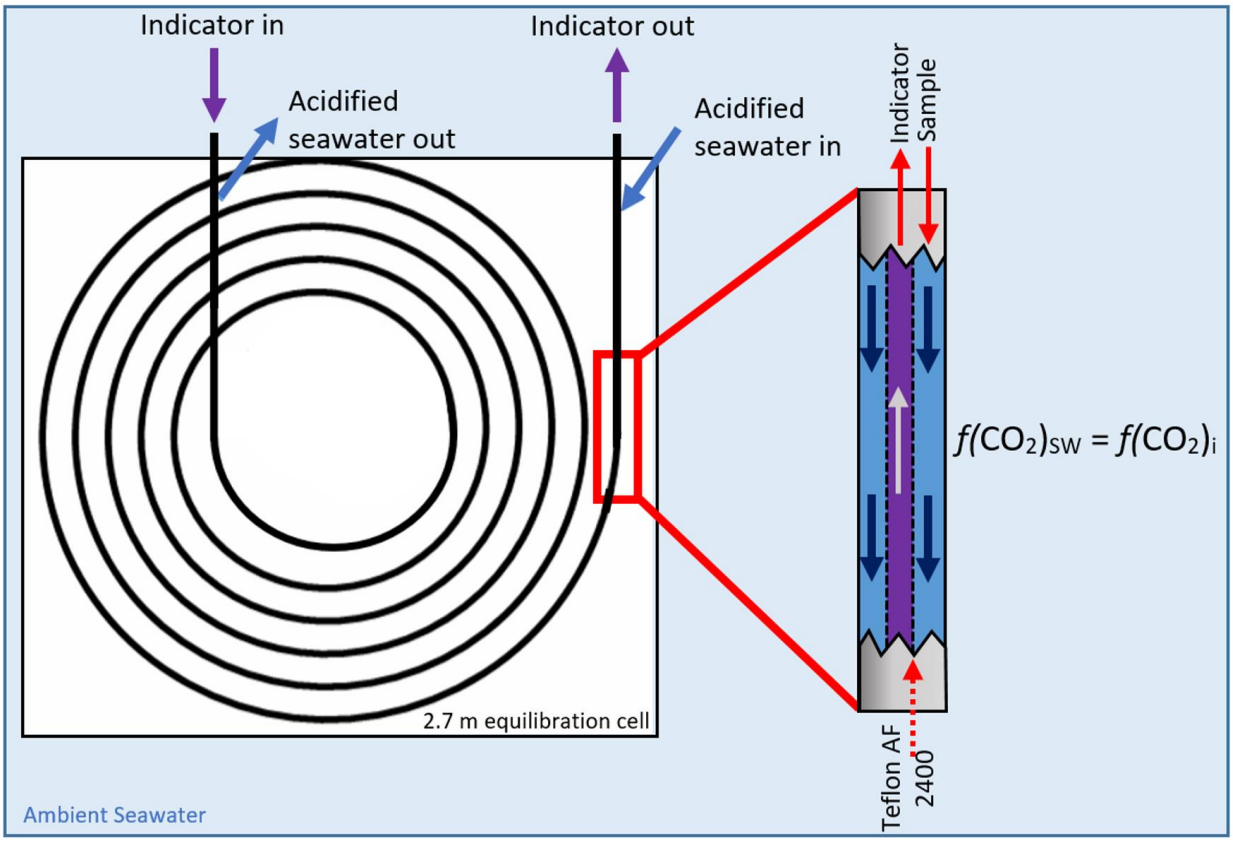

Figure 2.2: Schematic of the CO_2 equilibration cell (> 2.5 m) used in CHANOS II, featuring countercurrent acidified sample and indicator flow in a custom milled fluid manifold block.

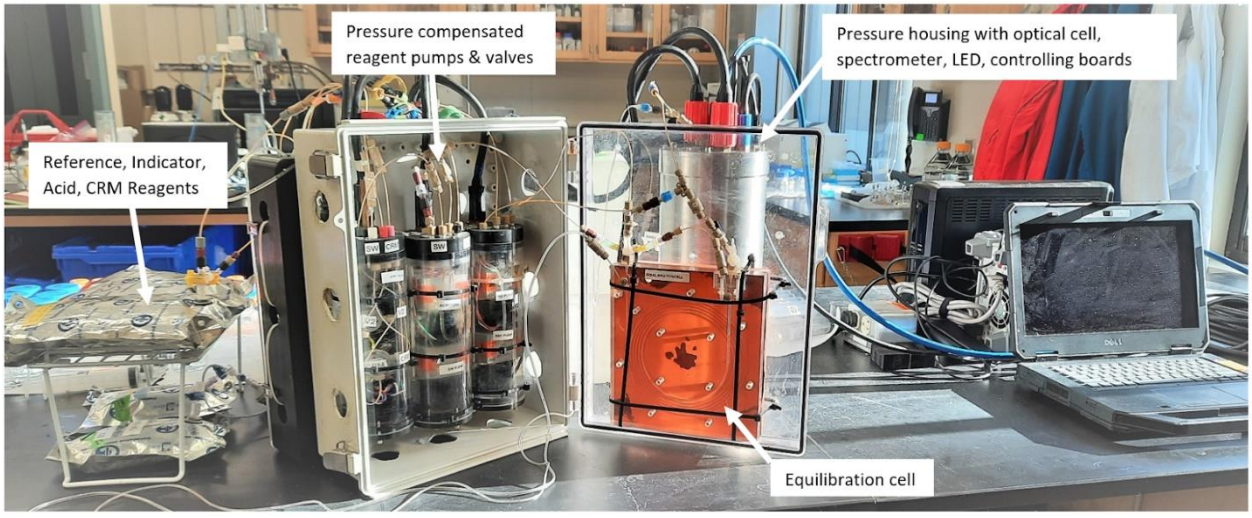

Figure 2.3: CHANOS II in benchtop mode. *From left*: working reagents stored in aluminum Calibond bags; sensor bay with pressure compensated pump/ valve housings and equilibration cell block; air-filled pressure housing containing optical cell, spectrometer, LED, and controlling boards. The sensor is controlled through a web browser-based software through an Ethernet connection. The sensor is deliberately modular and may be packed into various frames for deployment, depending on mission parameters (see Figure 2.4).

2.2.3 Reagents

Reagents (acid, reference, indicator, and CRM solutions) are carried onboard the sensor in customizable volumes depending on the length of a given deployment. Typically, 24 hours of near-continuous measurements require ~75 mL acid, ~20 mL reference, and ~180 mL indicator solutions. Each CRM measurement requires ~350 mL CRM. Hydrochloric acid (HCl, 3.0M) is used to acidify the seawater samples at a ~1:200 acid:seawater ratio. A working reference solution is made using Milli-Q water and extra-pure Na_2CO_3 at a TA concentration of ~1000 µmol kg^{-1}. Bromocresol purple sodium salt is added to the reference solution to make an indicator concentration of ~25 µM, optimized to maximize the detectable absorbance range encountered for seawater DIC concentrations (typically ~1500 - 3000 µmol kg^{-1}) with a known alkalinity. Working reference and indicator solutions are stored in gas-impermeable aluminum laminated bags (Calibrated Instruments, Inc.), which have been shown to retain the original solution composition for several months at a time (Wang et al., 2015). CRM (obtained from A.G. Dickson at Scripps Institution of Oceanography) or secondary standards are transferred to gas-impermeable aluminum laminated bags which have been shown to retain the original solution composition for up to one month (Wang et al., 2015). A typical time-series deployment as described in section 2.3.5 carries 0.5 L HCl, 0.5 L reference solution, 2 L indicator solution, and two 2 L bags of standards. These solutions will last for ~7 days of continuous measurements or ~18 days of intermittent measurements at hourly intervals.

2.2.4 Sensor Measurement Procedure

A custom controlling software allows for autonomous measurements at continuous, intermittent minimum hourly), or scheduled (at specific dates and times) operation. Seawater is filtered through nylon and copper meshes to remove particulate matter, then acidified with HCl to convert all dissolved inorganic carbon species (H_2CO_3, HCO_3^-, CO_3^{2-}) into dissolved CO_2. The acidified seawater is continuously pumped through the outer shell of the equilibration fluid manifold. Reference solution is flushed through the optical cell and a reference spectrum is recorded. Samples are typically measured continuously with reference spectra retaken every ~6 hours to correct for any existing absorbance baseline drift, though references may be recorded more or less frequently depending on the specifics of the deployment. Indicator solution is pumped countercurrent to the acidified seawater through the inner shell of the equilibration cell with a travel time of ~2 - 4 min, determined by the length of the equilibration cell and the flow rate of the indicator. The current cell uses ~2.7 m Teflon AF 2400 tubing in a custom milled fluid manifold block. The indicator flow rate is chosen to balance a high exchange efficiency (p) with a low consumption of the indicator, with consideration for the maximum allowable safe flow rate through the thin-walled Teflon AF 2400 tubing

available from distributors at the time of this publication, which can rupture and leak under high flow rates. The equilibrated indicator solution is then directed through the optical cell for absorbance detection at a frequency of ~1 Hz.

2.2.5 Calibration

Laboratory calibration is conducted before a sensor deployment to establish the full range of DIC concentrations and temperatures expected during a given mission. In theory, the spectrophotometric method can be calibration free for in-situ measurements provided that the indicator solution and optical measurement system are stable during a deployment (DeGrandpre et al, 2014; Wang et al., 2007). However, in practice, we can conduct in-situ calibrations during deployments by measuring CRMs on a regular schedule, determined by the deployment goals and strategy, to ensure in-situ measurement quality. Alternately, in-situ measurements of CRM may be used as an additional quality control check on sensor measurements, if they are not considered within sensor calibration curves. Before a deployment or after a change in reagent batches, laboratory calibration curves are generated by measuring CRM at varying temperatures in a controlled water bath to calculate the B(T) constant as a response to sampling temperature, which is a function of the chemical and optical properties of the indicator solution. B(T) of a given batch of indicator is assumed to be stable over several months (Wang et al., 2013). When in-situ CRM measurements are recorded during a deployment, they may replace the laboratory calibration curve to provide the best possible information on sensor operation. Bottle samples taken throughout a given deployment are used to check sensor measurement quality, accuracy, and precision, as discussed in Section 2.3.

2.2.6 Laboratory tests

The sensor's temperature response was established through a series of laboratory measurements inside a large cooler of seawater attached to an aquarium chiller capable of achieving steady temperatures from 4 - 32°C. Repeated measurements of an in-house secondary seawater standard (DIC ~2100 µmol kg^{-1}), calibrated via CRM, were taken at multiple temperatures to create a B(T) experimental calibration curve. Seawater samples of different DIC concentrations (range 1500 – 2500 µmol kg^{-1}) were measured to determine typical response times at a range of seawater and indicator flow rates, as well as to evaluate the efficiency of CO_2 equilibration (*p*, Equation 2.2).

2.2.7 Ground-truthing and Field Deployments

A variety of customizations to CHANOS II may be made to suit specific deployment platforms, durations, and goals, with key considerations including length of deployment, desired frequency of measurement, power requirements, and accessibility for maintenance. The CHANOS II sensor has been ground-truthed and deployed from several stationary and mobile platforms (Table 2.2 and Figures 2.4-2.5).

Table 2.2: CHANOS II field deployments in 2021

Platform, depth, and location	**Deployment type**	**Mode/ frequency**	**Additional sensors deployed**	**Length of deployment**	**Bottle sampling**
Boat dock near river mouth Submerged <3m depth Pocasset, MA 41.70, -70.62	Stationary/ time series	Continuous or hourly time series	Aanderaa 4330 dissolved oxygen (DO) optode Ruskin RBR*concerto* CTD	July – Nov 2021, total 59 days	148 samples, with 10 samples taken hourly across 3 full tidal cycles
Small catamaran *TriFly* Submerged <1m depth Waquoit Bay, MA 41.56, -70.52	Towed underway	Continuous	Aanderaa 4330 DO SBE 37 CTD Ruskin RBR*concerto* CTD	~2 hours each for 4 deployments over 3 days	~25 samples per towed deployment, taken every ~5 min

2.2.8 Stationary time-series in the Pocasset River, MA

We evaluated the performance of the CHANOS II in continuous and intermittent time-series measurements from the Scallop Bay Marina in the small tidal Pocasset River, MA (41.70 N, 70.62 W). This site is ~500 m from the mouth of the Pocasset River, which flows westward for ~3.2 km through a series of small ponds and wetlands into Buzzards Bay. We deployed the sensor from ~1 m below the surface of a powered dock between July 22 and November 14, 2021.

We collected a total of 59 days of measurements at this site. Breaks in the time-series of one day to one week included various elements of troubleshooting and routine maintenance (e.g., replacement of batteries,

filters, and reagents). A gap in the time-series from September 17 – 30 was due to the sensor's use in a towed deployment in Waquoit Bay, described in Section 2.2.9 below. Bottle samples were collected for sensor ground-truthing via laboratory measurement of DIC following the best practices of seawater CO_2 sampling and measurement as described in Dickson et al. (2007). Water samples were pumped through 0.45 µM capsule filters (Farr West Environmental Supply), collected into borosilicate glass bottles, and poisoned with saturated mercuric chloride solution. Bottle samples taken between October 28 and November 14 were not filtered due to pump and power failures at the site; in these cases, bottle samples were poisoned as usual and analyzed for DIC and TA as rapidly as possible, typically within one day of collection. Unfiltered bottle samples were typically analyzed for DIC and TA within two weeks.

CHANOS II was deployed with an Aanderaa 4330 dissolved oxygen (DO) optode and Ruskin RBR*concerto* CTD. In-situ CRM calibration measurements were taken every 6 - 36 hours throughout the deployment, depending on sampling mode (continuous or intermittent) and reagent availability. During intermittent periods, CHANOS II operated for 30 minutes out of every hour. Reference measurements interrupted sampling for ~15 minutes every 6 hours to allow for correction of potential baseline drift of absorbance measurements.

2.2.9 Small boat underway towing, Waquoit Bay, MA

To test the sensor's capability in high resolution spatial mapping from mobile platforms, the CHANOS II was towed just below the surface from the front of the small research catamaran *TriFly* in Waquoit Bay, MA (41.58 N, 70.52 W) on September 20, 27, and 28, 2021 (Figure 2.4). We conducted 4 towed deployments throughout the bay in transects of ~13-15 km total over 2 hours each, centered around 2 high (September 20 and 27) and 2 low (September 27 and 28) tides. The sensors ran continuously and autonomously, with minor operator intervention to clear shallow sandbars. Bottle samples were taken frequently for laboratory DIC analysis (every ~5 min). The sensor package included an auxiliary Aanderaa 4330 DO, SBE 37 CTD, Ruskin RBR*concerto* CTD sensor, and pro-Oceanus pCO_2 sensor. Due to limited space on the small boat, bottle samples were collected directly at the surface and were not filtered. Samples were immediately poisoned with mercuric chloride and stored in a dark box. Bottle samples were analyzed for DIC and TA as rapidly as possible, typically within 1 day of collection.

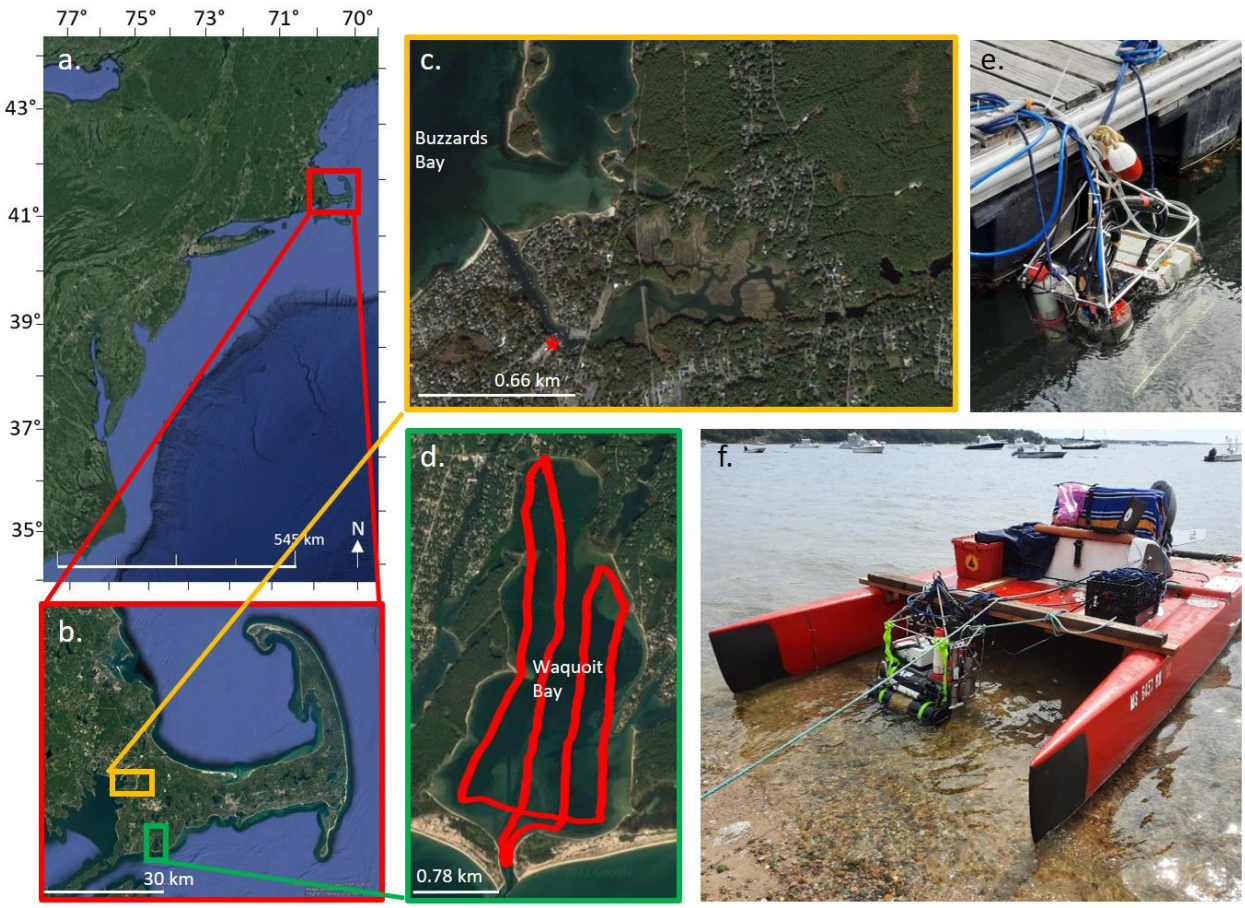

Figure 2.4: East Coast US (*a*) and Cape Cod, MA maps (*b*) show locations of CHANOS II deployments in the Pocasset River (*c*) and Waquoit Bay (*d*). The red star on panel *c* marks the location of the Scallop Bay Marina, ~500 m from the mouth of the Pocasset River entering Buzzards Bay. CHANOS II was deployed with auxiliary CTD and DO sensors (*e*). Red track lines in panel *d* show one tow path for the CHANOS II with auxiliary CTD, DO, and pro-Oceanus pCO_2 sensors deployed from the *TriFly* research catamaran (*f*) at the Waquoit Bay National Estuarine Research Reserve in Waquoit, MA.

2.2.10 Laboratory measurement of bottle samples

All DIC samples were measured with a DIC auto-analyzer (AS-C3 Apollo SciTech Inc., Newark, DE, USA). This system requires acidification of samples with 10% phosphoric acid. Evolved CO_2 gas is purged with N_2 and detected via a LiCOR7000 infrared instrument (Li-COR, Lincoln, NE, USA). CRMs were used for calibration of the analyzer and precision and accuracy of DIC measurements were ±2 µmol kg^{-1} (Song et al., 2020; Wang et al., 2017).

2.3 Results and Discussion

2.3.1 Laboratory testing and calibration

CHANOS II laboratory precision was determined by continuous, repeated measurements of known seawater samples poisoned with mercuric chloride and held at a constant temperature of 22.5 °C. This resulted in a laboratory precision of ± 5.5 µmol kg^{-1} and accuracy of ± 2.9 µmol kg^{-1} (n = 10 sets of standard measurements, with each standard measured at least 3 times). Precision was determined from a pooled standard deviation of repeated sensor measurements. Accuracy was derived from an average of the difference between sensor measurements and known sample DIC as determined via the Apollo auto-analyzer. A variety of factors contribute to these uncertainties, including the stability of the LED, noise in spectra measurements, and the potential for variability (or 'pulsing') of the peristaltic reagent pumps.

CHANOS II was calibrated for temperature in the laboratory before deployments, where field measurements of onboard CRM or secondary standard reference materials were available to contribute to or replace laboratory calibration curves, or to independently evaluate sensor performance. Figure 2.5 shows the results of repeated laboratory measurements of a secondary seawater standard at temperatures ranging from 4.6 to 28.5 °C. B(T), the constant describing the chemical and optical properties of the indicator at a given temperature, was experimentally determined from samples with known DIC concentration using Eq. 2.3. This allowed for the determination of a temperature calibration curve of B(T) that was applied when calculating DIC concentrations from sensor absorbance ratios measured for a given sample (Figure 2.6).

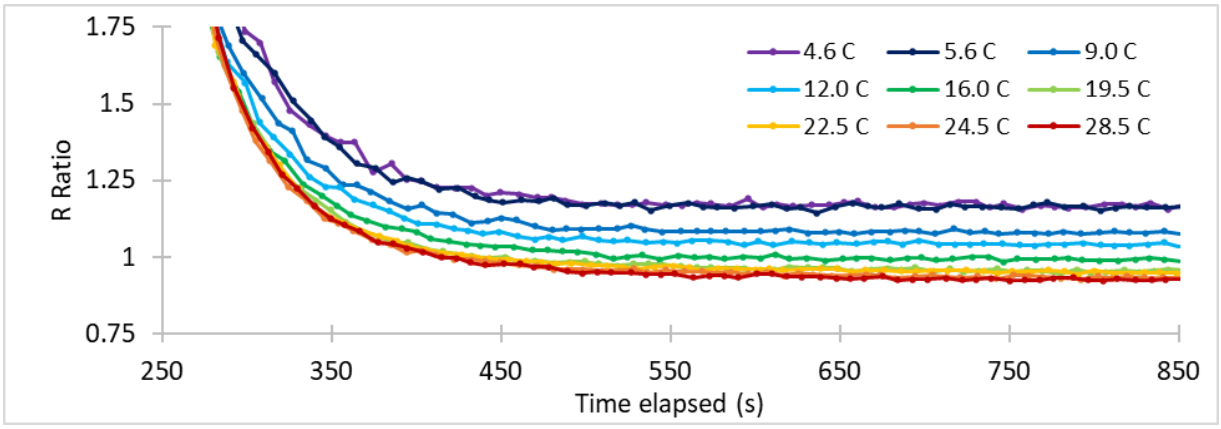

Figure 2.5. Absorbance ratio R vs time for repeated measurements of a secondary seawater standard at varying temperatures. Seawater is acidified and pumped through the outer shell of the equilibration cell, with indicator flowing through the inside of the Teflon AF 2400 tubing. As CO_2 equilibrates across the semi-permeable Teflon barrier, the change in pH of the indicator is monitored spectrophotometrically and converted to an R ratio, which is then used to calculate DIC. Stable R values ~450 s after indicator is introduced to the equilibration flow cell indicate that the seawater-indicator system has equilibrated.

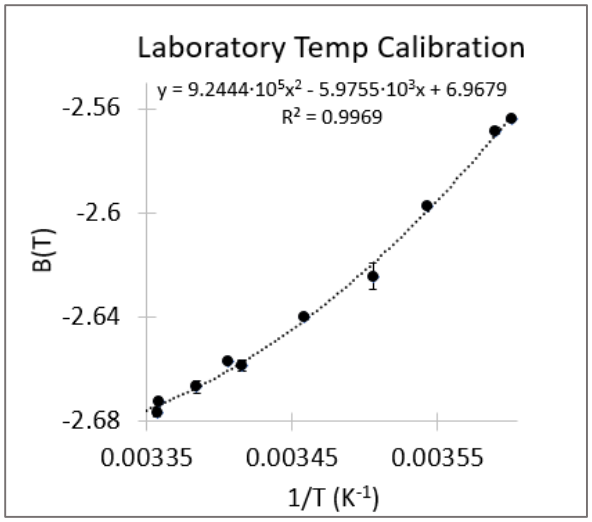

Figure 2.6. Experimentally derived indicator behavior as a function of temperature, B(T), determined from laboratory measurements. This curve is applied to laboratory sensor measurements when calculating DIC from sensor absorbance ratios.

CHANOS I (e.g., Wang et al., 2015) calculated the nonlinear percentage of CO_2 equilibration between an acidified seawater sample and indicator dye and chose the best indicator flow rate to balance indicator consumption, response time, and measurement stability. CHANOS II uses a fluid manifold block with Teflon AF tubing coiled in grooves to mimic the original 'tube-in-tube' design (Figure 2.2) to equilibrate acidified samples and indicator solution. Changes in the stock Teflon AF 2400 available have impacted the selected indicator flow rate through this equilibration cell, such that we have slowed indicator flow to ~0.125 mL min^{-1} to ensure that the indicator is not forced through the fragile, thin-walled Teflon tubing. In this way, equilibration can be maintained near ~100% and indicator consumption is reduced, but the trade-off is that response time is slowed relative to CHANOS I (Figure 2.7).

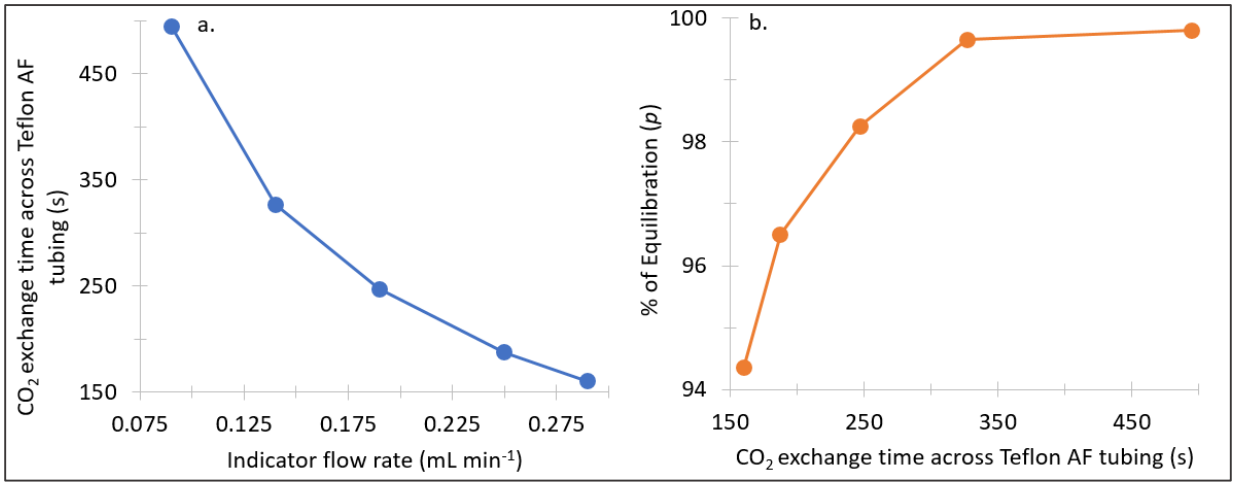

Figure 2.7. CO_2 exchange time in Teflon tubing (travel time or residence time) as a function of indicator flow rate *(a)*, and percentage of equilibration (*p*) as a function of exchange time (*b*). A CO_2 exchange time or travel time of ~450 s is required to reach ~100% equilibration.

2.3.2 In-situ sensor characteristics during time-series in the Pocasset River, MA

An in-situ B(T) temperature calibration curve was determined from measurements of secondary seawater standards throughout the time-series deployment at temperatures ranging from 12 to 22 °C (n = 31 sets of standard measurements throughout the time-series deployment, with each standard measured at least 3 times, Figure 2.8). A standard error calculated between the best fit B(T) curve and field data was propagated through DIC calculations (1 SE, B(T) ± 0.0026).

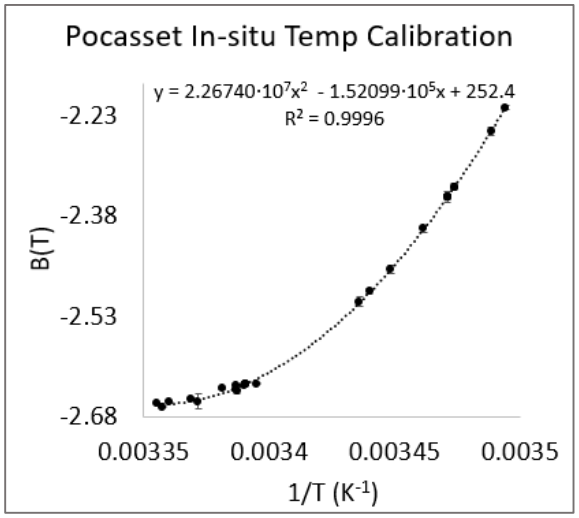

Figure 2.8. Experimentally derived indicator behavior as a function of temperature, B(T), from field measurements. This curve is applied to in-situ sensor measurements when calculating DIC from sensor absorbance ratios.

During the Pocasset River time-series deployment, we collected 59 days of CHANOS II DIC data with 148 discrete bottle samples for laboratory DIC analysis. 52 bottle samples collected during the deployment, chosen to best represent an accurate comparison between sensor and bottle measurements, were used to evaluate the sensor performance against standard laboratory DIC analyses. Only filtered bottle samples that were simultaneous to equilibrated CHANOS II DIC measurements were used in this evaluation. Of the 96 bottle samples that were not used in this comparison, 57 were not filtered at the time of collection, and the remainder were collected when the sensor was not measuring between intermittent timepoints, was measuring a CRM or reference, or was not yet equilibrated. A comparison of residuals between selected bottle samples and CHANOS II DIC measurements is shown in Figure 2.9, spanning the range of DIC recorded during this deployment from ~1300 - 1900 µmol kg^{-1}. The residuals had a mean and standard deviation of -3.79 ± 9.00 µmol kg^{-1}, respectively. These residuals indicate that there was no significant drift and limited measurement bias over the course of the deployment. Part of the difference between sensor measurements and discrete bottle samples may be due to discrete bottle sample analytical errors (±2.0 µmol

kg^{-1}), and the rest is comparable to the laboratory-determined precision of the sensor (±5.5 µmol kg^{-1}). A pooled standard deviation of repeated sensor measurements at the time of bottle sampling indicated a field precision of 4.9 µmol kg^{-1}.

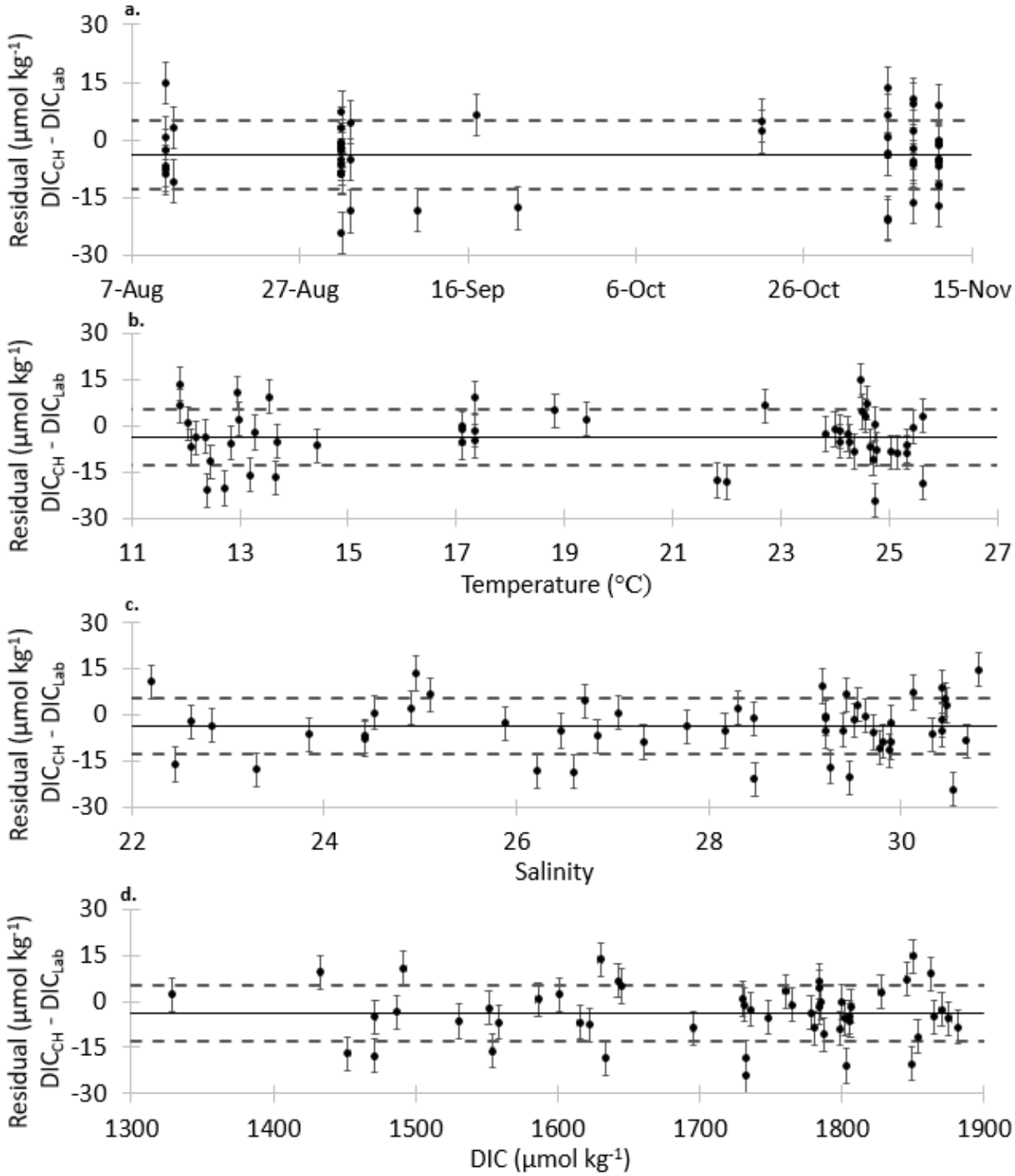

Figure 2.9. Residuals between bottle samples (DIC_{Lab}) and CHANOS II measurements (DIC_{CH}) versus sample date (*a*), temperature (*b*), salinity (*c*), and DIC (*d*). The black line represents the mean at -3.79 µmol kg^{-1}, with a standard deviation of 9.00 µmol kg^{-1} (dashed lines). Error bars represent estimated laboratory precision in CHANOS II measurements (e.g., 5.5 µmol kg^{-1}).

2.3.3 Sensor response time

The sensor response time during deployments can be estimated by switching between two distinct DIC samples, as similar to that demonstrated by Wang et al., (2013). For example, it took ~450 s to record a steady sensor measurement when switching between ambient seawater and an onboard CRM in the field, with a DIC difference of ~ 200 µmol kg^{-1} (Figure 2.10). As the concentration difference between two samples decreases, the response time decreases, such that the incremental concentration changes in actual flow-through samples can be approximately represented in Figure 2.10. The sensor response time must be assessed during data processing: sensor measurements may be within precision of the final value within 450 s, but could be slower in some cases if the DIC difference between successive samples is much larger.

This response time is ~ 7 times longer than that of the CHANOS I sensor, but still allows for high frequency measurements (Wang et al., 2015). This response time may be improved by further optimizing the stock and diameter of Teflon used in the equilibration cell (here, 0.010" ID and 0.020" OD versus 0.016" ID and 0.022" OD in CHANOS I, Wang et al., 2015). Response time may also be improved by accounting for percent equilibration, as in Wang et al., 2013 and 2015, using wider diameter Teflon to allow for tuning of the indicator flow rate. Given the limitation in Teflon tubing supply, this should not be a significant constraint of the response time of the sensor over the long term, as a more appropriate Teflon tubing can be substituted into the fluid manifold block without further modifications. For slow-moving mobile deployments, the current configuration can still capture most DIC variability during a given deployment. For example, for an ROV moving at 0.2 knots (6.2 m min^{-1}), a running average of DIC measurements over ~450 s will capture an attenuated spatial resolution of better than 50 m, which represents a significant improvement over individual bottle samples from this type of deployment.

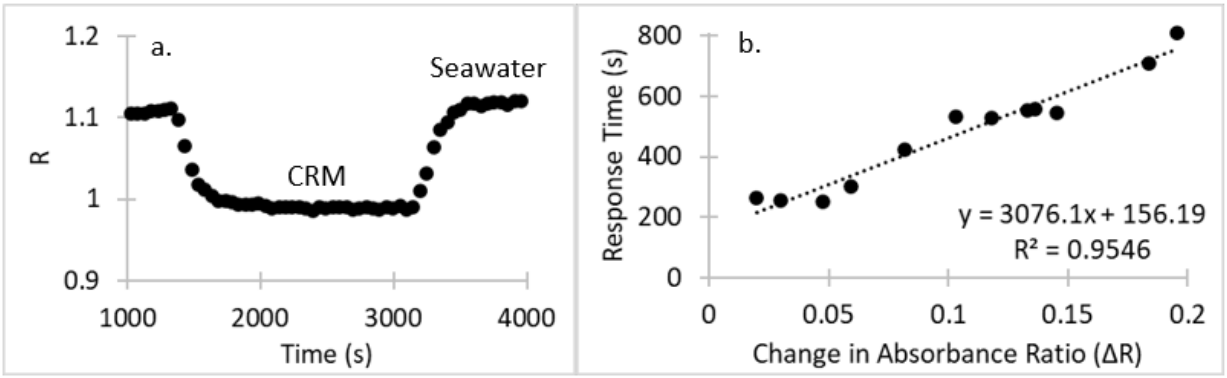

Figure 2.10. Assessment of sensor response time by measuring absorbance ratios when toggling from ambient seawater to a known CRM standard and back (*left*). Sensor response time as a factor of the difference in concentration between 2 consecutive samples (*right*), as measured during the Pocasset River deployment.

2.3.4 Biogeochemical signals in the Pocasset time-series

All CHANOS II DIC data and bottle samples were plotted against CTD measured salinity and dissolved oxygen, grouped by month throughout the time-series deployment (Figure 2.11). Several notable features are evident in this figure. First, we highlight two major storms: tropical storm Henri hit Pocasset on August 22, 2021, bringing rain and damaging winds to the area. The CHANOS measured both anomalously high and low DIC during this storm, circled in red. The blue oval highlights the low DIC and low salinity values measured during a nor'easter that arrived on October 27, 2021, primarily bringing heavy rains to the area.

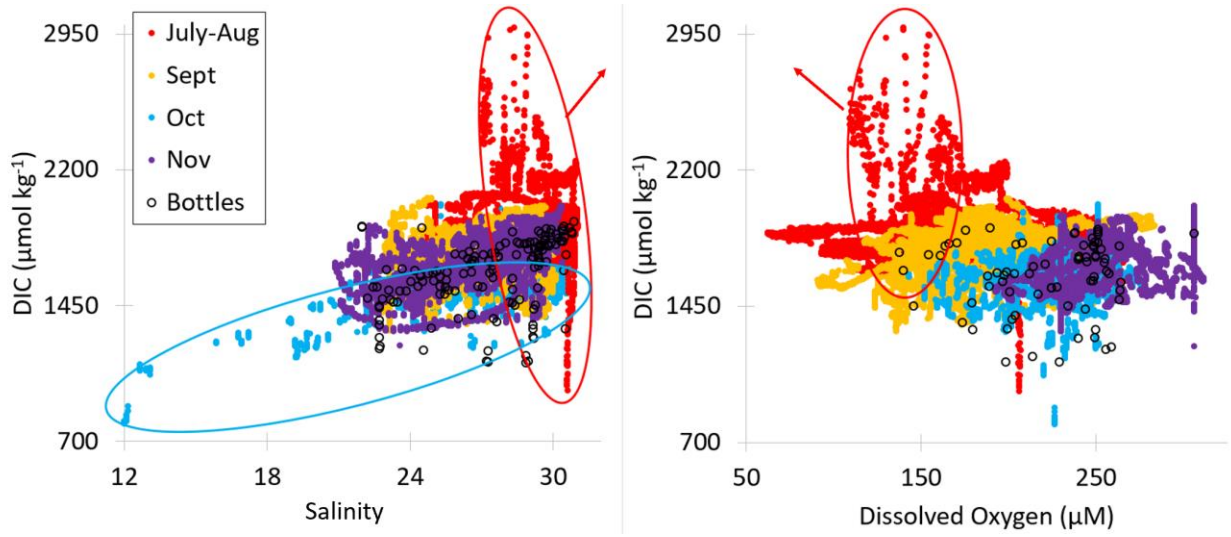

Figure 2.11. CHANOS II DIC measurements plotted against CTD measured salinity (*left*) and dissolved oxygen (*right*), grouped by color into months. Bottle samples are identified by black circles. The red ovals highlight both high DIC and low DO values measured during tropical storm Henri ~August 22, which brought rain and high winds and trapped debris-laden runoff at the dock of the deployment site. The blue oval highlights low DIC and low salinity values measured during a nor'easter on October 27, which primarily brought large volumes of fresh rain.

While the bulk of the DIC range measured by CHANOS II is also captured by bottle samples, no bottle samples were obtained during either storm due to site inaccessibility. Sensor evaluation is therefore difficult during these storm periods, though the baseline absorbance measurement at 700 nm indicated that the optical system was behaving acceptable, and an onboard secondary standard measurement during the nor'easter on October 27 was good ($\Delta DIC_{CH\text{-}Lab}$ = -4.27 µmol kg^{-1}, where the laboratory measurement of the secondary standard was ~1910 µmol kg^{-1}).

The sensor readings appear to illuminate two different biogeochemical responses to these storms. During the August tropical storm, a large volume of rain and runoff was flushed over land. Heavy winds generated waves and swept terrestrial biomass, including grasses, leaves, and large branches, into the Pocasset River.

Reeds, branches, and leaves were trapped by the docks for several tidal cycles above the CHANOS sensor, and visible damage was done to the seagrass beds on the sides of the river. The high winds and waves likely stirred up the sediment in these seagrass and reed beds, releasing DIC-rich and DO-poor sediment pore water into the water column. In contrast, the October nor'easter was primarily a dilution event, where large volumes of rain and runoff flushed into the river, resulting in a decreased salinity and DIC during the storm. At this time in late October, limited biomass remained onshore and no visible damage was done to the river beds by wind or waves. The low DIC and high DO during this storm indicated that pore water was not released into the water column as had occurred during the tropical storm. While bottle sampling was not possible during either storm, CHANOS II measurements were reasonable and illuminated biogeochemical signals that are difficult to capture without the development of such autonomous systems. This highlights the importance of deploying automated sensors in dynamic environments, even if they are not as precise as benchtop laboratory DIC analyzers.

Two subsets of time-series data, including the two storms discussed, are shown in Figures 2.13 and 2.14. Several tidal cycles of each of these subsets are shown in Figures 2.15 and 2.16.

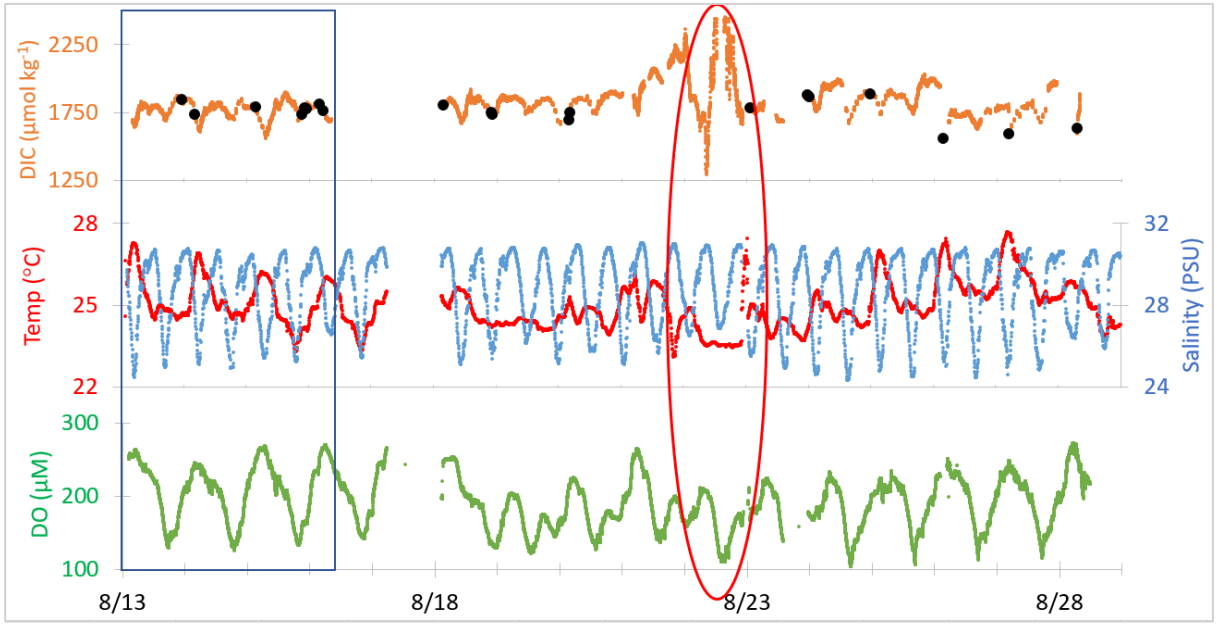

Figure 2.12. Time-series data from the Pocasset River between August 13 and 28, 2021, with CHANOS II DIC (*orange*) and bottle samples (*black*) (*top*), CTD temperature (*red*) and salinity (*blue*) (*middle*), and dissolved oxygen (*green*) (*bottom*). The red oval ~August 22 corresponds tropical storm Henri. Most CHANOS II data in this set was collected continuously, with some periods of intermittent (~hourly) measurement. The blue box indicates the time period shown in Figure 2.14.

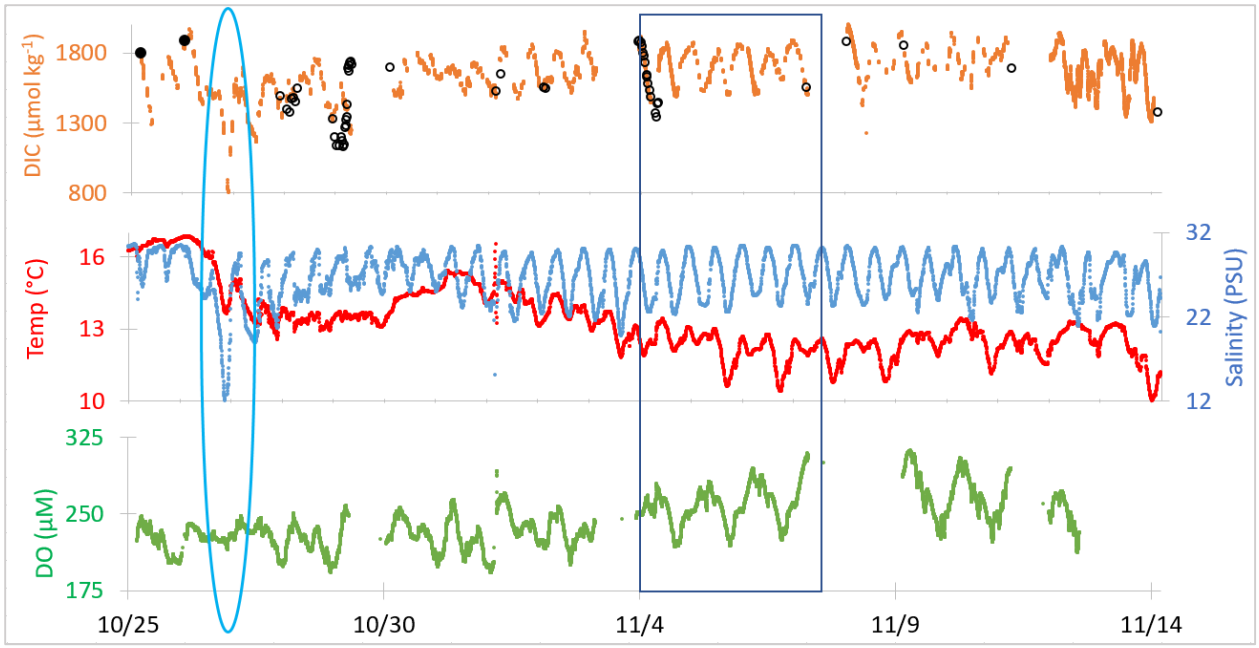

Figure 2.13. Time-series data from the Pocasset River between October 25 and November 14, 2021, with CHANOS II DIC (*orange*) and bottle samples (2 filtered samples are shown as filled black circles at the beginning of this dataset, followed by open circles designating unfiltered samples) (*top*), CTD temperature (*red*) and salinity (*blue*) (*middle*), and dissolved oxygen (*green*) (*bottom*). Most CHANOS data in this set was collected intermittently (~hourly). The blue box indicates the time period shown in Figure 2.15.

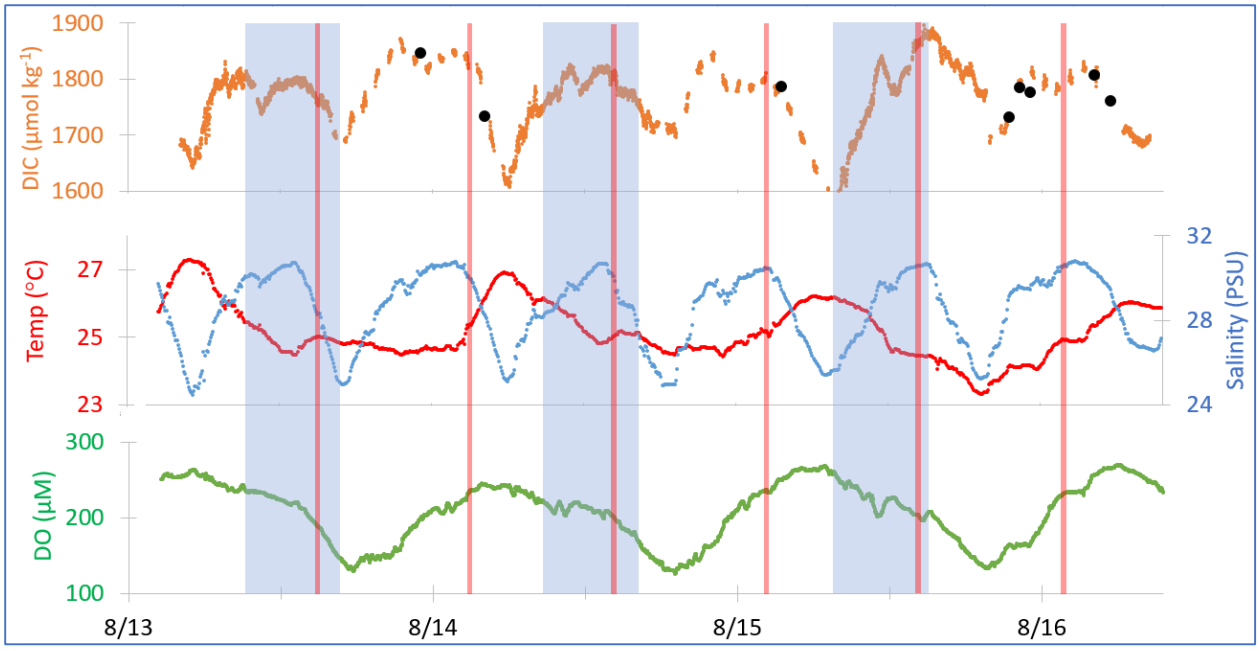

Figure 2.14. Time-series data from the Pocasset River between August 13 and 17, 2021, with CHANOS II DIC (*orange*) and bottle samples (*black*) (*top*), CTD temperature (*red*) and salinity (*blue*) (*middle*), and dissolved oxygen (*green*) (*bottom*). Blue shaded rectangles indicate nighttime. Red vertical lines indicate high tides. During this portion of the deployment, the sensor alternated between continuous and intermittent measurements every 12 hours.

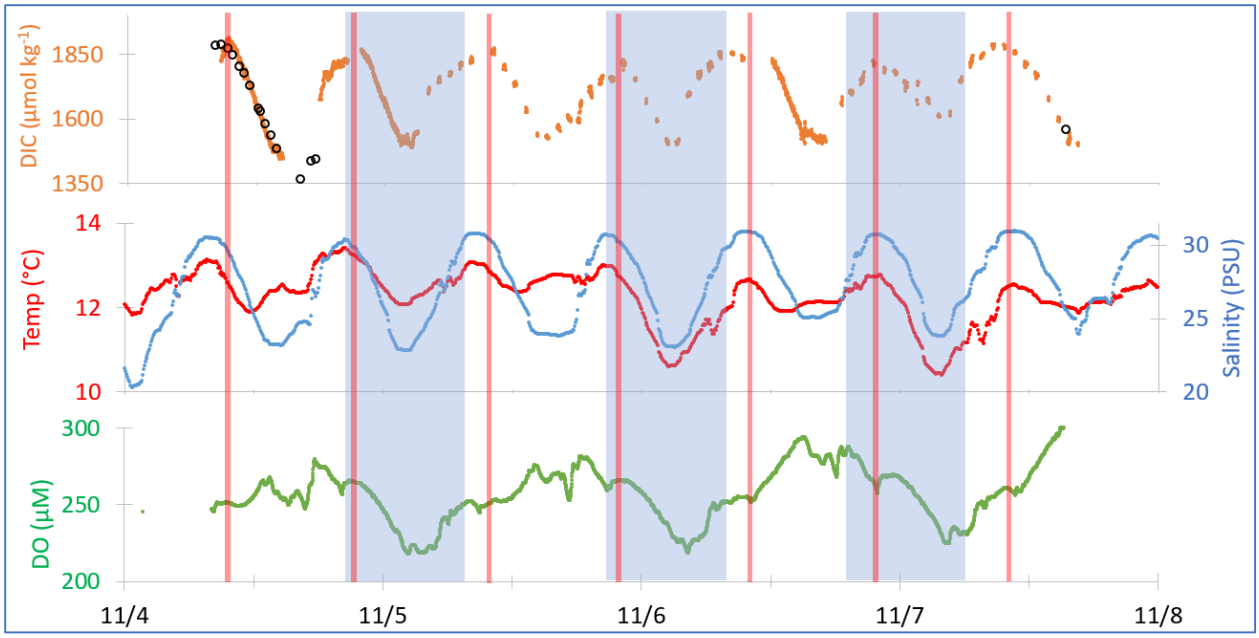

Figure 2.15. Time-series data from the Pocasset River between November 4 and 8, 2021, with CHANOS II DIC (*orange*) and bottle samples (*black*) (*top*), CTD temperature (*red*) and salinity (*blue*) (*middle*), and dissolved oxygen (*green*) (*bottom*). Blue shaded rectangles indicate night. Red vertical lines indicate high tides. During this portion of the deployment, the sensor measured continuously for ~6 hours followed by ~18 hours of intermittent measurements.

Aside from the occasional storms, DIC at this site typically tracked with salinity, such that high tides were typically characterized by high salinity and high DIC as water from the bay was swept into the Pocasset River. Low tides were characterized by low salinity and low DIC; the freshwater endmember likely comes from further upstream in the Pocasset River (Figures 2.14-2.15). Spring and neap tides influenced the relative range of salinities recorded at this site: during spring tide periods, the practical salinities observed at the low tides were slightly higher (1 - 2) than occurred during neap tides, as the river was inundated with more seawater from Buzzards Bay. However, there was no significant difference in the range of DIC values recorded during these tidal variations. Figure 2.16 shows the DIC plotted against salinity for summer and fall, both of which generally approximate a conservative mixing line.

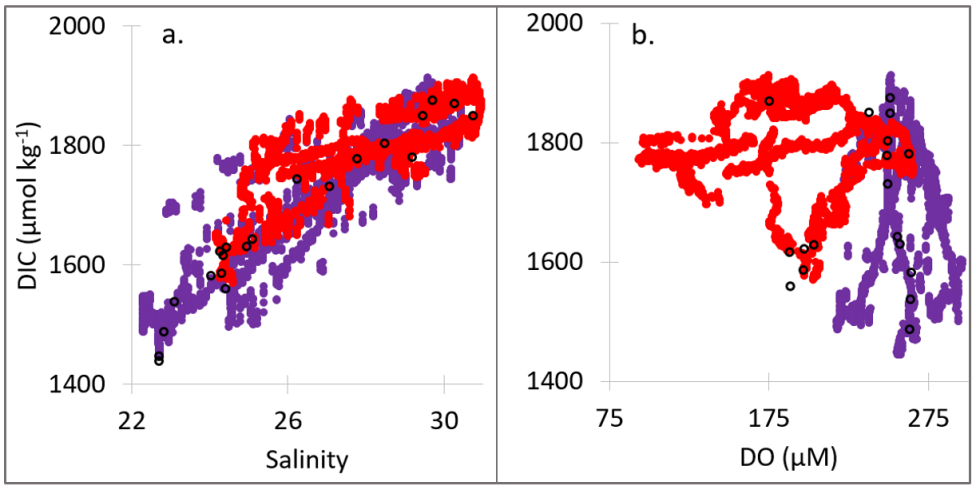

Figure 2.16: Panel *a*: DIC versus salinity for the data shown in Figure 2.14 (*red*, August 13-17, 2021) and Figure 2.15 (*purple*, November 4-8, 2021), showing a general mixing trend between bay and upstream endmembers, with seasonal shifts in DIC and salinity. Panel *b*: DIC vs DO for the same time periods.

Table 2.3 provides a comparison of the range of sensor measurements over several typical tidal cycles during late July and early November. DIC varied more widely in fall than in summer and was on average ~137 µmol kg^{-1} lower than in summer. Similarly, temperature and salinity ranged more widely in fall than in summer and were on average ~12 °C and 1.8 lower than in summer. DO was more variable in summer and was on average ~50 µM lower than in fall. These ranges reflect seasonal change in the Pocasset River: lower salinity values in fall are likely due to increased rainfall and decreased evaporation. DIC, temperature, and DO are closely linked: physically, dissolved oxygen is more soluble in fresher and colder water, raising DO values in fall. As phytoplankton die off in the fall under conditions of decreased light and temperature, respiration rates slow, such that DO increases on average but is less variable over day/night cycles. DIC decreases on average from summer to fall as respiration slows and salinity decreases.

Table 2.3: Range of sensor measurements recorded during August and November, 2021

	DIC (µmol kg^{-1})	Temperature (°C)	Practical salinity	DO (µM)
Summer (July 22 –24, 2021)	1575 - 1925	23.5 – 25.5	24.0 – 31.0	90 - 270
Fall (November 12 – 14, 2021)	1300 - 1950	10.0 – 13.5	21.0 – 30.5	210 - 300

2.3.5 Sensor characteristics during small boat underway towing, Waquoit Bay, MA

We collected ~8 hours of continuous CHANOS II DIC measurements, binned by minute for reporting and accounting for the time it takes for a sample to flow through the sensor system, during the small boat deployment at Waquoit Bay. 90 bottle samples were collected at 5 min intervals for sensor-bottle comparison. Each towed deployment included four parallel north/south paths, varying slightly depending

on the locations of sand bars and local boat traffic (Figure 2.17). Each tow covered a total of 13-15 km at an average speed of ~110 m min^{-1}. These tows took ~2 hours each and were centered around low or high tides on September 20, 27, and 28.

Figure 2.17. Underway towing transects at Waquoit Bay as recorded by GPS trackers carried on the *Trifly*. Individual transects vary slightly due to sandbars and local boat traffic.

All underway data are shown first as time-series in Figures 2.18 - 2.21.

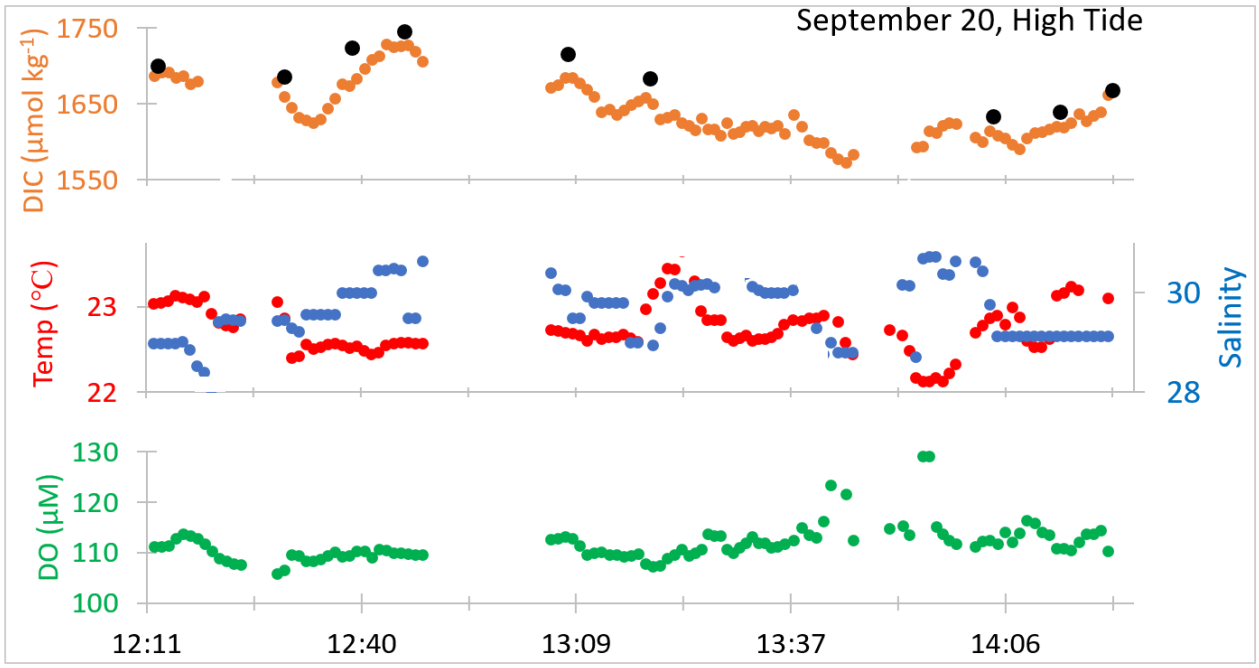

Figure 2.18. CHANOS II DIC data (*orange*) and bottle samples (*black*) measured continuously during a ~2-hour underway tow centered around the high tide on September 20. Temperature *(red)* and salinity (*blue)* were measured with a SBE 37 CTD, and DO (*green*) is measured with an Aanderaa 4330 Oxygen Optode.

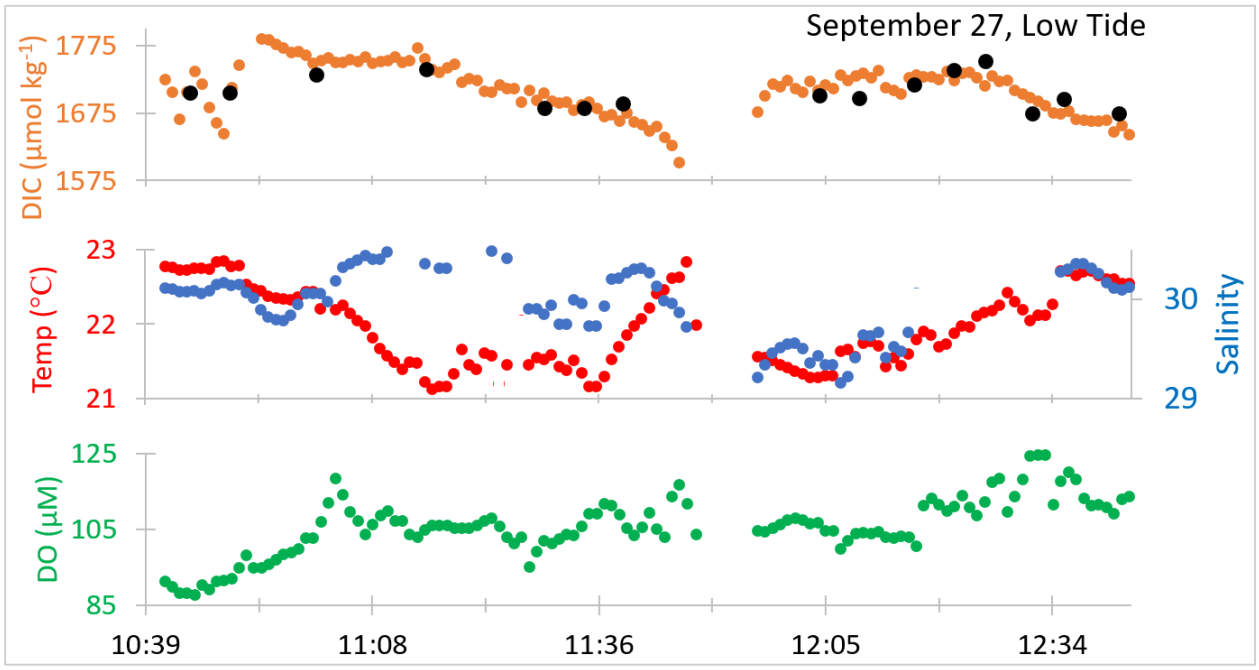

Figure 2.19. CHANOS II DIC data (*orange*) and bottle samples (*black*) measured continuously during a ~2-hour underway tow centered around the low tide on September 27. The middle panel shows temperature *(red)* and salinity (*blue)*, with DO (*green*) in the bottom panel.

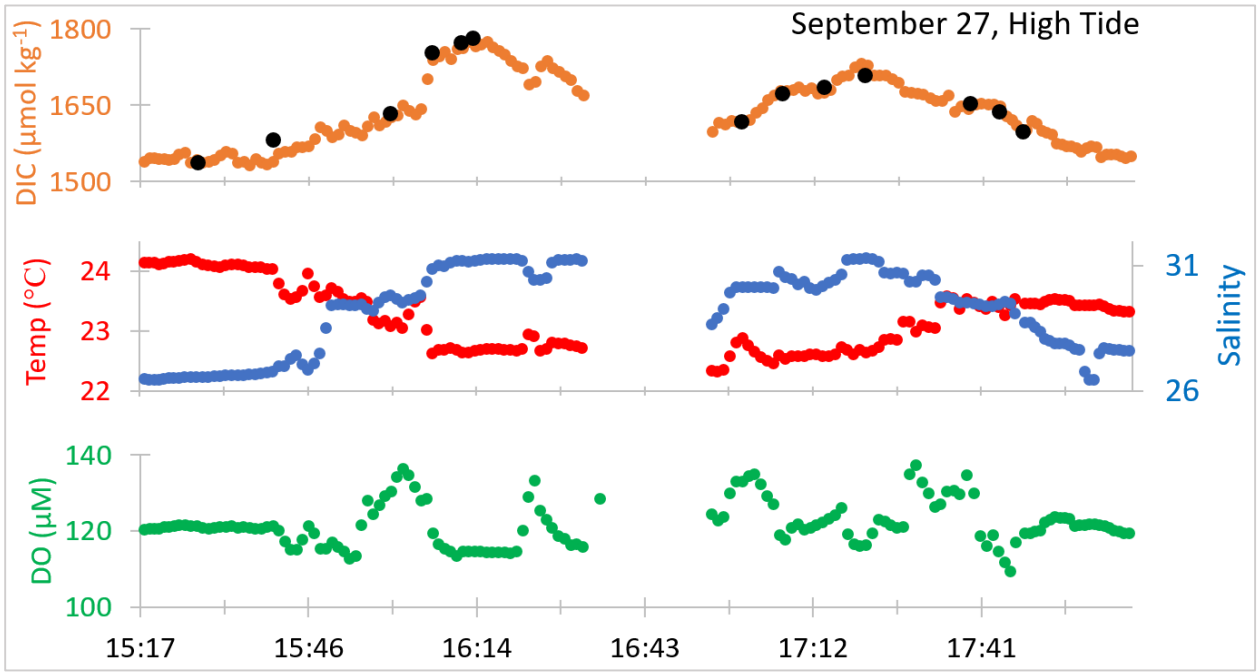

Figure 2.20. CHANOS II DIC data (*orange*) and bottle samples (*black*) measured continuously during a ~2-hour underway tow centered around the high tide on September 27. The middle panel shows temperature *(red)* and salinity (*blue)*, with DO (*green*) in the bottom panel.

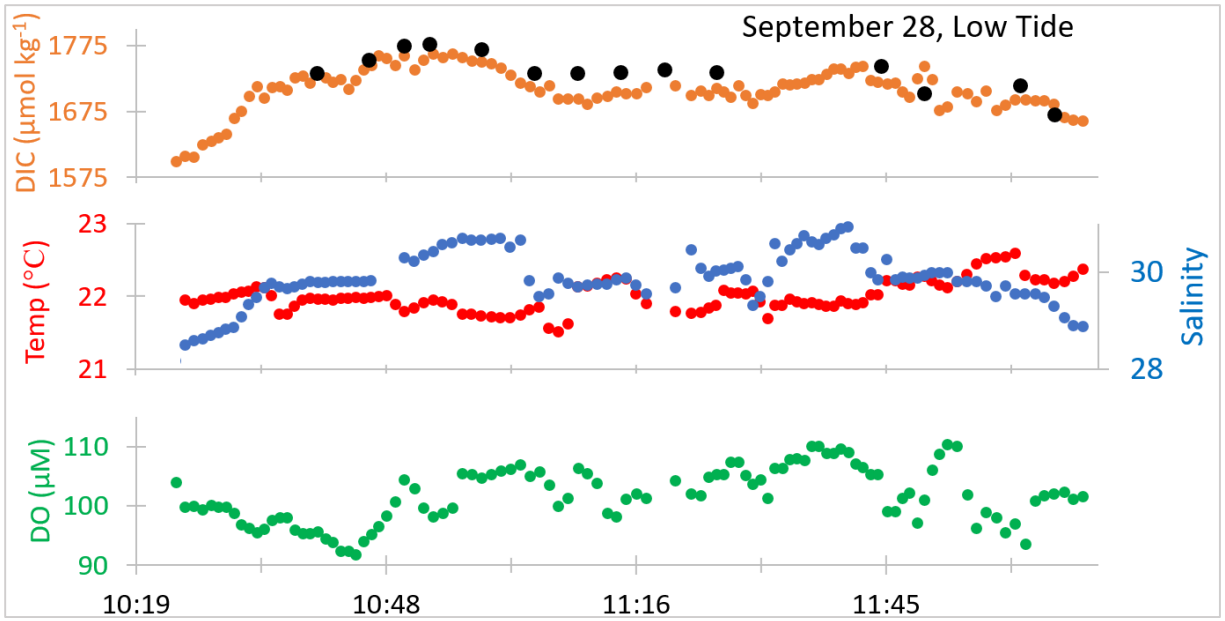

Figure 2.21. CHANOS II DIC data (*orange*) and with bottle samples (*black*) measured continuously during a ~2-hour underway tow centered around the September 28 low tide. The middle panel shows temperature *(red)* and salinity (*blue)*, with DO (*green*) in the bottom panel.

2.3.6 Comparison of bottle samples and towed sensor measurements

The residuals calculated between CHANOS II DIC data and bottle samples are shown in Figure 2.22. The 51 bottle samples selected for statistical analysis were well constrained for temperature and salinity. Some poor salinity data was removed during quality control of the first transect, likely due to turbulence and air bubbles generated over the CHANOS II package hanging from the front of the boat that impacted only the CTD; while no back-up salinity data were available for this transect, additional temperature measurements were available from the DO and CHANOS II sensors and were in good agreement. The position of the sensor package was adjusted before the next transect to ensure all sensors were fully submerged. DIC bottle samples taken during periods of questionable salinity were not used in statistical analysis of the sensor performance. The mean of these residuals was 6.76 µmol kg^{-1} with a standard deviation of 17.56 µmol kg^{-1}. This indicates that there was no significant drift and limited measurement bias throughout the deployment (Figure 2.22).

In general, there was good agreement between bottle samples and towed sensor measurements. However, the bottle samples taken during this deployment were not filtered. Because there was not enough space to operate a pump on the small boat, samples were scooped from the surface of the water and poisoned, then analyzed in the laboratory for DIC within one day of collection. These samples were taken within 1 m above the CHANOS II sensor. The discrepancy in sampling location, the potential for unfiltered particles collected

in bottle samples, potentially slow equilibration while towing quickly, noise from vibration and air bubbles from the turbulent mixing caused by movement of the boat, and the sometimes-poor resolution in salinity may account for the larger differences between sensor measurements and bottle samples compared to those of the Pocasset time series in Figure 2.10.

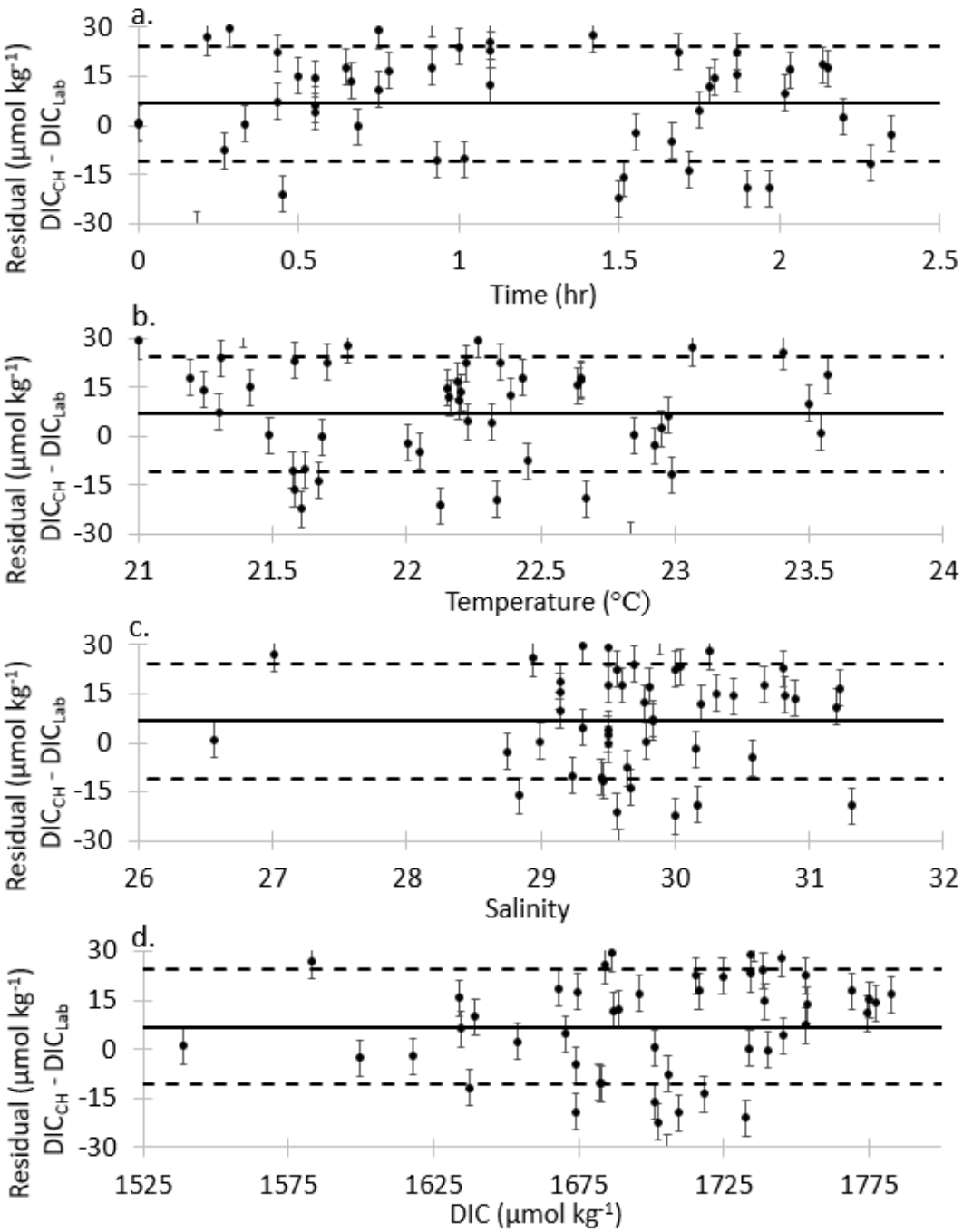

Figure 2.22. Residuals between bottle samples (DIC_{Lab}) and CHANOS II measurements (DIC_{CH}) versus sample date (*a*), temperature (*b*), salinity (*c*), and DIC (*d*). The black line represents the mean at 6.76 µmol kg^{-1}, with a standard deviation of 17.56 µmol kg^{-1} (dashed lines). Error bars represent estimated laboratory precision in CHANOS II measurements (e.g., 5.5 µmol kg^{-1}).

2.3.7 Biogeochemical signals in the Waquoit Bay tow

DIC values measured throughout the towed deployments were plotted on their GPS tracks along with bottle samples in Figure 2.23. DIC ranged between ~1550 and 1785 μmol kg^{-1} across all deployments with the highest DIC values by the mouth of the bay and lowest values in the northern portion of the bay. High tide transects (September 20 and 27) had a slightly lower range of DIC values (1550 – 1765 μmol kg^{-1}) than low tide transects (September 27 and 28) (1600 – 1785 μmol kg^{-1}). DIC was higher across a greater portion of Waquoit Bay during each low tide than during high tides. An anomalously low DIC (~1550 μmol kg^{-1}) was recorded in the southwestern portion of the bay during each high tide, but not during low tide; a high DO (~130 μM) was recorded at this location during the high tide on September 20. We note that low DIC values (~1550 μmol kg^{-1}) were also reported at tidal frequencies during a deployment of the RATS TCO_2 system in the northern portion of Waquoit Bay in 2013, potentially indicating groundwater inputs (Martin et al., 2013).

Surface maps for all 4 towed deployments for sensor measurements of temperature, salinity, dissolved oxygen, and pCO_2, as well as bottle sample TA and CO2SYS-calculated pH, pCO_2, and saturation state of aragonite (Ω_{Ar}) may be found in Figures 2.25-2.31 in the Supplementary Materials (CO2SYS version 2.1, using K_1 and K_2 constants from Leuker et al., 2000, K_{SO4} from Dickson, 1990, K_F from Perez and Fraga, 1987, and total boron from Lee et al., 2010; Pierrot et al., 2006). pCO_2 sensor measurements were in good agreement with CO2SYS-calculated pCO_2, where data was available (Figure 2.29). A comparison of CO2SYS-calculated pH and observed DO may be found in Figure 2.32 in the Supplementary Materials.

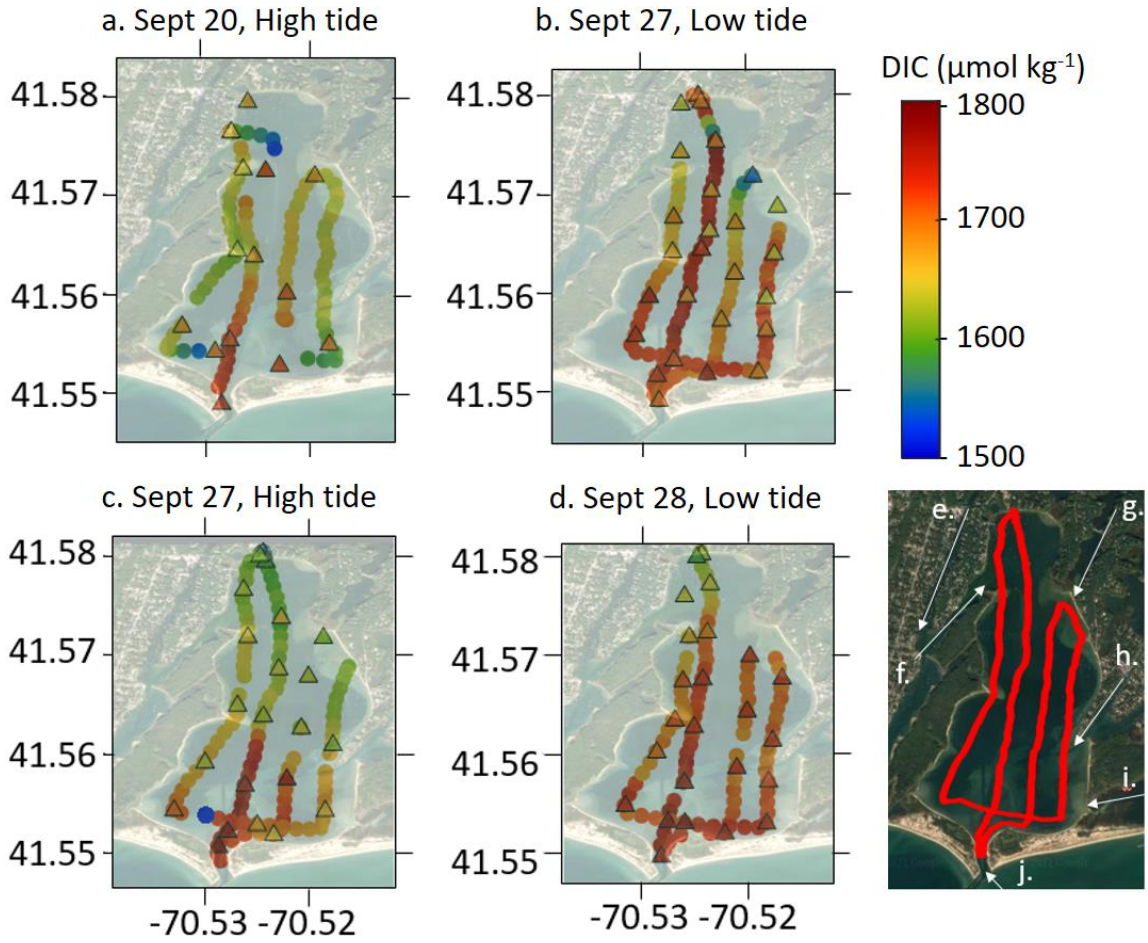

Figure 2.23. Waquoit Bay surface DIC maps generated with CHANOS II DIC data (*circles*) and bottle samples (*triangles*) across high and low tidal cycles (*a-d*), with axes representing latitude and longitude. Major river, pond, and bay inlets to Waquoit Bay include: e.) Childs River, f.) Seapit River, g.) Moonakis River, h.) Great River, i.) Sage Lot Pond, j.) mouth of the bay opening into Nantucket Sound. High salinity, high DIC water is primarily sourced from the mouth of the bay in the south. The Moonakis and Childs Rivers in the northern portion of the bay drain upstream saltwater marshes and ponds.

Figure 2.23 highlights some of the major river, pond, and bay inputs to the study site, most notably including the Moonakis and Childs River freshwater sources in the north and the high salinity mouth of the bay in the south. CHANOS DIC is plotted against salinity and dissolved oxygen for each tidal map in Figure 2.24. While the CTD data for the first high tide transect on September 20 was poor, the other three transects suggest that there are at least two endmembers mixing in the bay, one of which is strongly observed with low DIC and salinity in the northern end of the bay during the high tide on Sept 27. This follows previously observed trends in salt marshes: high DIC during low tides and low DIC during high tides suggests the export of DIC from the salt marshes through tidal water (Chu et al., 2018, Song et al., 2020). This shift in DIC between tides is particularly visible in Figure 2.24, where CHANOS II DIC measurements are plotted against salinity and DO.

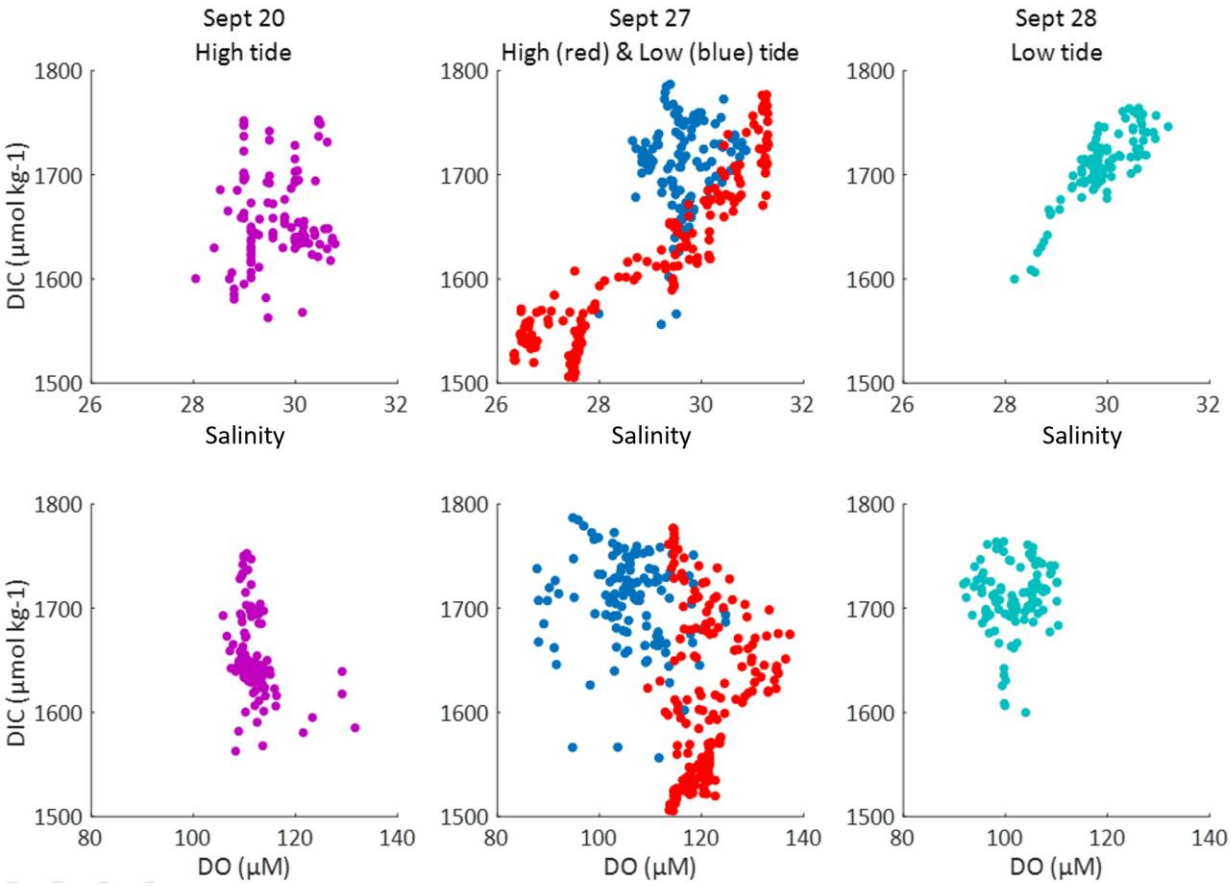

Figure 2.24. CHANOS DIC versus salinity (*top*) and dissolved oxygen (*bottom*) across high (*magenta, red*) and low (*blue, teal*) tidal cycles on September 20 *(left),* 27 *(middle),* and 28 *(right).*

2.4 Summary

Ground-truthing deployments in the Pocasset River and Waquoit Bay have shown that CHANOS II is capable of in-situ near-continuous or intermittent measurement of samples with a better than "weather quality" accuracy and precision (Newton et al., 2014). We report the observed laboratory accuracy and precision as ±2.9 and ±5.5 µmol kg^{-1}, respectively. The mean difference and standard deviation between bottle and sensor measurements was -3.8 ± 9.0 µmol kg^{-1} for time series and 6.8 ± 17.6 µmol kg^{-1} during the surface mapping deployment.

These results reflect a successful improvement from the CHANOS I sensor, retaining an acceptable measurement quality and allowing for deployments that were not achievable with the original CHANOS sensor, including mobile measurements from ROVs, small boats, and smaller stationary platforms. The CHANOS II shows a marked improvement for high frequency DIC sampling capacity over studies relying

on bottle sampling. The sensor is capable of calibrating or performing quality checks in-situ with CRMs and may be deployed from mobile platforms with low demand for power, reagents, maintenance, and waste. CHANOS II can achieve near-continuous measurements fully submerged and is designed for measurement from the surface to ~1200 m depth, as will be discussed in Chapter 3.

Due to its need for occasional maintenance (i.e, replacement of filters and reagents), the CHANOS II is well suited for unattended time-series DIC measurements on the order of weeks to 1-2 months. It is particularly useful for high-frequency mapping of DIC from towed vehicles and ROVs over fine spatial scales. Its broad adaptability for different missions, platforms, and deployment lengths is a major advantage of this system for use in dynamic environments such as the coastal ocean.

With minor modifications, specifically the removal of the acidification step, the CHANOS II can be readily adapted for pCO_2 measurements instead of DIC (Wang et al., 2003; 2007). The current system may also be modified to make continuous pH measurements (Wang et al., 2015). A second, simultaneous channel is in development to allow for this sensor to fully resolve the seawater inorganic carbon system via simultaneous measurement of DIC-pCO_2 or DIC-pH. A driving principle of this sensor design was to use inexpensive, off the shelf components wherever possible to reduce the cost of the unit itself and to allow for easy replacement of spare parts in the field. The fluidic connections between pressure-compensated pump housings and optical units are modular and modifiable, such that this sensor could be adapted for spectrophotometric in-situ measurement of other seawater chemical species, including nutrients and dissolved metal species.

2.5 Acknowledgements

The development of CHANOS II was supported by the National Science Foundation (1233654), NSF Ocean Technology and Interdisciplinary Coordination (1841092), MIT Seagrant (2017-R/RCM-51), and WHOI Ocean Ventures Funds and Grassle fellowship funds. We thank WHOI engineers Fritz Sonnichsen, Steve Lerner, Glenn MacDonald, and research assistant Jonathan Pfeifer. For assistance in local deployments, we thank Kate Morkeski, Eyal Wurgaft, and Dylan Titmuss; Dan Ward and Matty Paquette for access to the Scallop Bay Marina docks; and Vitalii Sheremet for his work on the *Trifly* deployments.

2.6 References

Amornthammarong, N., Ortner, P.B., Hendee, J., and Woosley, R., 2014. A simplified coulometric method for multi-sample measurements of total dissolved inorganic carbon concentration in marine waters. Analyst, v. 139, pp. 5263-5270.

Bell, R.J., Short, R.T., and Byrne, R.H., 2011. In-situ determination of total dissolved inorganic carbon by underwater membrane introduction mass spectrometry. Limnology and Oceanography: Methods, v. 9, pp. 164-175.

Briggs, E.M., Heinen De Carlo, H., Sabine, C.L., Howins, N., and Martz, T.R., 2020. Autonomous, ion sensitive field effect transistor-based total alkalinity and pH measurements on a barrier reef of Kāne'ohe Bay. AS Earth and Space Chemistry, v. 4, pp. 355-362.

Briggs, E.M., Sandoval, S., Erten, A., Takeshita, Y., Kummel, A.C., and Martz, T.R., 2017. Solid state sensor for simultaneous measurement of total alkalinity and pH of seawater. ACD Sensors, v. 2, pp. 1302-1309.

Bushinsky, S.M., Takeshita, Y., and Williams, N.L., 2019. Observing changes in ocean carbonate chemistry: Our autonomous future. Current Climate Change Reports, v. 5, pp. 207-220.

Byrne, R.H., Liu, X.W., Kaltenbacher, E.A., and Sell, K., 2002. Spectrophotometric measurement of total inorganic carbon in aqueous solutions using a liquid core waveguide. Analytica Chimica Acta, v. 451, pp. 221-229.

Chua, E.J., Savidge, W., Short, R.T., Cardenas-Valencia, A.M., and Fulweiler, R.W., 2016. A review of the emerging field of underwater mass spectrometry. Marine Science, DOI: 10.3389/fmars.2016.00209

Chu, S.N., Wang, Z.A., Gonneea, M.E., Kroeger, K.D., and Ganji, N.K., 2018. Deciphering the dynamics of inorganic carbon export from intertidal salt marshes using high-frequency measurements. Marine Chemistry, v. 206, pp. 7-18.

Clarke, J.S., Achterberg, E.P., Connelly, D.P., Schuster, U., and Mowlem, M., 2017. Developments in marine pCO_2 measurement technology; towards sustained *in situ* observations. Trends in Analytical Chemistry, v. 88, pp. 53-61.

Clayton, T.D., and Byrne, R.H., 1993. Spectrophotometric seawater pH measurement: Total hydrogen ion concentration scale calibration of m-cresol purple and at sea results. Deep-Sea Research, v. 40, pp. 2115-2129.

Colson, B., and Michel, A., 2022. C-SPEC: A deep sea laser spectrometer for measuring the carbon system (DIC and pCO_2). Poster, Ocean Sciences Meeting, virtual, February 24-March 4, 2022.

DeGrandpre, M.D., Spaulding, R.S., Newton, J.O., Jaqueth, E.J., Hamblock, S.E., Umansky, A.A., and Harris, K.E., 2014. Considerations for the measurement of spectrophotometric pH for ocean acidification and other studies. Limnology and Oceanography: Methods, v. 12, pp. 830-839.

Dickson, A.G., and Riley, J., 1978. The effect of analytical error on the evaluation of the components of the aquatic carbon-dioxide system. Marine Chemistry, v. 6, pp. 77-85.

Dickson, A.G., Sabine, C.L., and Christian, J.R., 2007. Guide to best practices for ocean CO_2 measurements. North Pacific Marine Science Organization.

Fassbender, A.J., Sabine, C.L., Lawrence-Slavas, N., De Carlo, E.H., Meinig, C., and Jones, S.M., 2015. Robust sensor for extended autonomous measurements of surface ocean dissolved inorganic carbon. Environmental Science and Technology, v. 49, pp. 3628-3635.

Huang, K., Cassar, N., Jönsson, B., Cai, W.J., and Bender, M.L., 2015. An ultrahigh precision, high-frequency dissolved inorganic carbon analyzer based on dual isotope dilution and cavity ring-down spectroscopy. Environmental Science & Technology, v. 49.

Hunt, C., 2021. Alkalinity and buffering in estuarine, coastal and shelf waters. PhD thesis, University of New Hampshire.

Liu, X., Byrne, R.H., Adornato, L., Yates ,K.K., Kaltenbacher, E., Ding, X., and Yang, B., 2013. In situ spectrophotometric measurement of dissolved inorganic carbon in seawater. Environmental Science & Technology, v. 27, pp. 11106-11114.

Martz, T.R., Daly, K.L., Byrne, R.H., Stillman, J.H., and Turk, D., 2015. Technology for ocean acidification research: Needs and availability. Oceanography, v. 28, pp. 40-47.

Martin, W.R., Sayles, F.L., McCorkle, D.C., and Weidman, C., 2013. Continuous, autonomous measurement of the CO_2 system in Waquoit Bay, MA. AGU Fall Meeting Abstracts, OS53D-07.

Millero, F.J., 2007. The Marine Inorganic Carbon Cycle. Chemical Reviews, v. 107, pp. 308-341.

Newton, J.A., Feely, R.A., Jewett, E.B., Williamson, P., and Mathis, J., 2014. Global ocean acidification observing network: Requirements and governance plan. GOA-ON, 57.

Nightingale, A.M., Beaton, A.D., Mowlem, M.C., 2015. Trends in microfluidic systems for in situ chemical analysis of natural waters. Sensors and Actuators, B: Chemical. v.221, pp. 1398-1405.

Pierrot, D., Lewis, E., and Wallace, D.W.R., 2006. MS Excel program developed for CO2 system calculations. ORNL/CDIAC-105a. Carbon Dioxide Information Analysis Center, Oak Ridge National Laboratory, U.S. Department of Energy, Oak Ridge, Tennessee.

Sayles, F.L., and Eck, C., 2009. An autonomous instrument for time series analysis of TCO_2 from oceanographic moorings. Deep Sea Research, Part I, v. 56, pp. 1590-1603.

Schuster, U., Hannides, A., Mintrop, L., and Körtzinger, A., 2009. Sensors and instruments for oceanic dissolved carbon measurements. Ocean Science, v. 5, pp. 547-558.

Shangguan, Q., Lai, C., Beatty, C.M., Young, F.L., Spaulding, R.S., and DeGrandpre, M.D., 2021. Autonomous in situ measurements of freshwater alkalinity. Limnology and Oceanography: Methods, v. 19, pp.51-66.

Song, S., Wang, Z.A., Gonneea, M.E., Jroeger, K.D., Chu, S.N., Li, D., and Liang, H., 2020. An important biogeochemical link between organic and inorganic carbon cycling: Effects of organic alkalinity on carbonate chemistry in coastal waters influenced by intertidal salt marshes. Geochimica et Cosmochimica Acta, v. 275, pp. 123-139.

Tue-Ngeun, O., Sandford, R.C., Jakmunee, J., Grudpan, K., McKelvie, I.D., Worsfold, P.J., 2005. Determination of dissolved inorganic carbon (DIC) and dissolved organic carbon (DOC) in freshwaters by sequential injection spectrophotometry with on-line UV photo-oxidation. Analytica Chimica Acta, v. 554, pp. 17-24.

Wallace, R.B., Baumann, H., Grear, J.S., Aller, R.C., and Gobler, C.J., 2014. Coastal ocean acidification: The other eutrophication problem. Estuarine, Coastal and Shelf Science, v. 148, pp. 1-13.

Wang, Z.A., Cai, W.J., Wang, Y., and Upchurch, B.L., 2003. A long pathlength liquid-core waveguide sensor for real-time pCO_2 measurements at sea. Marine Chemistry, v. 84, pp. 73-84.

Wang, Z.A., Chu, S.N., and Hoering, K.A., 2013. High-frequency spectrophotometric measurements of total dissolved inorganic carbon in seawater. Environmental Science & Technology, v. 47, pp. 7840-7847.

Wang, Z.A., Lawson, G.L., Pilskaln, C.H., and Maas, A.E., 2017. Seasonal controls of aragonite saturation states in the Gulf of Maine. Journal of Geophysical Research: Oceans. v. 122, pp. 372-389.

Wang, Z.H.A., Liu, X.W., Byrne, R.H., Wanninkhof, R., Bernstein, R.E., Kaltenbacher, E.A., and Patten, J., 2007. Simultaneous spectrophotometric flow-through measurements of pH, carbon dioxide, fugacity, and total inorganic carbon in seawater. Analytica Chimica Acta, v. 596, pp. 23-36.

Wang, Z.A., Sonnichsen, F.N., Bradley, A.M., Hoering, K.A., Lanagan, T.M., Chu, S.N., Hammar, T.R., and Camilli, R., 2015. In-situ sensor technology for simultaneous spectrophotometric measurements of seawater total dissolved inorganic carbon and pH. Environmental Science & Technology, v. 49, pp. 4441-4449.

2.7 Supplementary materials

The following figures show the spatial distribution of sensor measurements and bottle samples taken during 4 small boat towing deployments across Waquoit Bay on September 20, 27, and 28.

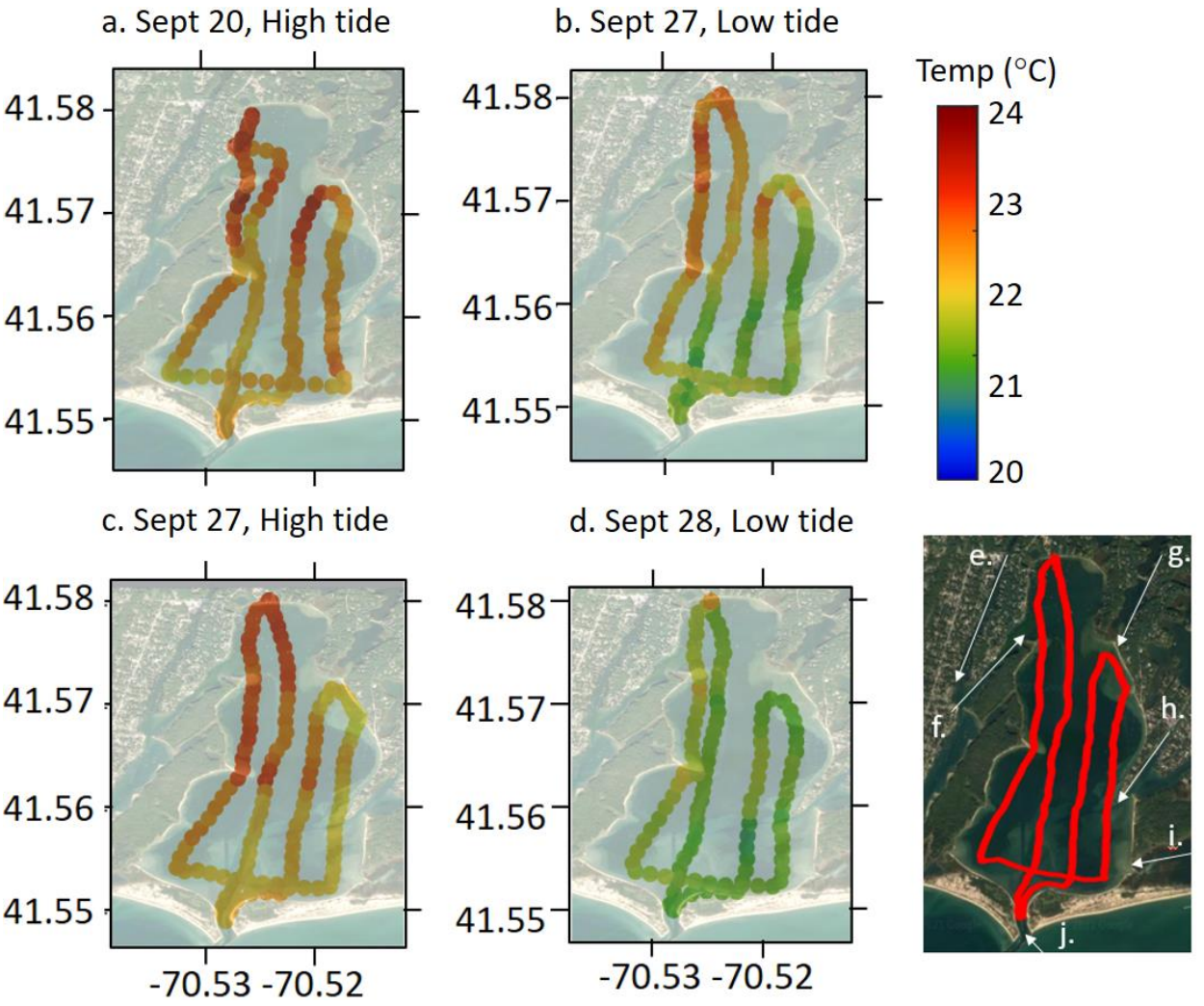

Figure S2.25. Waquoit Bay surface temperature maps generated via CTD across high and low tidal cycles (*a-d*). Major river, pond, and bay inlets to Waquoit Bay include: e.) Childs River, f.) Seapit River, g.) Moonakis River, h.) Great River, i.) Sage Lot Pond, j.) mouth of the bay opening into Nantucket Sound. Low tide tows were conducted in the morning and high tide tows in the afternoon, resulting in generally lower temperatures during low tide tows.

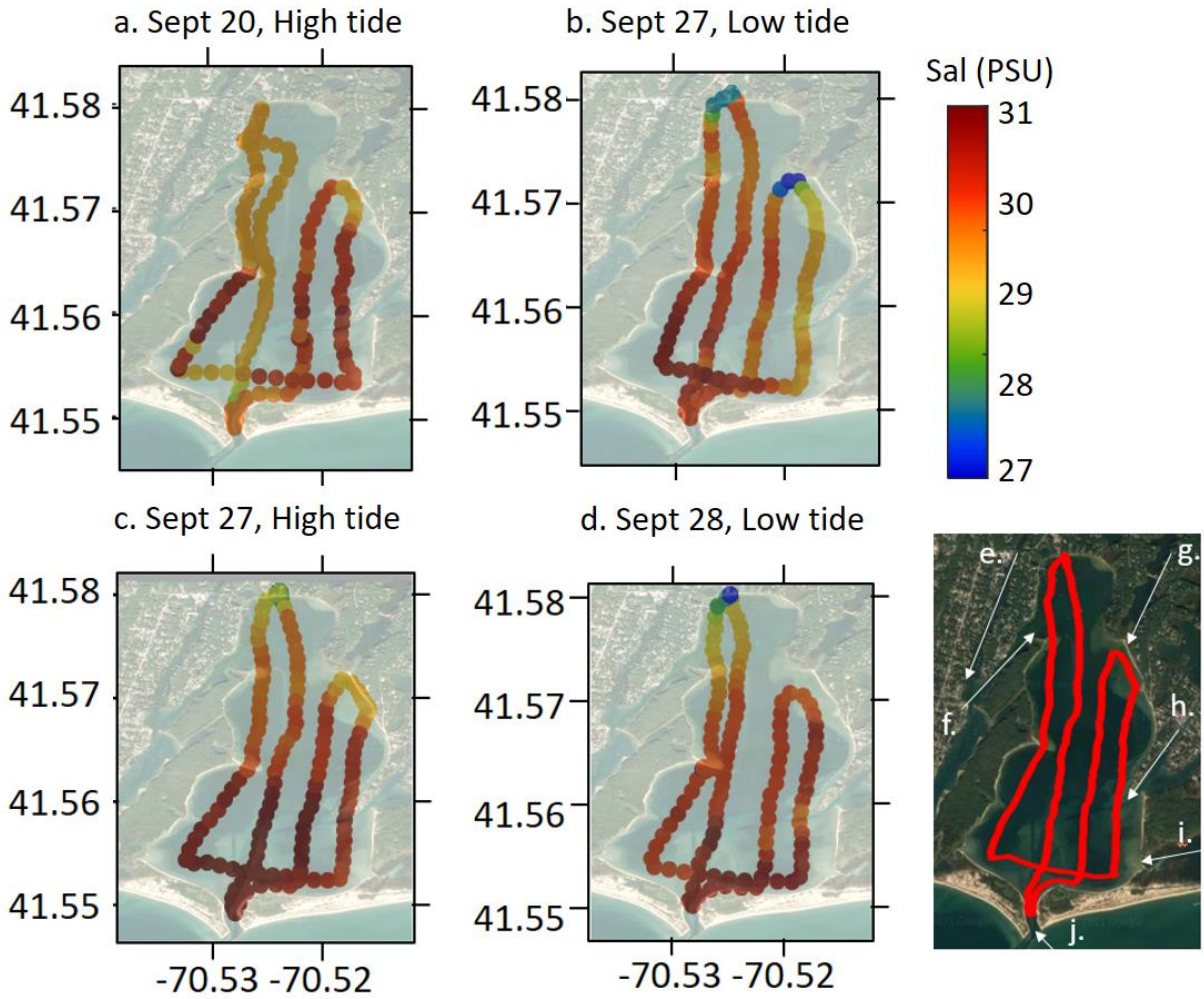

Figure S2.26. Waquoit Bay surface salinity maps generated via CTD across high and low tidal cycles (*a-d*). Salinity measurements during most of the September 20 tow (*a*) were poor due to the CTD's placement in the sensor package. Salinities are lower in the northern portion of the bay during low tides due to fresher water inputs from the rivers and marshes in the north. Major river, pond, and bay inlets to Waquoit Bay include: e.) Childs River, f.) Seapit River, g.) Moonakis River, h.) Great River, i.) Sage Lot Pond, j.) mouth of the bay opening into Nantucket Sound. Low tide tows were conducted in the morning and high tide tows in the afternoon, resulting in generally lower temperatures during low tide tows.

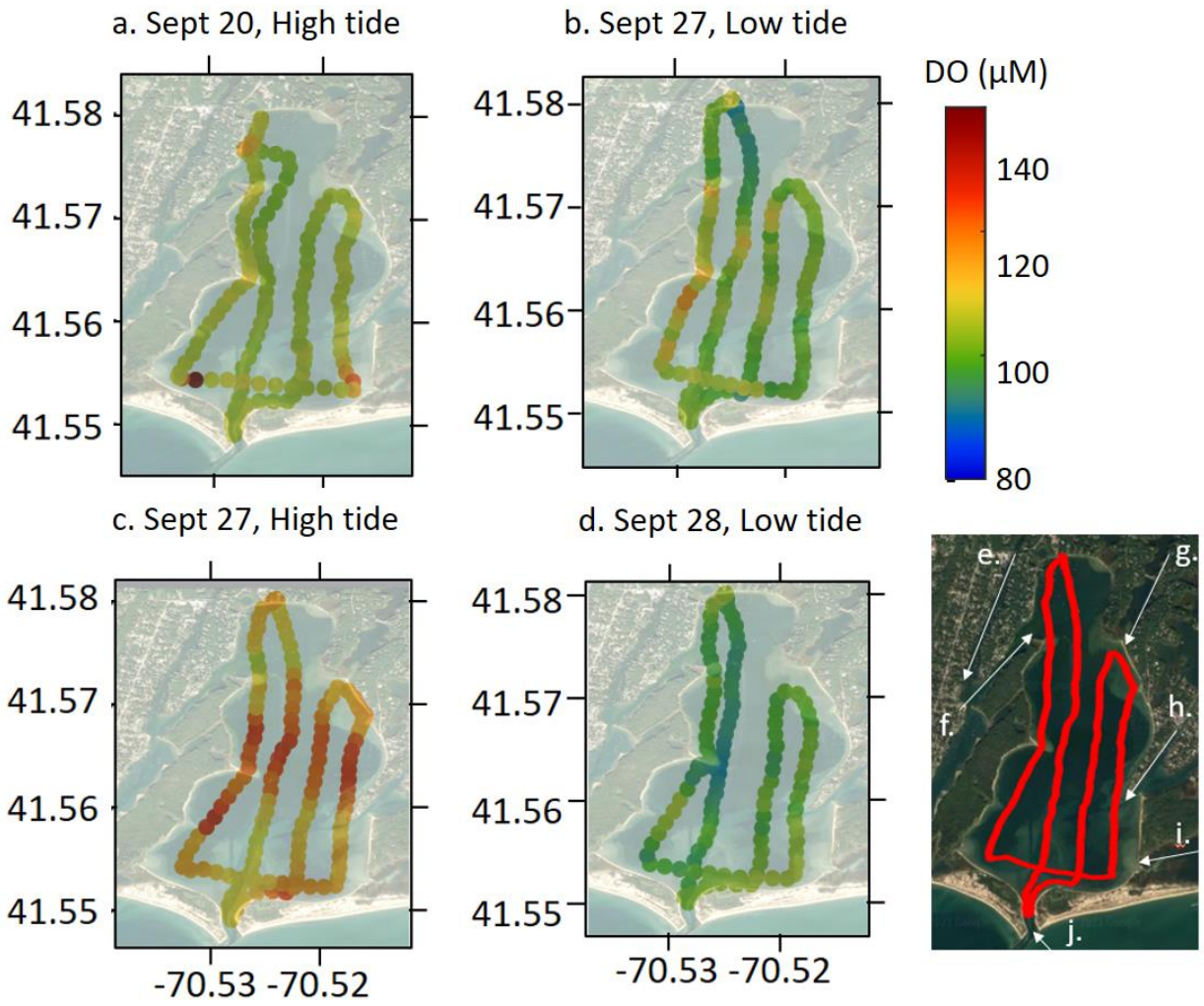

Figure S2.27. Waquoit Bay surface dissolved oxygen maps generated with an Aanderaa 4330 Oxygen optode attached to the CHANOS II during high and low tidal cycles (*a-d*). DO was generally lower across Waquoit Bay during low tides, despite the lower temperatures during these tows. Major river, pond, and bay inlets to Waquoit Bay include: e.) Childs River, f.) Seapit River, g.) Moonakis River, h.) Great River, i.) Sage Lot Pond, j.) mouth of the bay opening into Nantucket Sound. Low tide tows were conducted in the morning and high tide tows in the afternoon, resulting in generally lower temperatures during low tide tows.

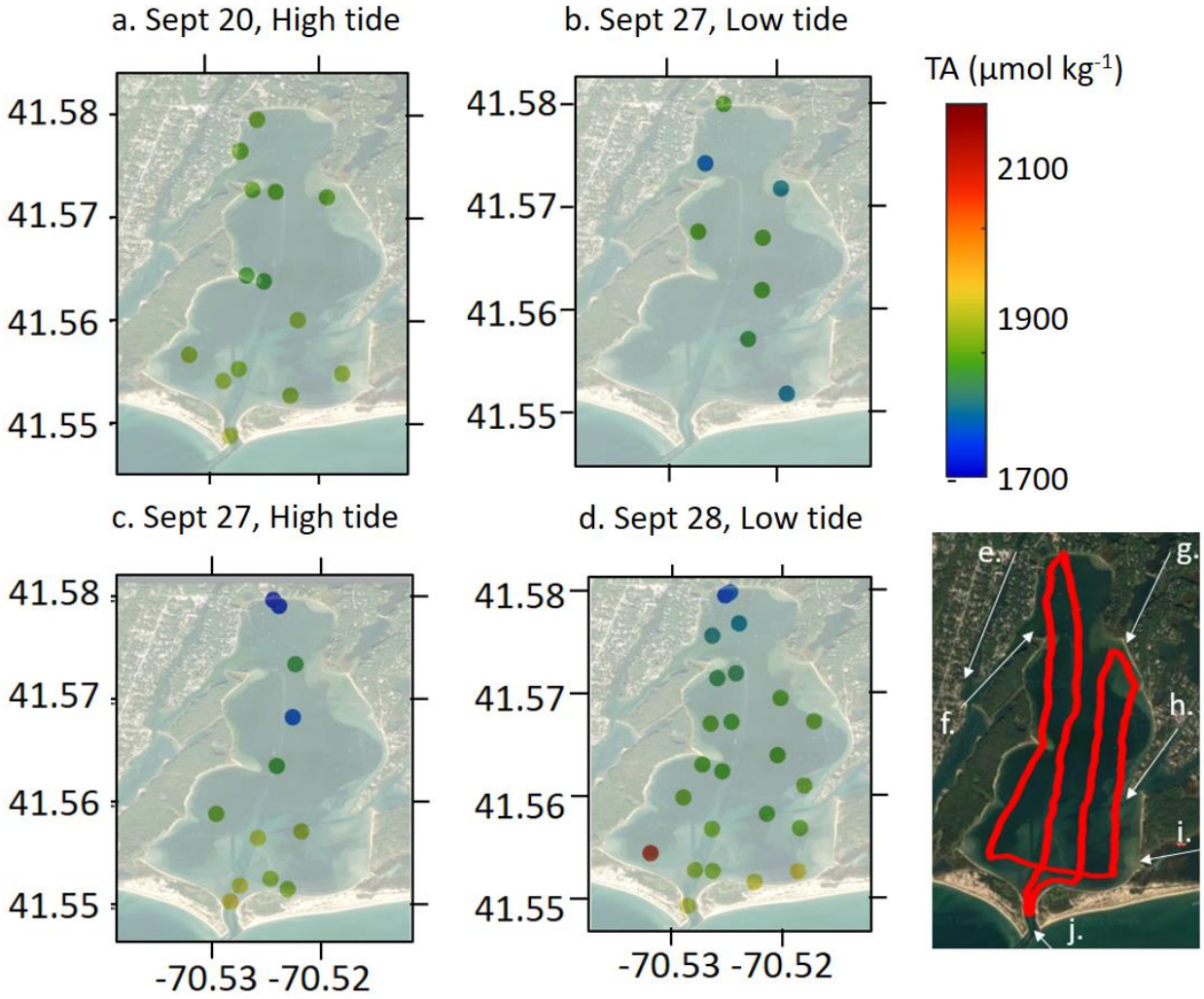

Figure S2.28. Waquoit Bay TA maps across high and low tidal cycles generated via bottle samples analyzed in the laboratory (*a-d*). TA was generally higher toward the mouth of Waquoit Bay. Major river, pond, and bay inlets to Waquoit Bay include: e.) Childs River, f.) Seapit River, g.) Moonakis River, h.) Great River, i.) Sage Lot Pond, j.) mouth of the bay opening into Nantucket Sound. Low tide tows were conducted in the morning and high tide tows in the afternoon, resulting in generally lower temperatures during low tide tows.

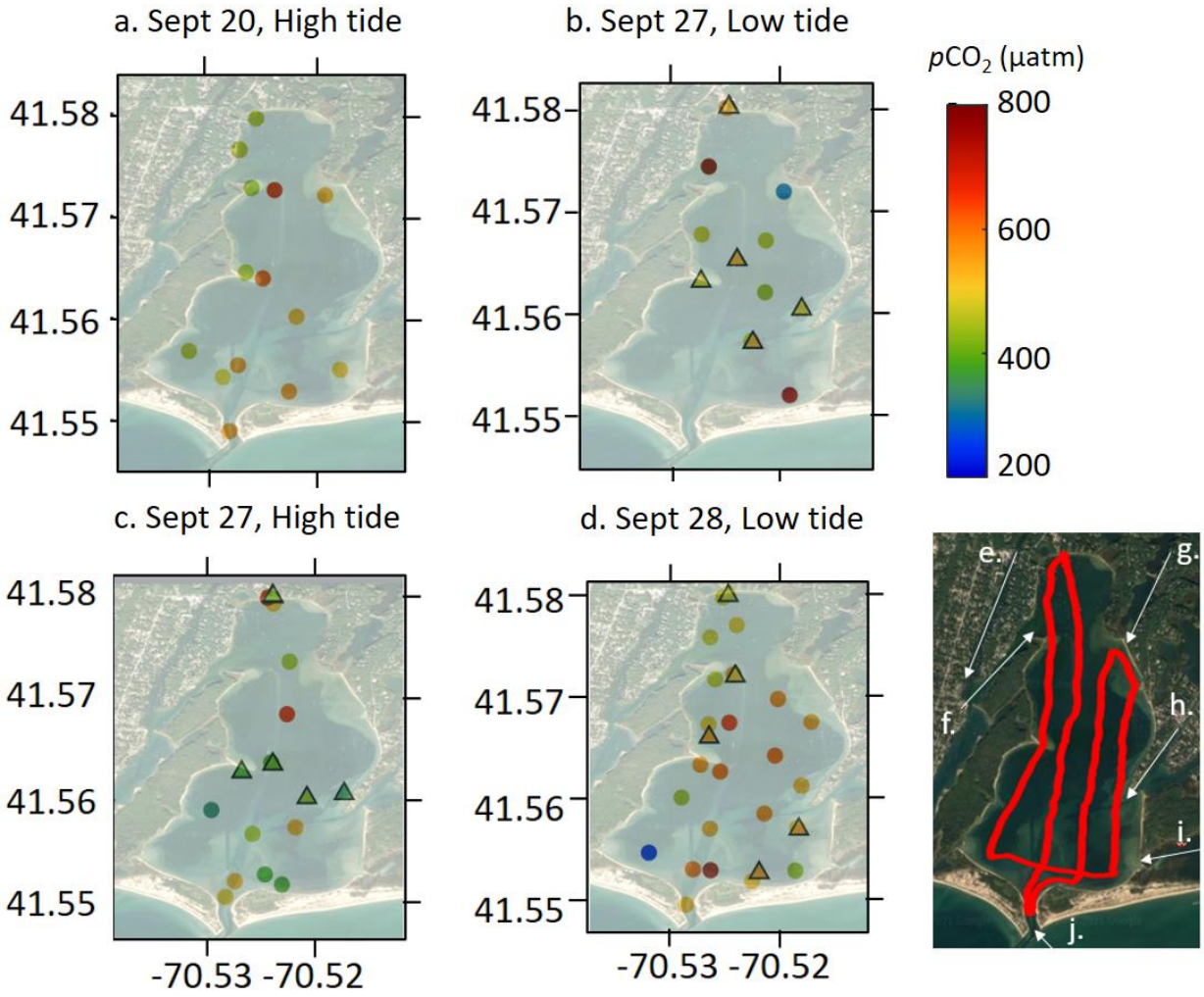

Figure S2.29. Waquoit Bay surface pCO_2 maps across high and low tidal cycles generated via pro-Oceanus sensor measurements (*triangles*) and CO2Sys calculations using bottle sample DIC, TA, and CTD values (*circles*) (*a-d*). pCO_2 measurements were variable across the bay and were generally higher during low tide. Major river, pond, and bay inlets to Waquoit Bay include: e.) Childs River, f.) Seapit River, g.) Moonakis River, h.) Great River, i.) Sage Lot Pond, j.) mouth of the bay opening into Nantucket Sound. Low tide tows were conducted in the morning and high tide tows in the afternoon, resulting in generally lower temperatures during low tide tows.

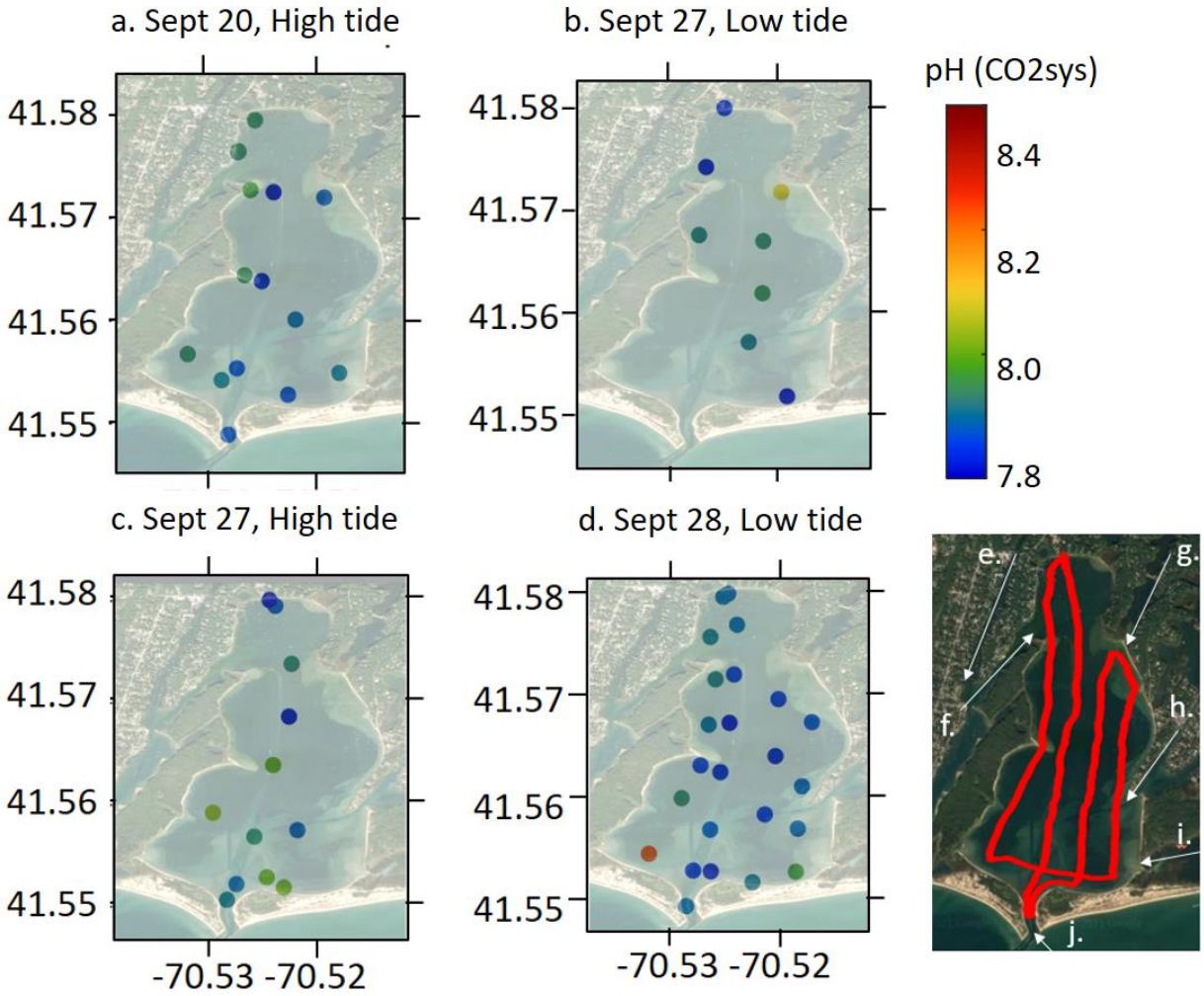

Figure S2.30. Waquoit Bay surface pH (total scale) maps across high and low tidal cycles generated CO2Sys calculations using bottle sample DIC, TA, and CTD values (*a-d*). Major river, pond, and bay inlets to Waquoit Bay include: e.) Childs River, f.) Seapit River, g.) Moonakis River, h.) Great River, i.) Sage Lot Pond, j.) mouth of the bay opening into Nantucket Sound. Low tide tows were conducted in the morning and high tide tows in the afternoon, resulting in generally lower temperatures during low tide tows.

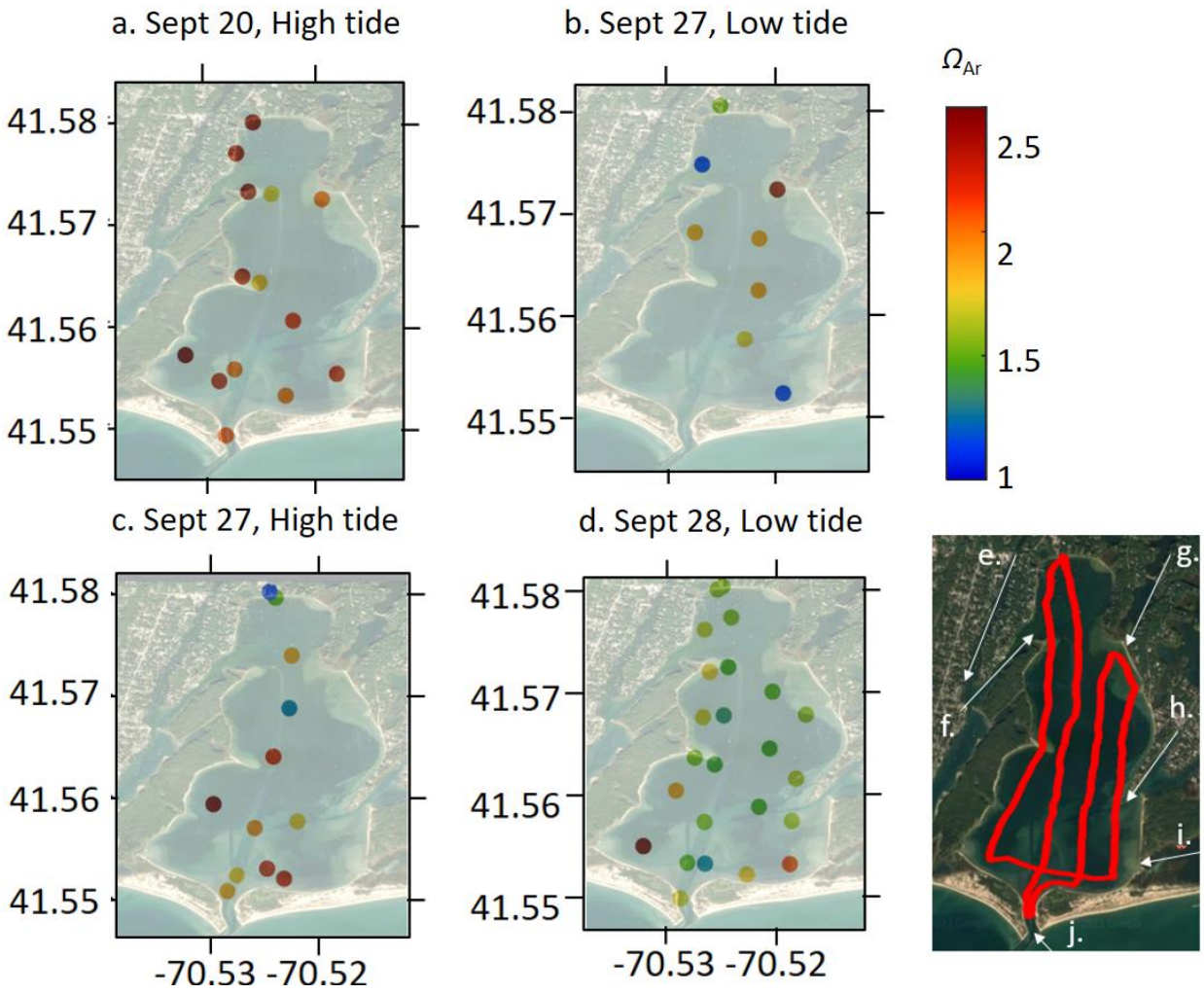

Figure S2.31. Waquoit Bay surface Ω_{Ar} maps across high and low tidal cycles generated via CO2Sys calculations using bottle sample DIC, TA, and CTD values (*circles*) (*a-d*). Ω_{Ar} measurements were variable across the bay and were generally higher during high tide. Major river, pond, and bay inlets to Waquoit Bay include: e.) Childs River, f.) Seapit River, g.) Moonakis River, h.) Great River, i.) Sage Lot Pond, j.) mouth of the bay opening into Nantucket Sound. Low tide tows were conducted in the morning and high tide tows in the afternoon, resulting in generally lower temperatures during low tide tows.

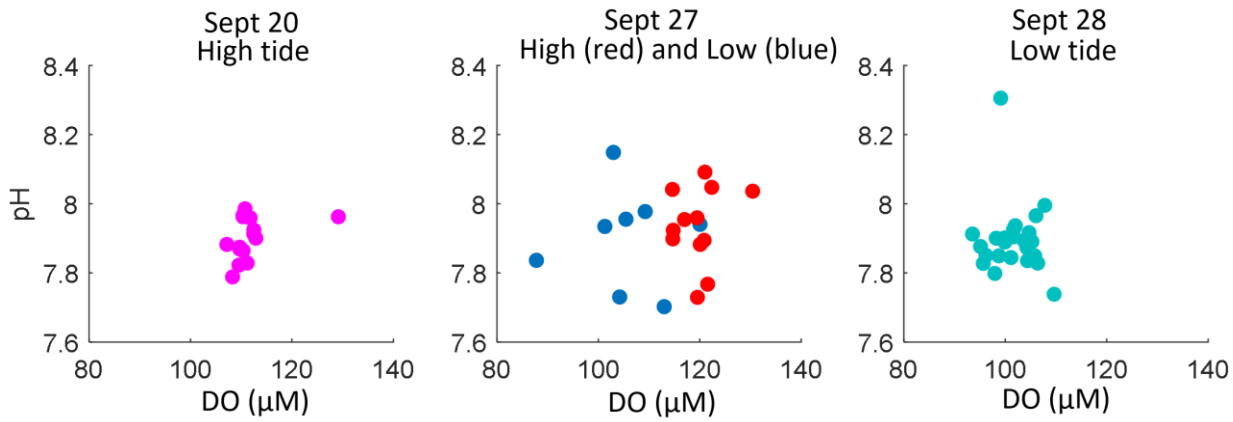

Figure S2.32. CO2SYS-calculated pH versus observed dissolved oxygen across high (*magenta*, *red*) and low (*blue*, *teal*) tidal cycles on September 20 *(left)*, 27 *(middle)*, and 28 *(right)*.

Chapter 3

Exploration of fine-scale spatial biogeochemistry over deep coral reefs on the West Florida slope using the CHANOS II dissolved inorganic carbon sensor on ROV *Global Explorer*

Abstract

Deep-sea corals create complex habitats that support rich reef ecosystems and the communities that depend on them. Understanding spatial variations in physical conditions and biogeochemistry, particularly inorganic carbon chemistry, may provide insight into both the distribution of deep coral ecosystems and how they may be affected in warming and acidifying oceans. Seafloor inorganic carbon chemistry data has been limited by the scarcity of seafloor bottle samples and precise *in-situ* sensors for deep deployment from mobile platforms. In 2019, the ROV *Global Explorer* conducted visual surveys over four deep scleractinian (*Lophelia pertusa, Desmophyllum pertusum*) reefs and rocky slope habitats on the West Florida slope, Gulf of Mexico. The ROV was equipped with the dissolved inorganic carbon (DIC) sensor CHANnelized Optical System (CHANOS) II. We collected high resolution (<100 m) DIC data across four deep coral reef habitats on the West Florida slope, Gulf of Mexico. The sensor data was in close agreement with the few bottle samples collected during the dives (n = 5, average $DIC_{bottles}$= 2190.9 ± 1.0 µmol kg^{-1}, $\Delta DIC_{sensor\text{-}bottles}$ = 1.2 ± 12.2 µmol kg^{-1} DIC), but also recorded a wide range of ~1900 – 2900 µmol kg^{-1} DIC across the seafloor and coral habitats that has not previously been observed through bottle samples. Multiple linear regression models trained on historical water column CTD bottle samples and CHANOS II seafloor DIC provide a conservative estimate of seafloor TA, pH, and Ω_{Ar}, which all vary significantly at the seafloor. Ω_{Ar} fluctuates between conditions of under and oversaturation, which may be important to the ability of deep corals to flourish under ocean acidification, warming, and other changing oceans. This work highlights the need to investigate deep sea biogeochemistry at high spatial scales in order to understand the range of environmental variation encountered by benthic communities, and to provide baseline measurements for future studies.

Chapter 3

3.1 Introduction

Deep sea coral reefs, typically dominated by branching scleractinians, octocorals, and black corals, are found on bathymetric highs with elevated currents. These habitats support highly dynamic ecosystems that may be impacted by ocean acidification (OA), warming, deoxygenation, and circulation changes. OA caused by the uptake of anthropogenic CO_2 by the oceans, may have detrimental effects on coral reefs over time due to decreasing seawater pH and aragonite saturation state (Ω_{Ar}) that results in a reduction of biological calcium carbonate production by corals (Gómez et al., 2018). In turn, these effects may impact the diverse fisheries and ecosystems that rely on the reef structures (Andersson et al., 2009; Bates et al., 2010; Carpenter et al., 2008; Hoegh-Guldberg et al., 2007; Pandolfi et al., 2011; Turley, Roberts, and Guinotte, 2007). Deep sea corals living in the 400-800m depth range are typically situated in oxygen minimum zones of high CO_2 and low pH where aragonite saturation may be near corrosive. Rising temperatures and CO_2 concentrations may increase physiological stress on coral communities, resulting in reduced suitable habitats for the corals and the fish and benthic communities they support (Roberts et al., 2009).

Existing environmental variability may allow for some resilience to physical and chemical changes at deep sea coral communities. These corals already live in hydrodynamically active areas that may experience rapid shifts in currents, temperature, and inorganic carbon chemistry due to tides, meandering boundary currents, and mesoscale eddies (Roberts et al., 2009; Ross et al., 2015). In particular, on the West Florida Slope, Loop Current cyclonic eddy interactions with currents and bottom bathymetry may induce strong upwelling over rapid timescales, bringing cold, CO_2 rich waters to the mid/upward slope where deep sea coral habitats are found (Jiang et al., 2020). While the biological responses of coral communities in general are heavily impacted by variability in environmental conditions, some studies have suggested that exposure to variable carbonate chemistry conditions, coupled with genetic variations, may allow for relative resilience to chemical changes resulting from OA (Brooke et al., 2013; Kurman et al., 2017; Lunden et al., 2013; 2014). Due to site inaccessibility, studies on deep coral responses to OA are significantly limited relative to shallow reef research. Deep coral studies often focus on one of the most widespread habitat-forming species, *Lophelia pertusa*, which primarily grows in the Atlantic in thickets or bioherms ("mounds"). This species provides habitat for many other marine organisms through its slow growth of branching aragonite skeletons. Changes to live and dead *L. pertusa* mounds driven by OA are likely to be more impactful on the benthic community than other types of deep sea corals, including black corals and

gorgonians, that may be more patchily distributed and build less long-lasting structures. Incubations of *L. pertusa* in OA studies with perturbed pH or pCO_2 have produced mixed results, with short-term exposures (weeks – months) resulting in reduced growth and respiration, with acclimatization in the long term (year). For example, Maier et al. (2009) observed reduced calcification from young *L. pertusa* polyps under reduced pH conditions, while retaining a net positive calcification even at undersaturated aragonite states. Hennige et al., (2014; 2015), did not observe a change in calcification rates between ambient and increased CO_2 conditions on *L. pertusa* samples, but did observe a decrease in the strength of exposed reef framework. Thresher et al. (2011) found that carbonate undersaturation had little effect on the depth distribution, growth, or skeletal composition of stony corals on Tasmanian seamounts, suggesting that changes in the carbonate saturation horizon as a result of ocean acidification are unlikely to have a large impact on live calcifiers in their study area. While these corals may physiologically acclimatize to changing carbonate chemistry conditions, much is still unknown about their outlook on timescales greater than the ~1-2 years of available incubation studies, or under conditions of multiple stressors introduced by OA, including thermal stress and food availability. Exploration and characterization of deep coral sites is therefore necessary to establish a baseline of biogeochemical conditions over current deep sea corals, and to allow for investigation of future changes in biogeochemistry and their impacts on biodiversity of deep reefs over time.

Fine-scale biogeochemical variability has been observed in some deep coral communities. Mesoscale eddies and internal tides responsible for vertical water mass movements in the Florida Straits resulted in rapid temperature changes (>4 °C) over short distances (<1 km) in regions supporting deep coral communities (Leichter et al., 2007; Gula et a., 2015; Jiang et al., 2020). Diurnal internal waves causing vertical water mass displacement may result in significant temperature and salinity changes over deep reefs, as observed over the *L. pertusa* community at Viosca Knoll (Davies et al., 2010). Internal tides impact the Rockall Trough in the northeast Atlantic, where a dissolved inorganic carbon (DIC) range of 58 μmol kg^{-1} was observed across deep coral mounds using CTD Rosettes cast to 2 m above the corals. Findlay et al., (2014) reported that the carbonate mounds supporting corals at this site may provide an alkalinity source to the water column. Georgian et al. (2016) also found slightly elevated DIC (up to 35 μmol kg^{-1} relative to non-coral sites) and Total Alkalinity (TA, up to 44 μmol kg^{-1} relative to non-coral sites) above some large deep coral mounds in the northern Gulf of Mexico, suggesting that the dissolution and remineralization of dead coral skeletons in the interior of mounds may result in upwelling of high alkalinity seawater over some coral structures (Lunden et al., 2013; Georgian et al., 2016).

However, the relative inaccessibility of deep coral sites and the scarcity of high-resolution environmental sensor and sampling capabilities has limited our analysis and understanding of these environmental variations and their impacts on deep corals and benthic ecosystems. Most deep water inorganic carbon data comes from CTD rosette casts. To protect the rosette from colliding with the seafloor and/or benthic communities, these casts typically stop at 2 m off bottom at best, and more frequently terminate 10 m or more off bottom. ROVs and other submersibles may more closely approach the seafloor, but seawater sampling is frequently limited to 1 – 6 Niskin bottles per dive on such vehicles. Seafloor ROV transects often travel at ~0.5 kts to produce high quality video and may remain on the seafloor for hours to days, such that seafloor inorganic carbon samples may be separated by kilometers. Since the amount of seafloor data at the sediment-water column interface is so limited, we must turn to high-resolution chemical sensors, including the CHANOS II as described in Chapter 2, to address fine-scale spatial variability in the inorganic carbon system.

The objectives of this study are to explore and characterize the fine-scale variability in inorganic carbon chemistry across 4 deep coral habitats in the West Florida slope. Key questions in this study include: 1) What are the short-term (hours) spatial heterogeneities of DIC, pH, and aragonite saturation state (Ω_{Ar}) experienced by deep corals? 2) How frequent and persistent are conditions of low pH and low Ω_{Ar} across the seafloor and coral bathymetry? 3) What correlations exist between coral habitats and seafloor inorganic carbon conditions? This study will serve as an important step to understanding fine-scale variability of the inorganic carbon system across deep coral reefs, and may enable future deep coral research to better understand coral distributions and adaptations to variable environmental conditions.

3.2 Methods

3.2.1 Description of field sites

Many deep sea coral communities have been documented on the gently sloping carbonate platform of the West Florida Slope at depths of 400-1000 m (Figure 3.1). *L. pertusa* bioherms or mounds dominate here, and are particularly abundant in the region of the slope depicted in Figure 3.1. These mounds may range from 5 – 15 m tall and are often capped with thickets of live and/or dead *L. pertusa* (Newton et al., 1987; Reed et al., 2006). Deep coral communities here may also include a variety of octocorals, black corals, and sponges (Brooke et al., 2007; Brooks et al., 2015; CSA International, 2007; Reed et al., 2013; Ross and Nizinski, 2007).

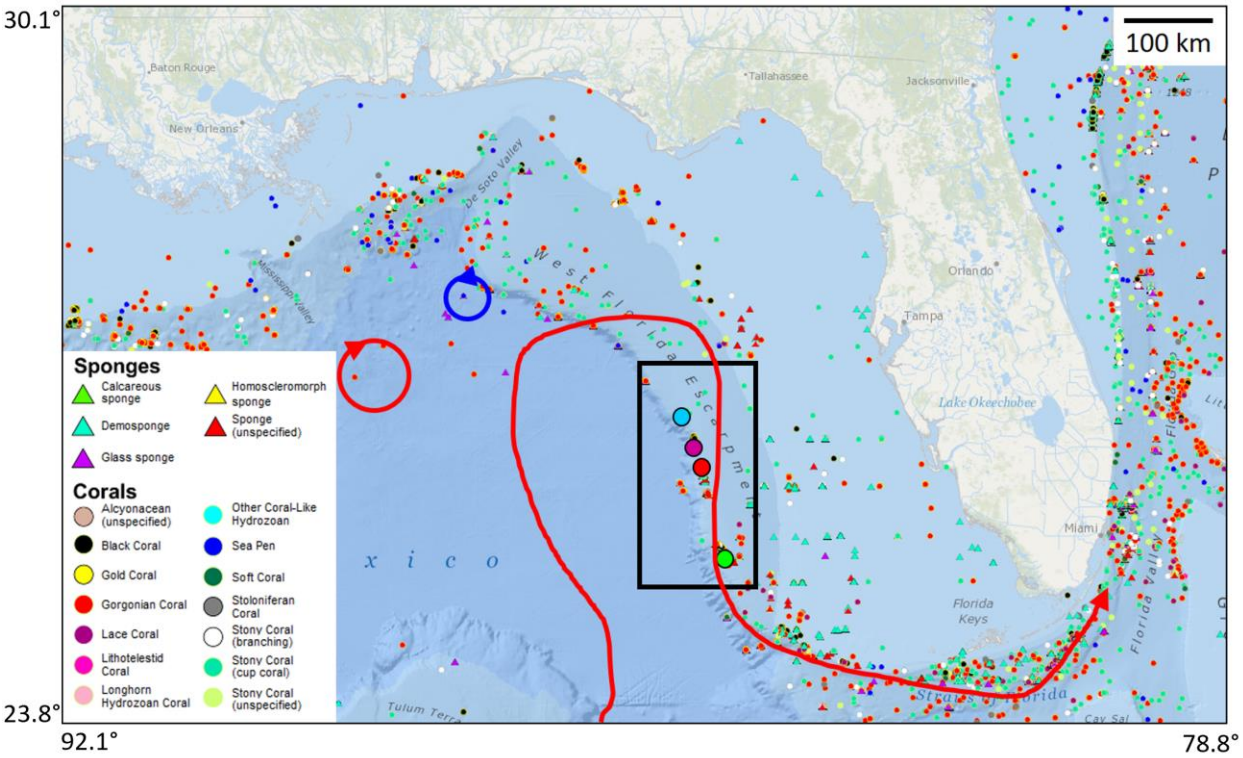

Figure 3.1: Deep-sea coral records from the southeastern US region from the NOAA National Database for Deep-Sea Corals and Sponges (v. 20190117-0. NOAA Deep Sea Coral Research & Technology Program). The thick red arrow indicates the flow of the Loop Current; the red and blue arrow circles denote the spin-off eddies from the Loop Current. The black box shows our study area including Many Mounds (*red*), Okeanos Ridge (*green*), North Wall (*blue*), and Long Mound (*magenta*).

The West Florida Slope is a highly dynamic region subject to the meandering of the Loop Current and the cyclonic Loop Current Frontal Eddies (LCFEs) that it spawns. These LCFEs are ~80-120 km in size and frequently migrate east along the Loop Current in the northern Gulf, then south along the West Florida Slope toward the Florida Straits (Vukovich and Maul, 1985; Cherubin et al., 2006; Le Henaff et al., 2012). Anticyclonic rings spawned by the Loop Current may also move west and south. The interactions between the Loop Current and LFCEs with bottom bathymetry may produce strong submesoscale eddies. Such eddies may induce strong, rapid upwelling, bringing cold, nutrient and CO_2-rich deep water onto the upper slope (Kourafalou and Kang, 2012; Jiang et al., 2020). These events may produce phytoplankton blooms that eventually die and sink to the seafloor, feeding the deep coral communities.

We focus on four sites on the West Florida Slope known to support *L. pertusa* mounds from prior ROV dives, particularly those of the Southeast Deep Coral Initiative (SEDCI, Wagner et al., 2018). The most studied of these, 'Many Mounds' (26.2095 N, 84.72884 W), hosts many dense, live *L. pertusa* bioherms and other coral species supported by strong currents that bring food and nutrients. 'Okeanos Ridge' (25.620

N, 84.5582 W) is less explored than Many Mounds due to strong southerly currents that complicate ROV surveys. *L. pertusa* has been observed at this site, but octocorals and black corals are more dominant. 'North Wall' (26.7629 N, 84.8650 W), is dominated by octocorals and black corals with some live *L. pertusa* colonies, but has a generally lower coral density than Many Mounds or Okeanos Ridge. Finally, 'Long Mound' (26.3992 N, 84.7655 W) contains a series of mounds and ridges populated by *L. pertusa*, other corals, and sponges. As of 2017, more than 14 coral species were identified in the Long Mound and Many Mounds areas. Both sites were identified as part of the West Florida Wall Habitat of Particular Concern (HAPC) by the Gulf of Mexico Fishery Management Council (GMFMC, 2017). This designation marks these sites as exploration priorities and seeks to protect dense coral habitats by prohibiting bottom tending gear, including bottom trawls, traps, and anchoring.

3.2.2 R/V *Point Sur* and R/V *Hogarth* cruises

We conducted two cruises to study these sites. The first, onboard the R/V *Point Sur* in October 11 – 17, 2019, explored deep coral habitats with detailed visual surveys using ROV *Global Explorer* (Section 3.3.3). This ROV was equipped with standard CTD sensors, 2 Niskin bottles for water chemistry sampling at depth, and the CHANnelized Optical System (CHANOS) II Dissolved Inorganic Carbon (DIC) sensor with an onboard SBE FastCat 49 CTD sensor and Aanderaa 4330 Oxygen Optode (Section 3.3.4). A CTD rosette was used to conduct hydrographic surveys of the water column around each field site after ROV dives, with seawater samples collected following the best practices for laboratory carbonate chemistry analysis (see Section 3.3.5, Dickson et al., 2007). A second cruise, onboard the R/V *Hogarth* in September 2020, conducted similar hydrographic water column surveys via CTD rosette with collection of seawater samples for carbonate chemistry analysis.

3.2.3 ROV *Global Explorer* transects

We conducted five ROV dives on the *Point Sur* cruise, with two dives at the Many Mounds site and one dive each at Okeanos Ridge, North Wall, and Long Mound. ROV transects for Many Mounds, Okeanos Ridge, and North Wall began at the deepest part of each planned dive, then flew generally east/northeast upslope over coral mounds and escarpments. The Long Mound dive was conducted over a relatively flat seafloor, where the ROV was directed to fly a 'lawnmower' pattern over coral mounds in four ~500 m parallel transects. The ROV speed ranged from 0.1-0.5 knots to ensure high quality video and image recording. Wherever conditions allowed, the ROV flew within 1-2 m of the seafloor or coral communities,

occasionally settling on or next to corals for biological and/ or chemical sampling. A summary of transect lengths, bottom times, and speeds is given in Table 3.1.

Table 3.1: Summary of ROV *Global Explorer* dives

Location	Date	On bottom GPS (°N, W)	Off bottom GPS (°N, W)	Depth range (m)	Time on bottom (hr)	Transect length (km)	Average ROV speed (kt)	Niskin bottle samples
Many Mounds 1	10/12/19	26.200, 84.729	26.210, 84.723	502 – 463	4.0	0.86	0.13	2
Many Mounds 2	10/13/19	26.205, 84.738	26.212, 84.711	572 – 401	6.5	2.73	0.24	2
Okeanos Ridge	10/14/19	26.671, 84.593	25.666, 84.581	606 – 509	4.5	1.34	0.17	2
North Wall	10/15/19	26.778, 84.883	26.773, 84.864	880 – 486	5.0	1.89	0.21	1
Long Mound	10/16/19	26.408, 84.782	26.409, 84.780	528 - 513	2.5	2.18	0.43	0

3.2.4 CHANOS II DIC sensor deployment on ROV *Global Explorer*

The CHANOS II is an autonomous sensor developed for high resolution, near-continuous measurements of DIC from mobile platforms including ROVs, as described in Chapter 2. Briefly, it operates by an improved spectrophotometric method for DIC detection (Wang et al., 2013; 2015). Seawater is acidified and pumped through the outer shell of an equilibration flow cell; a pH sensitive sulfonephthalein indicator is pumped countercurrent through the inner shell of Teflon AF 2400 tubing that is semi-permeable to CO_2. CO_2 is allowed to equilibrate between the two solutions, followed by the spectrophotometric pH measurement of the indicator solution. CO_2 concentration in the equilibrated indicator is calculated from the measured indicator pH and known alkalinity, and is related back to the total CO_2 or DIC of the seawater sample. The sensor carries onboard Certified Reference Material (CRM) seawater of known DIC, supplied by the Dickson Laboratory at Scripps Institute of Oceanography, for in-situ calibration to ensure data quality, or secondary standard seawater calibrated with CRM.

CHANOS II is capable of high-frequency near-continuous measurements, with a laboratory accuracy and precision of: ~2.9 and 5.5 μmol kg^{-1}, respectively, with a field accuracy of 9.0 μmol kg^{-1}. The sensor response time during this deployment was ~2 min, faster during this deployment than that discussed in Chapter 2 due to the use of a different length and diameter of Teflon AF tubing in the equilibration cell.

With an average ROV speed of ~0.2 knots or 6.2 m min^{-1}, we average DIC at a resolution of better than 20 m, allowing us to map the seafloor DIC during each dive at high resolution.

CHANOS II was developed for deployment to 3000 m and has been tested to 1200 m. It is equipped with a Seabird 49 FastCat DTC and Aanderaa 4330 dissolved oxygen (DO) optode. The sensor was loaded into the belly of the ROV *Global Explorer* behind the bio collection box. The seawater inlet was located at the bottom and middle the ROV, such that DIC measurements were as close to the bottom as possible (typically 1.2 m off bottom, approaching closer while settling the ROV for coral or water sampling) (Figure 3.2). It was hardwired into the ROV systems for power and communication, allowing for constant real-time operator control from the ROV control van. DO and CTD values were used to calculate the Apparent Oxygen Utilization (AOU) for all dives (McDougall and Barker, 2011).

Figure 3.2: CHANOS II on ROV *Global Explorer*. The sensor is mounted in the belly of the ROV to allow the inlet to be as close to the seafloor and coral mounds as possible.

3.2.5 CTD Rosette seawater sampling

After each ROV dive, we conducted a series of CTD Rosette casts at 3 - 10 hydrographic stations over the center of the ROV transect and evenly distributed around the area to determine water column profiles of temperature, salinity, and dissolved oxygen. Bottle samples were collected from Niskin samplers and poisoned with mercuric chloride following the best practices for carbonate chemistry (Dickson et al., 2007). These samples were measured at WHOI within three weeks of sampling. DIC samples were measured via

DIC auto-analyzer (AS-C3, Apollo SciTech; precision and accuracy better than ±2 μmol kg^{-1}). In this method, CO_2 gas is stripped with an inert nitrogen gas from acidified samples. The total CO_2 or DIC in the gas stream is determined by non-dispersible infrared CO_2 analyzer (LiCOR 7000) calibrated with CRMs. Seawater total alkalinity was determined potentiometrically using an automated open-cell titrator with a ROSS™ combination electrode, following a modified Gran titration procedure (AS-ALK2, Apollo SciTech, precision and accuracy better than ±2 μmol kg^{-1}).

3.2.6 Multilinear regression modeling to simulate seafloor carbonate conditions

With the above methods, we collect in-situ physical (temperature, pressure, salinity) and chemical (dissolved oxygen, DIC) data in order to understand the variation in environmental conditions experienced by deep corals. However, DIC is not enough to provide a full picture of inorganic carbon chemistry in the deep sea. Pairing DIC with in-situ TA, pH, or pCO_2 would allow for full resolution of the inorganic carbon system, including carbonate saturation states, but the handful of bottle samples collected by Niskins on the ROVs is not enough to provide this information. CTD casts provide valuable information about the water column above reef habitats, but such casts typically measure at least 2-10 m above the seafloor, missing potentially valuable information at the intersection of the seafloor and benthic communities with the base of the water column. We attempt to fill in the gaps by modeling seafloor TA, which, taken together with CHANOS II DIC measurements, allow us to estimate pH, pCO_2, and aragonite saturation state (Ω_{Ar}).

To obtain seafloor TA estimates, we first model water column TA:DIC over our study sites based on historical CTD casts in the region. The product of the deepest TA:DIC values produced by this model with seafloor CHANOS II DIC data results in an indirect estimate of seafloor TA. We note that this method has two major weaknesses: first, if sediment and coral biogeochemistry alters carbonate chemistry at the seafloor, then an application of even the deepest water column TA:DIC, generated from CTD casts that do not reach the sediment-water interface, may not appropriately estimate benthic conditions. Second, modeled seafloor TA becomes a function of CHANOS II or modeled seafloor DIC, such that errors are compounded in further carbonate parameter calculations (e.g., pH, pCO_2, and Ω_{Ar}). However, given the scarcity of seafloor data available, we argue that the conservative estimates provided by this method provide at least a range of seafloor conditions to consider.

In the first step of this modeling effort, we collected all publicly available inorganic carbon data from CTD casts and ROV dives in the Gulf of Mexico, including GOMECC, GOMRI, ECOGIG, and GISR cruises, sourced through NOAA and NSF data portals and is available upon request. Using a subset of data near our

study sites with available DIC and TA data, (n = 892, ranging in depth from 300 – 3417 m, in the bounds of latitude 21.63 - 21.17 °N and longitude 80.61 - 90.00 °W), we trained a simple multilinear regression using the built-in MATLAB multiple linear regression function (version 2018b). Data from the surface to 300 m depth were excluded to avoid seasonally varying surface processes in the mixed layer, including air-sea exchange and biological production. We modeled the water column ratio of TA:DIC, varying regression parameters of depth, temperature, and salinity. These parameters were chosen to reduce the error of the fit, evaluated via calculation of R^2 between model outputs and the training set. DO, AOU, and nutrients were tested in models with one or a combination of parameters. Where available, including silicate most improved the fit for water column data, but since nutrients were not included in the R/V *Point Sur* and *Hogarth* CTD cast analyses, this model was excluded analysis at our study sites. The addition of DO or AOU to these models worsened the fit to historical water column data.

We trained a separate multilinear regression on the CHANOS II DIC values measured during our dives to create a model for seafloor DIC given depth, temperature, and salinity. DO and AOU were considered as parameters for these models, but the inclusion of either worsened the fit to CHANOS II DIC data. Taking together the water column TA:DIC and either seafloor CHANOS II DIC or modeled seafloor DIC, we produced a conservative, indirect estimate of seafloor TA. We then used CO2SYS to estimate seafloor pCO_2, and Ω_{Ar} based on our DIC and TA estimates (CO2SYS version 2.1, using K_1 and K_2 constants from Leuker et al., 2000; Pierrot et al., 2006).

3.3 Results

3.3.1 Water column characteristics

To understand water mass movements during the ROV dives, GoMex forecasts were created using a numerical model based on the Regional Ocean Modeling System (ROMS), Gulf of Mexico Hybrid Coordinate Ocean Model (HYCOM), and surface meteorological data derived from the North American Regional Reanalysis (NARR) during the *Point Sur* cruise (Figure 3.3), courtesy of physical oceanographer Mingshun Jiang (Shchepetkin and McWilliams, 2005; Mesinger et al., 2006; Chassignet et al., 2009). The northern edge of the Loop Current was above Okeanos Ridge during the ROV dives, resulting in a southward flow at this site. Eddy interactions with the Loop Current resulted in a bifurcation of currents between Many Mounds and Okeanos Ridge, such that Many Mounds, Long Mound, and North Wall experienced a northward flow from the eastern edge of a cyclonic eddy. This behavior of the Loop Current, flowing south of our main study site, is common in the fall (Ross et al., 2017).

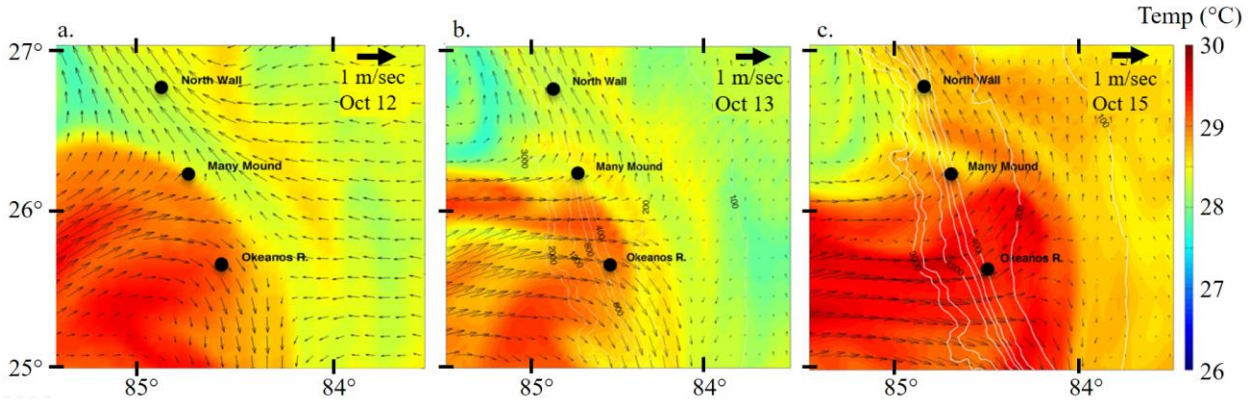

Figure 3.3: GoMEX forecasts at 250 m of the North Wall, Many Mounds, and Okeanos Ridge dive sites for Oct 12 (*a*), 13 (*b*), and 15 (*c*), 2019 during ROV dives. During this time, Okeanos Ridge was experiencing a southward flow under the northern edge of the Loop Current, while the Many Mound and North Wall sites experienced the eastern, northward flowing edge of a cyclonic Loop Current eddy. Currents are represented by arrows and temperature by color. Figure provided courtesy of collaborator Mingshun Jiang.

18 water column CTD casts were conducted during the *Point Sur* cruise, with one cast taken over the center of each ROV transect and remainder evenly distributed across each site (Figure 3.4). Due to cruise time constraints, no CTD casts were conducted above the Long Mound site. 65 bottle samples total were taken from nine casts at Many Mounds, 23 bottles were taken from four casts at Okeanos Ridge, and 30 samples were taken from five casts at North Wall. All 118 bottle samples collected were analyzed for DIC and TA. A total of six water column CTD casts were conducted during the *Hogarth* cruise, with three casts each taken above the Many Mounds and Okeanos Ridge study areas. A total of 30 bottle samples were collected from these casts (5 bottles fairly evenly distributed over the depth of each cast) and analyzed for DIC and TA.

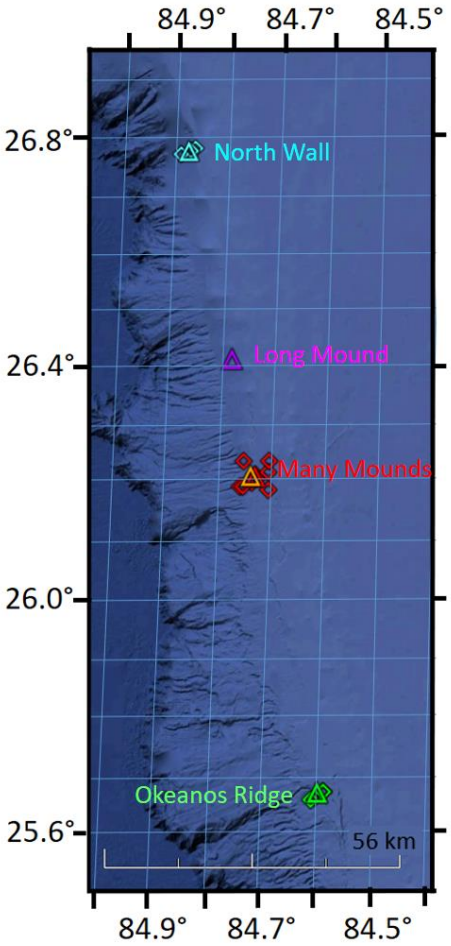

Figure 3.4: Large scale view of CTD cast locations (*diamonds*) and starting locations of ROV transects (*triangles*) at North Wall (*blue*), Long Mound (*magenta*), Many Mounds (*orange* and *red*), and Okeanos Ridge (*green*).

CTD cast data collected above and around the Many Mounds and Okeanos Ridge sites were plotted together for each cruise in Figure 3.5.

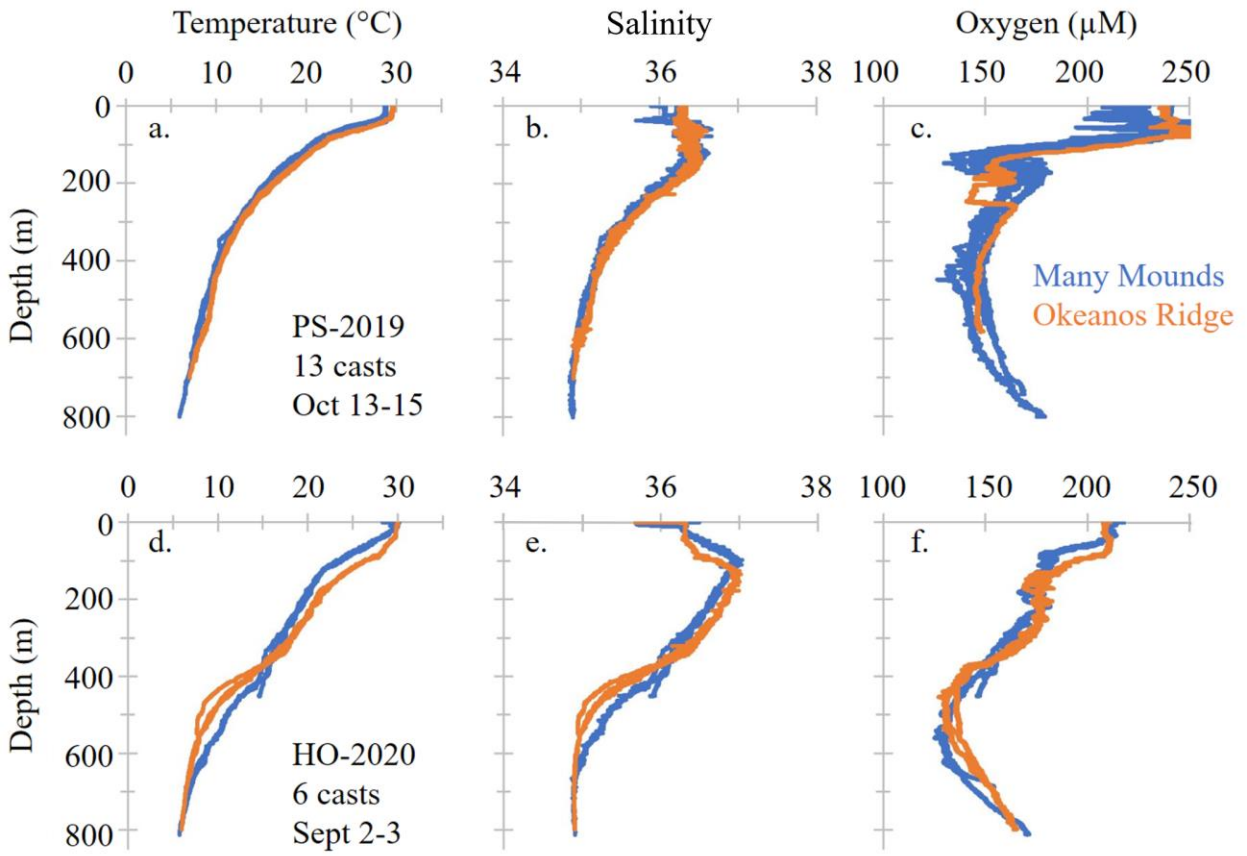

Figure 3.5: Temperature (*a*,*d*), salinity (*b*,*e*), and dissolved oxygen (*c*,*f*) plots versus depth. The upper panels show CTD casts conducted during the *Point Sur* cruise (October 13 – 15, 2019) over Many Mounds (*blue*) and Okeanos Ridge (*orange*). Bottom panels show CTD casts conducted during the *Hogarth* cruise (September 2-3, 2020) over Many Mounds (*blue*) and Okeanos Ridge (*orange*).

In all the *Point Sur* casts, temperature held steady at ~29.7 °C from the surface to ~35 m depth, followed by a thermocline as temperature declined rapidly to ~16.1 °C at 200 m, then declining gently to ~6.0 °C at ~800 m depth. A maximum salinity of ~36.6 was observed between ~65- 140 m depth, declining to 34.9 at 800 m depth. The DO signal was more complex, with near-surface (0 – 80 m depth) values ranging from 194 – 250 µM (Many Mounds) and 215 – 255 µM (Okeanos Ridge). Above the Many Mounds site, DO decreased rapidly to reach an oxygen minimum ~136 µM between 132 and 166 m depth, with a secondary oxygen minimum falling to ~140 µM between 410 – 475 m. DO then rose to ~177 µM at 800 m depth. Above the Okeanos Ridge site, DO decreased to an oxygen minimum zone ranging between 130 – 160 µM between 150 and 250 m depth. DO then decreased to a secondary minimum of ~145 µM at 550 m depth, before rising back to ~ 160 µM at 700 m depth.

Hogarth casts at the same sites, conducted 11 months later, showed a greater range in temperature, salinity, and DO with depth. The thermocline was less pronounced during these casts: temperatures decreased more

gently between the same values recorded during the *Point Sur* casts at the surface and 800 m (~29.7 °C and ~6.0 °C, respectively). The salinity maximum occurred at the same depth but at a higher magnitude, ~ 37.0. The first oxygen minimum between ~ 150 and 180 m depth was less pronounced at ~160 µM for both sites. The second oxygen minimum between ~500 and 600 m (Many Mounds) and 450 – 500 m (Okeanos Ridge) was deeper and lower than that of the *Point Sur* casts, at ~125 µM and 135 µM, respectively. *L. pertusa* often tolerate low (< 135 µM) DO conditions, but studies have shown that this species cannot survive prolonged exposure to DO < 70 µM (Brooke et al., 2009; Dodds et al., 2007; Hebbeln et al., 2020 Lunden et al., 2014).

Temperature and salinity were plotted for all CTD casts from the *Point Sur* cruise, with temperature scaled by DO (Figure 3.6). These plots highlight several water masses at the time of the *Point Sur* cruise and ROV dives when the northern edge of the Loop Current was passing over the Okeanos Ridge site, with eddy interactions resulting in the bifurcation of currents discussed above (Portela et al., 2018). Warm, salty shallow water comes from the central basin of the Gulf of Mexico. North Atlantic Subtropical Underwater (NASUW) is present as the subsurface salinity maximum with temperatures ranging from 16-21 °C at depths between 100-300 m. Waters with temperatures below 16 °C are the North Atlantic Central Water (NACW, or Tropical Atlantic Central Water, TACW). This water mass is defined by its low oxygen concentration in the 400 – 500 m depth range.

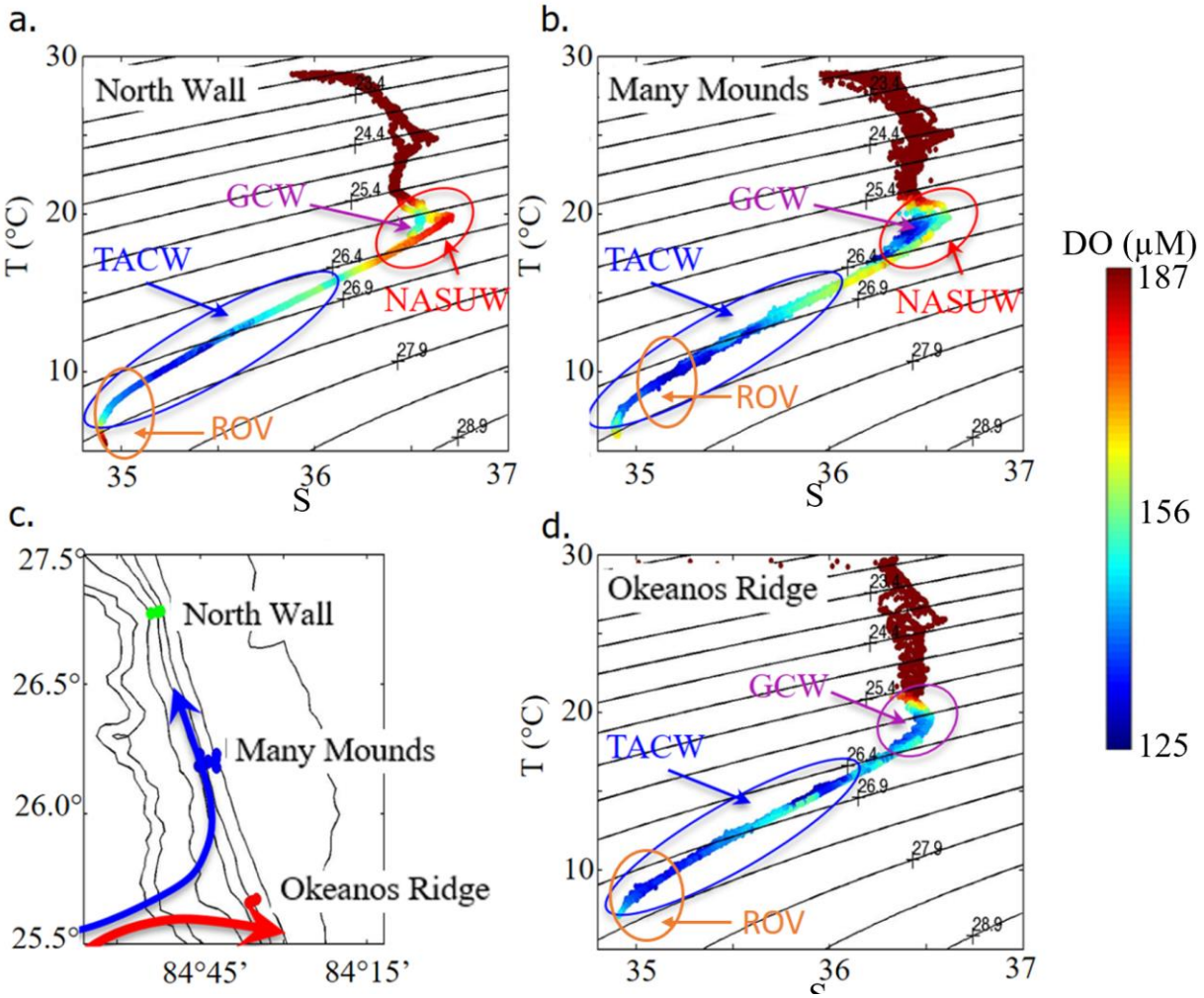

Figure 3.6: Temperature-salinity plots for all CTD casts above (*a*) North Wall, (*b*) Many Mounds, and (*d*) Okeanos Ridge. Water masses are identified as Gulf Central Water (GCW), North Atlantic Subtropical Underwater (NASUW), and Tropical Atlantic Central Water (TACW). Colors represent DO in µM. The range of temperature and salinity for each ROV dive is circled in orange. The bifurcation of currents during the ROV dives is illustrated in panel *c*. Image provided courtesy of collaborator Mingshun Jiang.

3.3.2 Bottom characteristics

ROV dive tracks were reprocessed to restore GPS tracks after an ROV beacon failure. All locations were plotted in ArcGIS (version10.8.2) and dive tracks were smoothed by creating a moving average of GPS locations and corresponding CTD data grouped by minute. ROV tracks for all dives are plotted in Figure 3.7, with the two Many Mounds dives plotted together on the same panel.

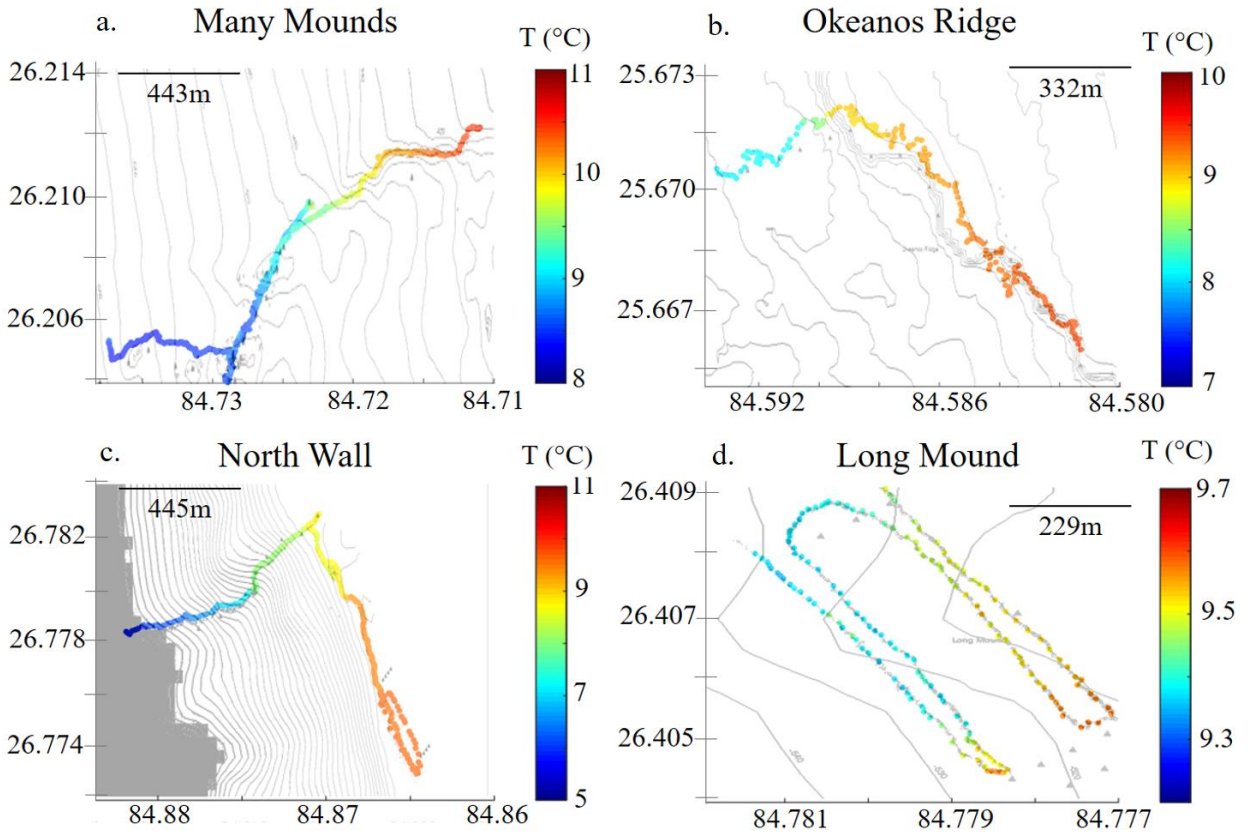

Figure 3.7: Reconstructed ROV *Global Explorer* dive tracks conducted between October 12-16, 2019. Length, depth, and locations of transects may be found in Table 3.1. Each dive began in the west and proceeded generally upslope to the east, with the exception of the Long Mound dive (*d*) that featured a series of lawn-mowing transects across corals mounds. Bottom bathymetry is noted by black lines on each plot. Each data point represents the average of one minute of ROV GPS coordinates, with colors denoting average temperatures recorded by the ROV's CTD.

ROV CTD sensors showed minor variations in temperature, salinity, and DO during the Long Mound dive, conducted in a relatively flat region, and in the relatively flat portions of the other dives before or after rising upslope. The greatest vertical rise encountered was that of North Wall, where the ROV gradually ascended ~360 m while following along a rocky wall feature, before leveling out to fly east over a relatively flat plain. The Okeanos Ridge dive also passed over a rocky wall feature, gradually ascending ~60 m along the edge of the wall before leveling out to the east. Both Many Mounds dives saw a gradual rise while heading east throughout the dive. A summary of environmental data recorded by the ROV at depth is available in Table 3.2.

Table 3.2 Summary of bottom environmental data recorded during *Global Explorer* dives on the West Florida slope deep sea reefs. See Table 3.1 for dive dates, locations, and bottom times.

Dive	Depth range (m)	Temperature (°C)	Practical Salinity	DO (µM)
Many Mounds 1	502 – 463	8.5 – 9.6	34.9 – 35.2	96.0 – 106.1
Many Mounds 2	572 – 401	8.4 – 10.5	35.0 – 35.3	102.6 – 106.3
Okeanos Ridge	606 – 509	8.1 – 9.4	34.8 – 355.2	102.3 – 109.9
North Wall	880 – 486	5.8 – 9.7	34.7 – 35.2	102.5 – 138.6
Long Mound	528 - 513	9.4 – 9.6	35.1 - 35.2	100.8 – 101.6

3.3.3 Bottom terrain and benthic habitat characterization

The bottom terrain and benthic habitats were characterized to one-minute resolution during analysis of high quality ROV videos recordings. Coral species were counted and identified, and seafloor substrate and percent coral coverage were characterized, courtesy of biological oceanographer Sandra Brooke and Gabby Fulton (Figure 3.8). A brief overview of coral types identified in Figure 3.8 is provided in Table 3.3.

Table 3.3: Summary of coral classifications

Grouping	Class, Order	Genus observed	Characteristics
Stony corals	Anthozoa, Scleractinia	*Lophelia, Madrepora, Solenosmilia, Desmophyllum*	Typically colonial, hard skeleton reef builders, requiring exposed, hard substrate for attachment.
Black corals	Anthozoa, Antipatharia	*Bathypathes, Stichopathes, Leiopathes*	Patchily distributed structure-forming corals that may be locally abundant.
Gorgonians	Anthozoa, Gorgonacea	Unidentified	Patchily distributed structure-forming corals that may be locally abundant, requiring exposed, hard substrate for attachment.
Soft corals	Anthozoa, Alcynoacea	*Paramuricea, Eunicella, Anthothela, Bamboo, Primnoidae, Plumerella, Anthomastus*	Mostly non-reef building. They include sea fans and sea whips, and are also known as tree corals. Common on sandy seafloor.
Lace corals	Hydrozoa, Stylasterina	*Stylaster*	Structure-forming, often erect species that require exposed, hard substrate for attachment. Patchily distributed.

Coral coverage across all four dives is visualized in Figure 3.9. In general, live, dense *L. pertusa* were most prevalent at Many Mounds, where they primarily colonized the high points of existing mounds and escarpments. A variety of *bathypathes*, *stichopathes*, and other coral species were identified, but were uncommon, throughout the dive. More than 25% coverage of structure forming corals was seen throughout a majority of the dive, with several regions exhibiting 75-100% coral coverage within the ROV's field of view, primarily dense live or dead *L. pertusa*. With the exception of areas where *L. pertusa* obscured the

view of the seafloor and a handful of rocky escarpments, the seafloor was mostly soft sediment with occasional emergent hard substrate.

L. pertusa was far less prevalent at Okeanos Ridge, where *bathypathes, stichopathes,* and other coral species dominated much of the dive. Most of the dive saw at least 25% coverage by structure forming corals, but >50% coverage was rarely exhibited. The initial ascent in this dive was soft sediment, with rubble and emergent hard substrate common along the ridge feature followed during the dive where most corals were located.

North Wall saw the lowest overall coral coverage, never exceeding 25% of the ROV field of view. *L. pertusa* were rarely observed and only clustered at the top of the wall structure dominating the first portion of the dive, with few to no *L. pertusa* present as the ROV proceeded southeast along the top edge of the wall. *Bathypathes and stichopathes* dominated in this region. The majority of this dive saw soft sediment, with some occurrences of steep slopes of rock or consolidated sediment.

Dense *L. pertusa* were present throughout the Long Mound dive. *Stichopathes* was common in this area and *bathypathes* was uncommon but fairly evenly distributed. Coral coverage in this area frequently surpassed 25 or 50% of the ROV field of view, interspersed with regions of soft sediment with occasional emergent hard substrate.

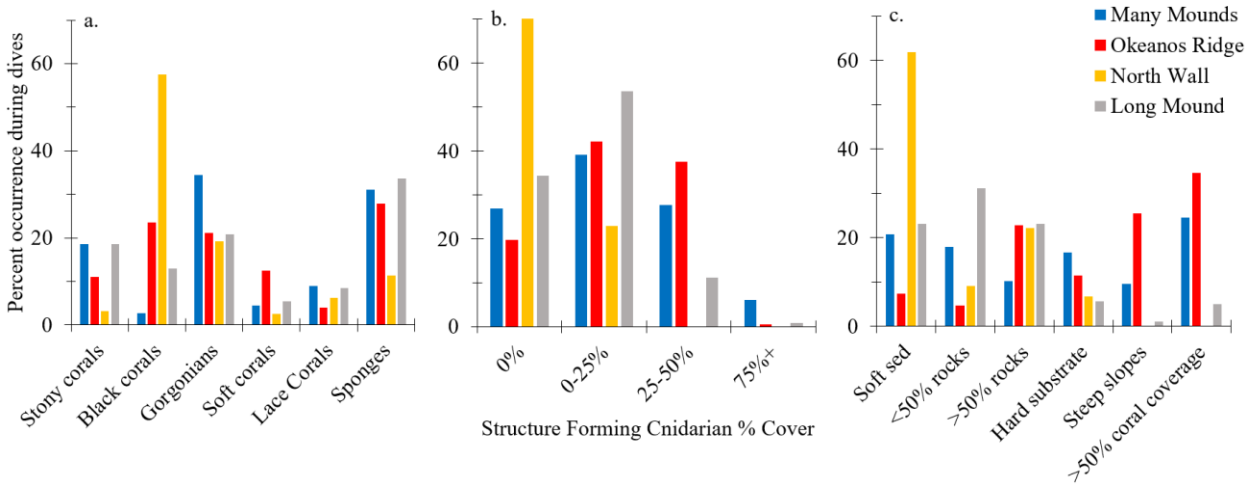

Figure 3.8: Distribution of seafloor communities and substrate grouped by percent occurrence during each dive, averaged by minute in the ROV field of view, including: *a*) type of Structure Forming Cnidarians (SFCs), *b*) SFC percent coverage of the seafloor in the ROV field of view, *c*) benthic substrate.

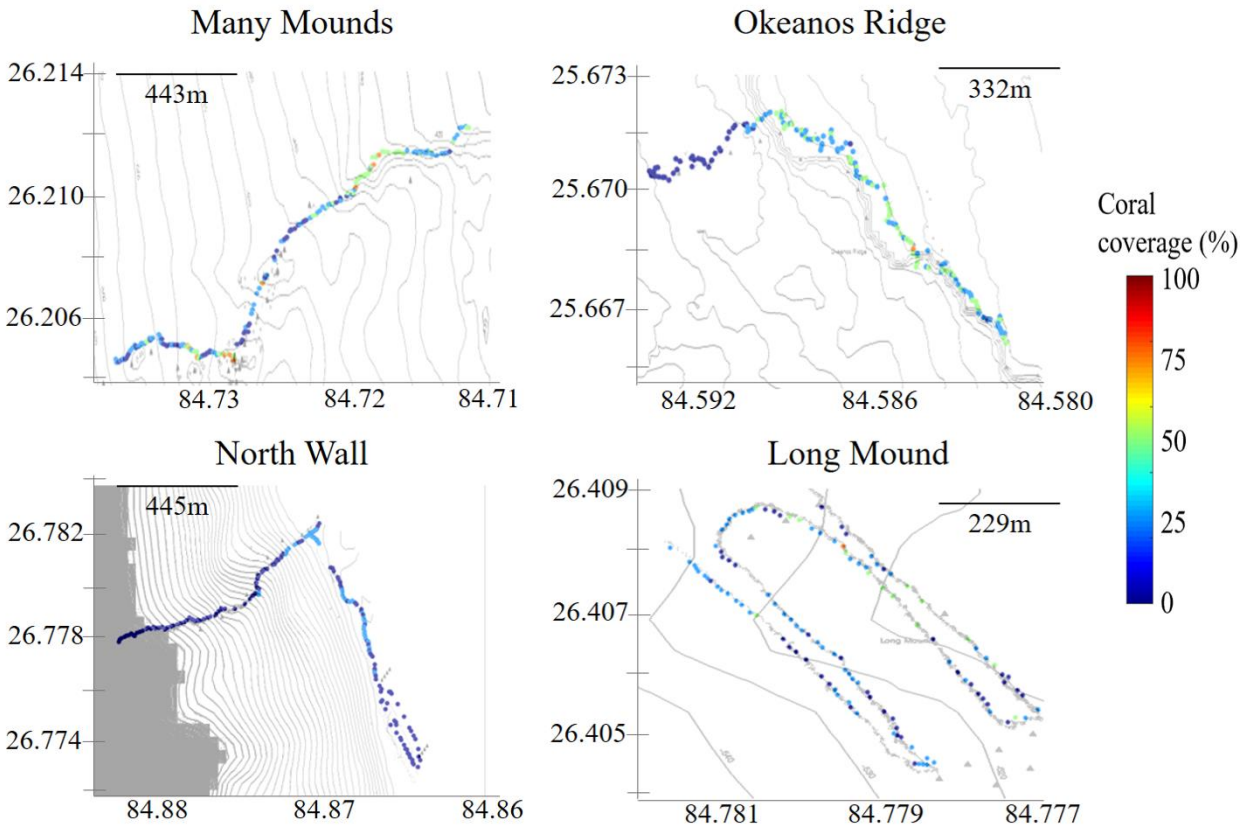

Figure 3.9: Structure Forming Cnidarian coverage (%) grouped by ROV field of view per minute across 4 ROV *Global Explorer* dive tracks conducted between October 12-16, 2019.

3.3.4 Mapping seafloor DIC with CHANOS II

CHANOS II DIC data was collected on 4 of 5 dives. While the spectrophotometric method allows for sensor measurements to be "calibration free," CRMs and secondary standards were carried onboard each dive to ensure measurement quality. These CRM measurements were not used for sensor calibration, for which a laboratory temperature calibration curve was used generated over 5 - 32°C, as described in Chapter 2, but were instead measured in-situ as a quality check in lieu of frequent bottle samples. DIC data was processed, calibrated, and plotted for each deployment, as seen in Figures 3.10 – 3.13. Niskin seafloor bottle samples collected during the dives were not included in the sensor calibration, and were plotted alongside CHANOS II DIC data. There was no significant statistical difference between CHANOS II DIC and salinity-normalized DIC and all ROV DIC data herein is presented as normalized to the average salinity for a given field site, though we note that the salinity changes reported throughout these dives are so small that normalization does not significantly change DIC data.

The Many Mounds dive resulted in ~3.5 hours of seafloor DIC, with breaks taken between 9:51 - 10:43 am and 12:51 - 1:46 pm to measure CRM (Figure 3.10). These in-situ calibrations were unsuccessful, likely due to an issue with the fluidic connections to the bag of CRM carried onboard this dive (see Table 3.4). Two bottle samples were taken during this dive: the first (8:38 am, ~ 2192.6 ± 1.1 µmol kg^{-1} DIC) was collected before CHANOS II readings had stabilized at the seafloor. The CHANOS II recorded a DIC of ~2188.1 ± 5.5 µmol kg^{-1} at the time of the second bottle sample (10:43 am, ~ 2190.5 ± 0.2 µmol kg^{-1}).

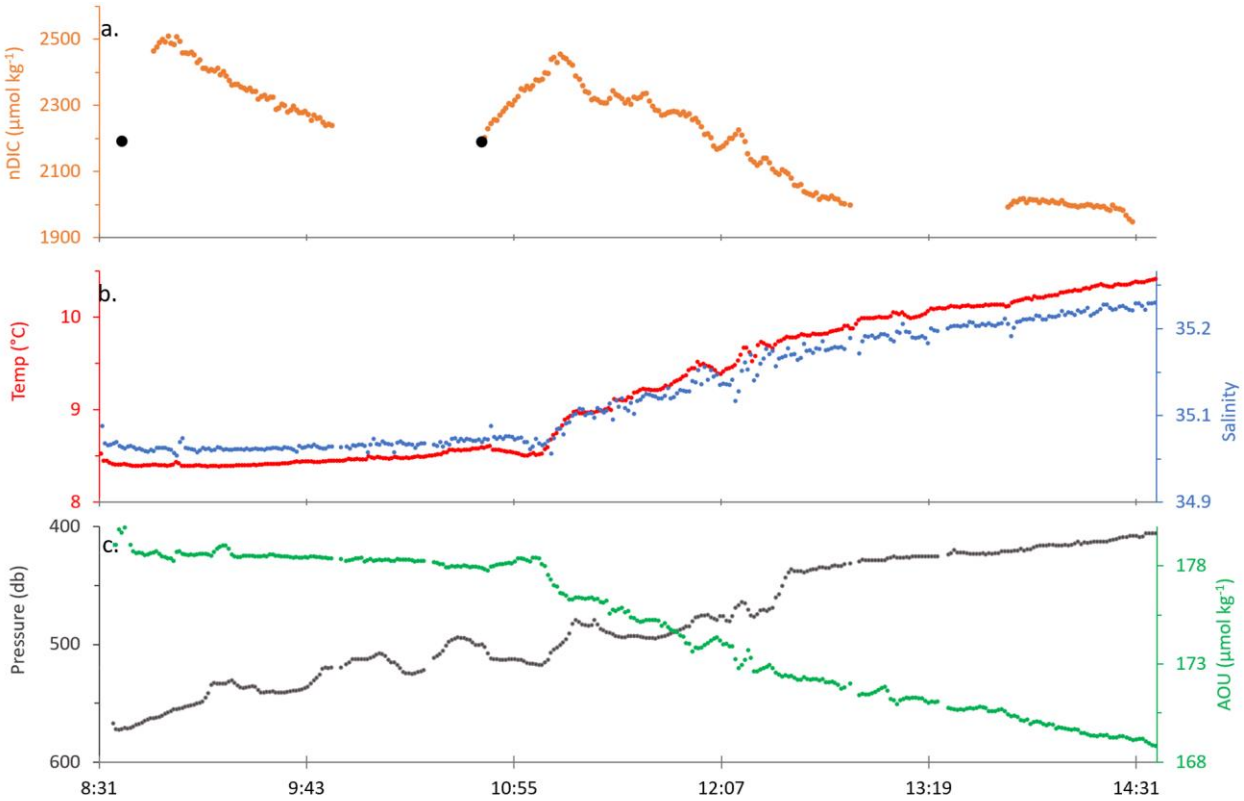

Figure 3.10: Salinity-normalized CHANOS II DIC (*orange*) (*a*), ROV temperature (*red*) and salinity (*blue*) (*b*), pressure (*grey*) and AOU (*green*) (*c*) during the Many Mounds dive, which included two ROV bottle samples (*black*).

The Okeanos Ridge dive resulted in ~2.5 hours of seafloor DIC measurements (Figure 3.11). The sensor was programed to repeatedly measure an onboard secondary standard material (analyzed in the laboratory at DIC 2235.0 ± 2.0 µmol kg^{-1}) from 7:30 - 8:00 am. This measurement began while the ROV was hovering just below the surface, during which time the CHANOS II recorded a value of 2243.4 ± 5.5 µmol kg^{-1} (ΔDIC of ~8.3 µmol kg^{-1}). The ROV then dove at ~30 m min^{-1} while the CHANOS II continued to repeatedly measure this standard, but sensor values during the descent were poor, likely due to vibration of the optical cell and fibers. One seafloor bottle sample was taken at 9:22 am (~ 2190.2 ± 0.2 µmol kg^{-1}), at which time the CHANOS II recorded a DIC of ~2193.7 ± 5.5 µmol kg^{-1} (ΔDIC of ~3.5 µmol kg^{-1}). CHANOS II was not measuring seawater at the time the second bottle sample was collected at 11:09 am just before the ROV ascended to the surface.

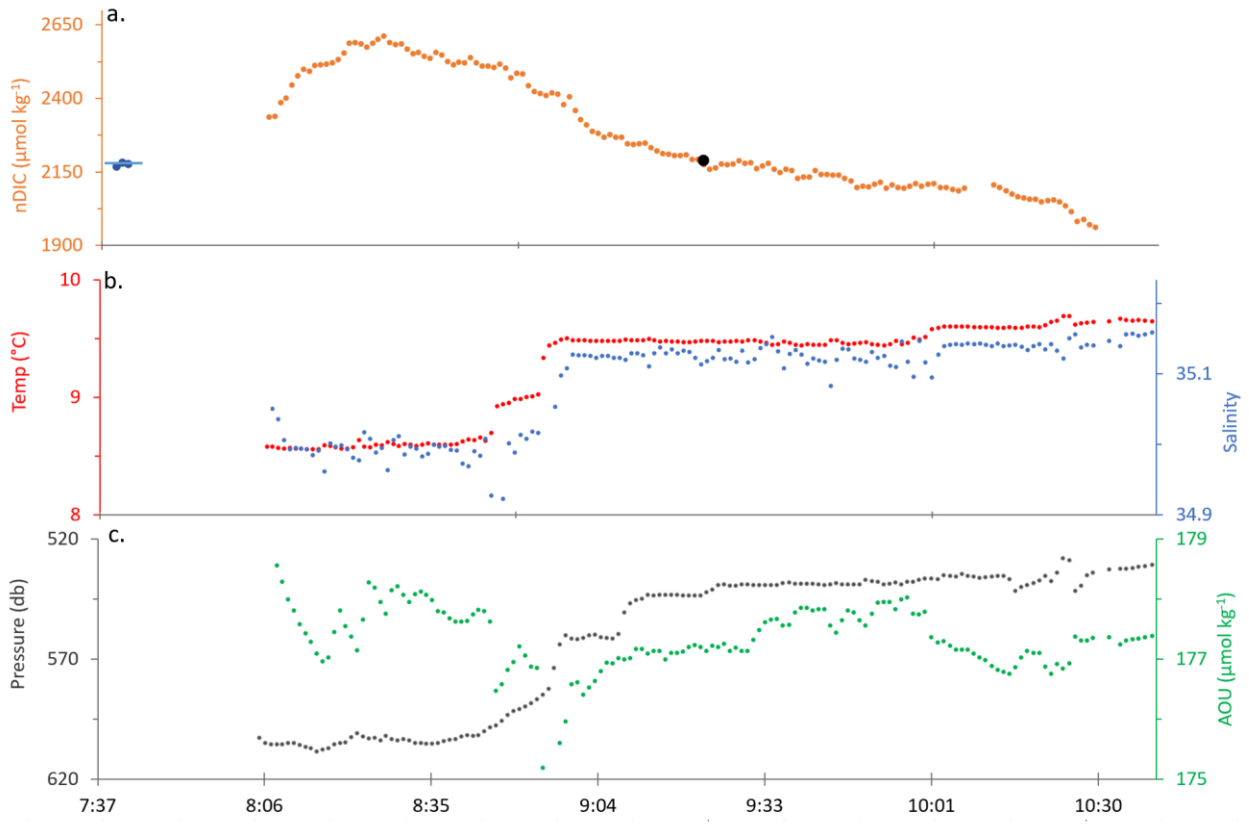

Figure 3.11: Salinity-normalized CHANOS II DIC (*orange*) (*a*), ROV temperature (*red*) and salinity (*blue*) (*b*), pressure (*grey*) and AOU (*green*) (*c*) during the Okeanos Ridge dive, which included one ROV bottle sample (*black*) and onboard standard measurements (*dark blue*) at ~7:40 am. The thin blue line in the top panel ~7:40 am indicates the expected DIC value of onboard standard seawater.

The North Wall dive resulted in ~3.5 hours of seafloor DIC (Figure 3.12). There were two breaks in the ambient seawater sensor measurements, between 10:10 - 10:42 am and 12:57 - 1:22 pm, to measure onboard

standard seawater (analyzed in the laboratory at DIC 2260.0 ± 2.0 µmol kg^{-1}). During these times the CHANOS II recorded 2266.2 and 2238.3 ± 5.5 µmol kg^{-1} (ΔDIC of ~6.2 and -21.7 µmol kg^{-1}), respectively. The variability in the first set of repeated standard measurements (10:10 - 10:42 am) is likely due to vibration from the movement of the ROV in the water column while maneuvering up and over the ridge (transiting from 623 m to 523 m depth during this standard measurement). The CHANOS II value for this standard measurement is therefore reported as an average over the last few minutes of the repeated measurement cycle, at which ROV depth was held steady at 524 m depth and ΔDIC between the expected and measured CRM value was 6.2 µmol kg^{-1}. It is likely that the 2nd standard measurement was not fully equilibrated at the time its value was recorded, as this measurement cycle was shortened due to operator error. Only one bottle sample was taken during this dive due to a Niskin sampler failure (11:10 am, ~2191.9 ± 1.0 µmol kg^{-1}). CHANOS II measurements had not yet stabilized at the time this sample was collected. A value of 2294.2 ± 5.5 µmol $kg^{-1}$was recorded 8 min later, ~60 m away from the bottle sampling location and ~7m higher upslope.

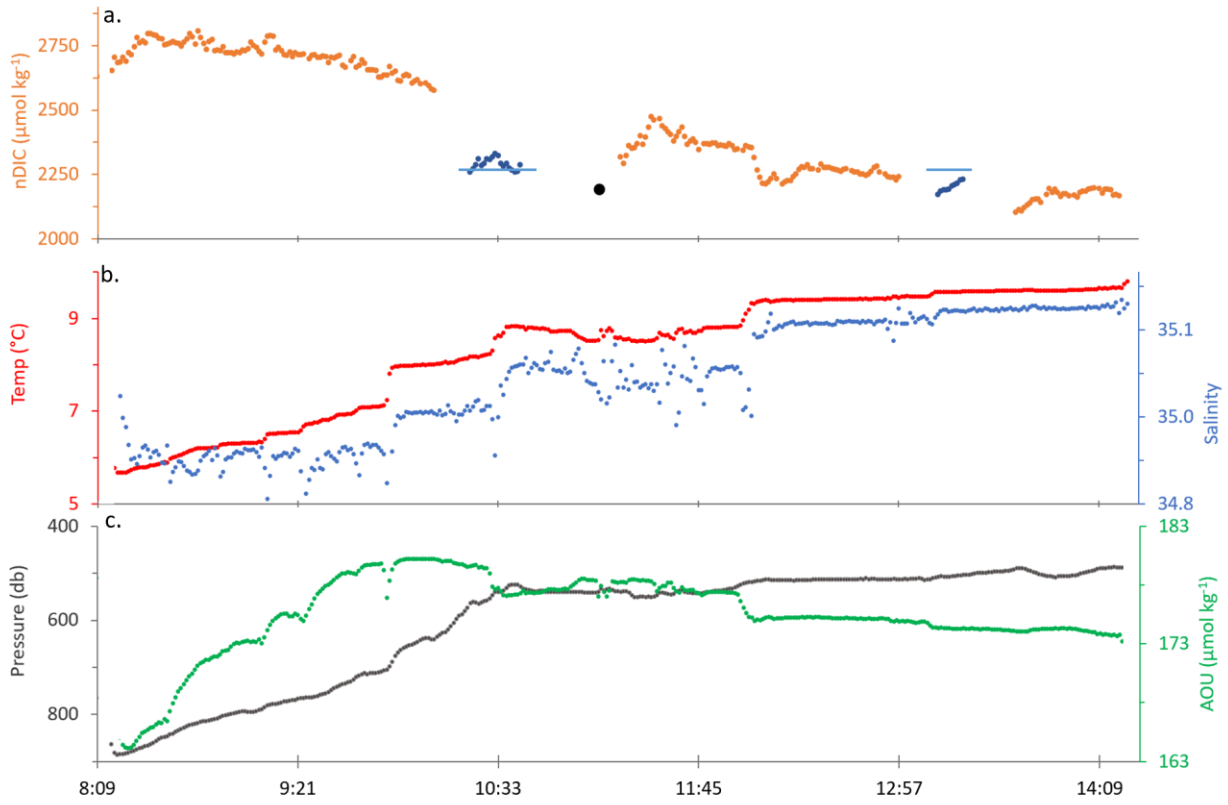

Figure 3.12: Salinity-normalized CHANOS II DIC (*orange*) (*a*), ROV temperature (*red*) and salinity (*blue*) (*b*), pressure (*grey*) and AOU (*green*) (*c*) during the North Wall dive, which included one ROV bottle sample (*black*) and two onboard standard measurements (*dark blue*) at ~10:40 am and 13:10 pm. The thin blue lines in the top panel ~10:40 am and 13:10 pm indicate the expected DIC value of onboard standard seawater.

The Long Mound dive resulted in ~2.2 hours of seafloor DIC (Figure 3.13). Due to cruise time constraints and Niskin failures, no CRM measurements or bottle samples were taken during this dive.

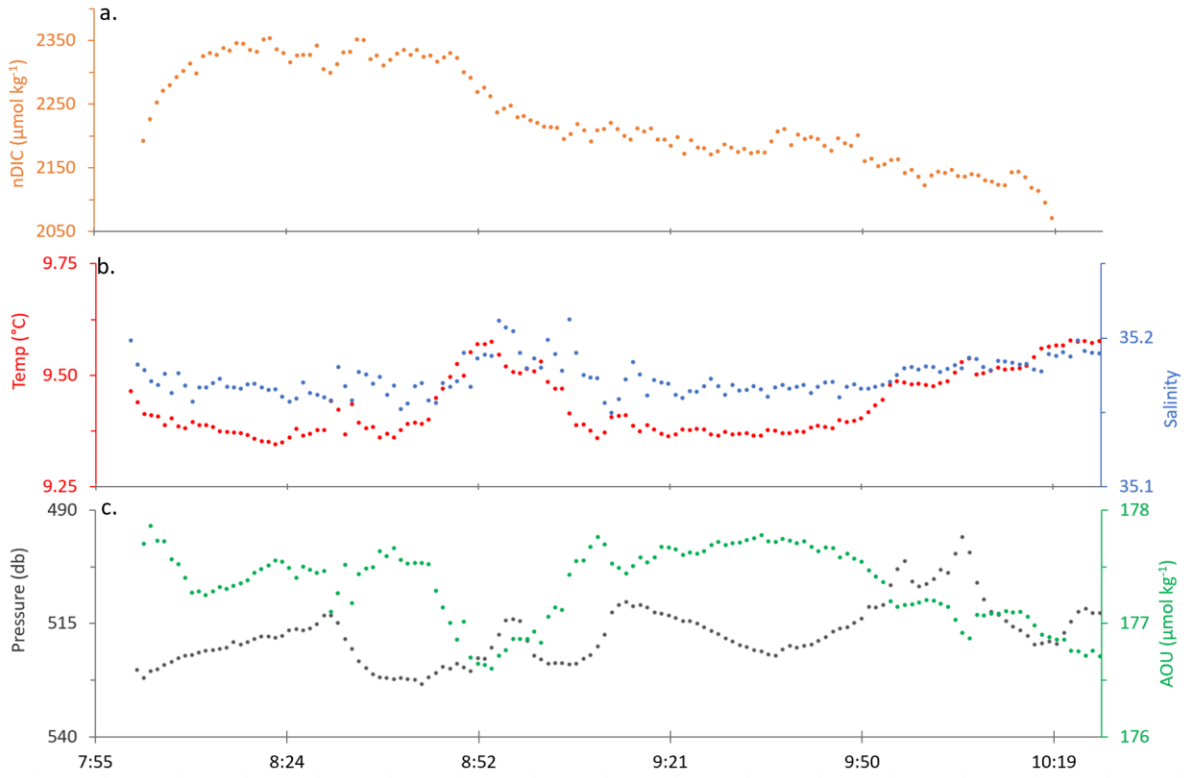

Figure 3.13: Salinity-normalized CHANOS II DIC (*orange*) (*a*), ROV temperature (*red*) and salinity (*blue*) (*b*), pressure (*grey*) and AOU (*green*) (*c*) during the Long Mound dive, which did not include either bottle samples or onboard standard measurements.

Table 3.4: Summary of CRM and bottle sample measurements

Dive	Sample type	Time	Depth (m)	Laboratory DIC (µmol kg^{-1})	CHANOS II DIC (µmol kg^{-1})	Used in analyses?
Many Mounds	Secondary standard	9:51 - 10:43 am	522 m	N/A	N/A	No—potential leaking from bag
	Secondary standard	12:51 - 1:46 pm	424 m	N/A	N/A	No—potential leaking from bag
	Bottle	8:38 am	572 m	2192.6 ± 1.1	N/A	No—before sensor equilibrated
	Bottle	10:43 am	500 m	2190.5 ± 0.2	2188.1	Yes
Okeanos Ridge	Secondary standard	7:30 - 8:00 am	2 m	2235.0 ± 2.0	2243.4	Yes
	Bottle	9:22 am	542 m	2190.2 ± 0.2	2193.7	Yes
	Bottle	11:09 am	520 m	2193.7 ± 5.5	N/A	No—sensor was offline
North Wall	Secondary standard	10:10 - 10:42 am	524 m	2260.0 ± 2.0	2266.2	Yes
	Bottle	11:10 am	532 m	2191.9 ± 1.0	2294.2	No—unequilibrated
	Secondary standard	12:57 - 1:22 pm	503 m	2260.0 ± 2.0	2238.3	No—CRM sequence terminated before sample had equilibrated

3.3.5 Comparison of bottle sample and sensor measurements

The range of CHANOS II DIC measurements was significant, varying by as much as 650 µmol kg^{-1} during the North Wall dive. While it is reasonable to expect that much of that variation could be attributed to changes in sensor performance due to changes in depth throughout the dives (see Discussion section 3.4), in many cases we see significant variations in seafloor DIC while the ROV crossed relatively flat terrain. The range of bottle sample DICs collected during the Many Mounds, Okeanos Ridge, and North Wall dives was insignificant: the five bottle samples have a mean and standard deviation of 2191.25 ± 1.0 µmol kg^{-1}. These samples were collected at depths ranging from 500 - 572 m with temperatures ranging from 8.4 – 9.3 °C, salinities of 34.98 - 35.10, DO of 101.7 – 105.5 µM, and AOU of 164 - 183 µmol kg^{-1}. A comparison of the residuals between bottle samples and CRMs versus CHANOS II DIC is shown in Figure 3.14. While few data points were available for these deployments, the mean of the residuals is denoted by the line at 1.2 µmol kg^{-1} with a standard deviation of 12.2 µmol kg^{-1}. Neglecting the second North Wall CRM measurement in which sensor measurements had likely not yet equilibrated, the mean of the residuals becomes -3.9 µmol kg^{-1} with a standard deviation of 4.7 µmol kg^{-1}.

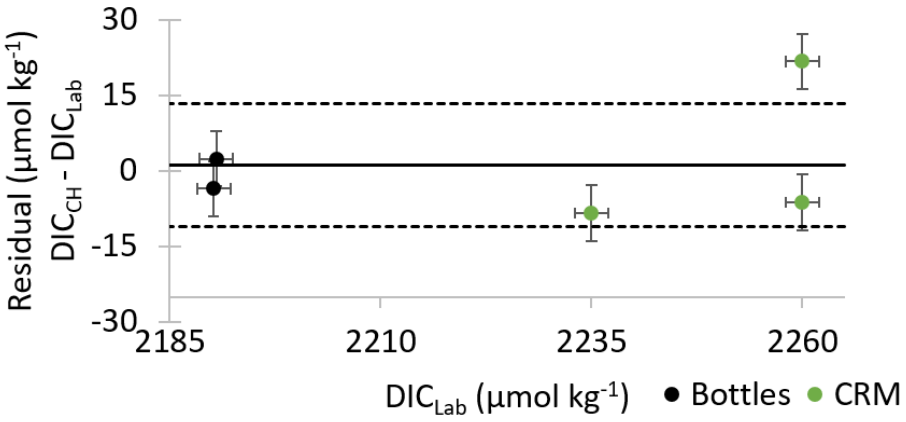

Figure 3.14: Residuals between CHANOS II (DIC_{CH}) and laboratory (DIC_{AP}) measured bottle samples and CRM. The black line represents the mean of 1.2 µmol kg^{-1}, with a standard deviation of 12.2 µmol kg^{-1} (*dashed lines*). Error bars represent estimated precision in CHANOS II measurements (e.g., 5.5 µmol kg^{-1} as determined by repeated laboratory tests).

3.3.6 Multilinear regression modeling

The lack of seafloor measurements limits our understanding and interpretation of environmental conditions experienced by deep sea corals on the West Florida slope. Taking into account the variability in DIC observed by the CHANOS II, it is likely that these coral sites experience significant variation in pH and

aragonite saturation state on a <100m resolution scale. We do not have enough bottle samples available from our or previous dives to fully resolve the seafloor inorganic carbon system directly. To address this gap, we build multilinear regression models using water column and seafloor measurements to conservatively estimate seafloor TA, allowing for full calculation of the seafloor inorganic carbon system with CHANOS II DIC data.

First, we collected publicly available historical DIC and TA data from CTD casts in the Eastern Gulf of Mexico, ranging from 21.6 - 29.2 N and 80.6 - 90.0 W. Data was primarily sourced from Gulf of Mexico Ecosystems and Carbon (GoMECC) cruises, and also included cruises from the Global Ocean Data Analysis Project (GLODAP v2.2021, Lauvset et al., 2021), Gulf of Mexico Research Initiative (GoMRI), ECOGIG, and Gulf of Mexico Integrated Spill Response Consortium (GISR) projects. *Point Sur* and *Hogarth* CTD samples described above were added into this data set. Samples with low salinity near the mouth of the Mississippi River were excluded, as were samples above 300 m depth. The remaining set of 893 individual samples was used to train a multilinear regression of water column TA, DIC, and TA:DIC ratios, using depth, temperature, and salinity as variables, then applied to *Point Sur* CTD casts to evaluate the model fit (Figures 3.15 and 3.16). Of this data set, only 25 samples came from ROVs or submersibles, with the remainder collected from CTD casts.

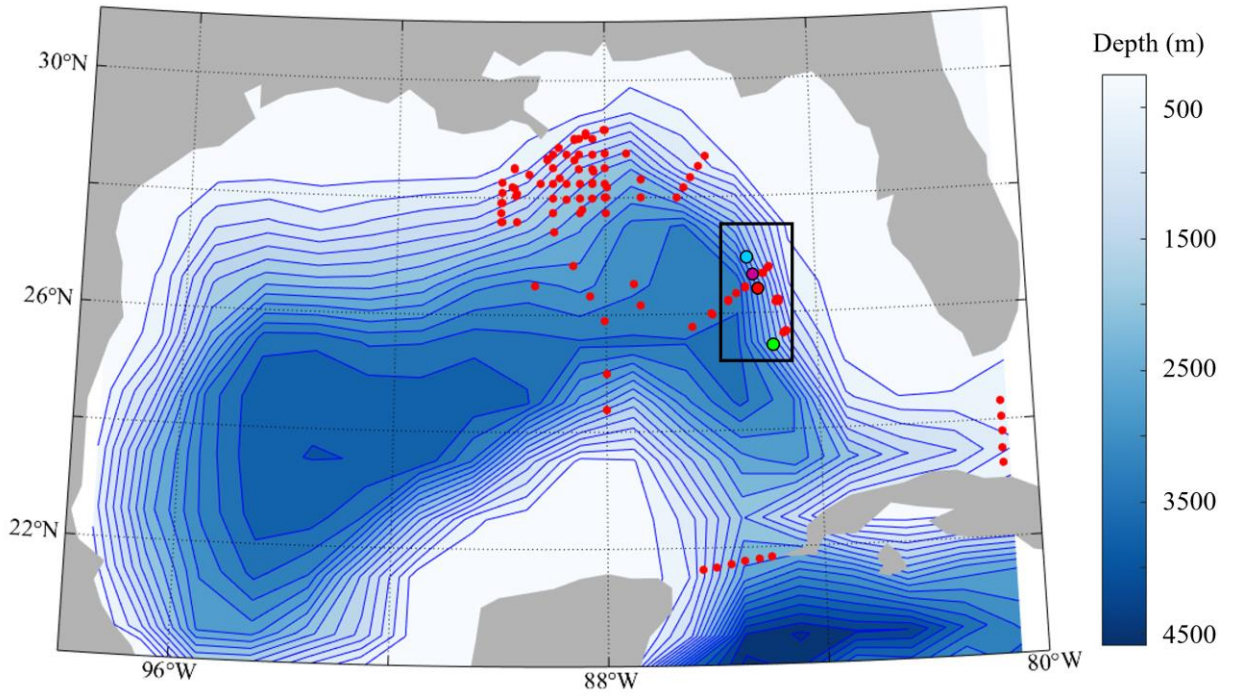

Figure 3.15: Locations of 893 samples included in water column TA, DIC, and TA:DIC models, consisting of publicly available bottle samples with full CTD, DIC, and TA data, but excluding samples that were above 300 m depth or that exhibited low salinity near the mouth of the Mississippi River. The ROV study area is highlighted in the black box.

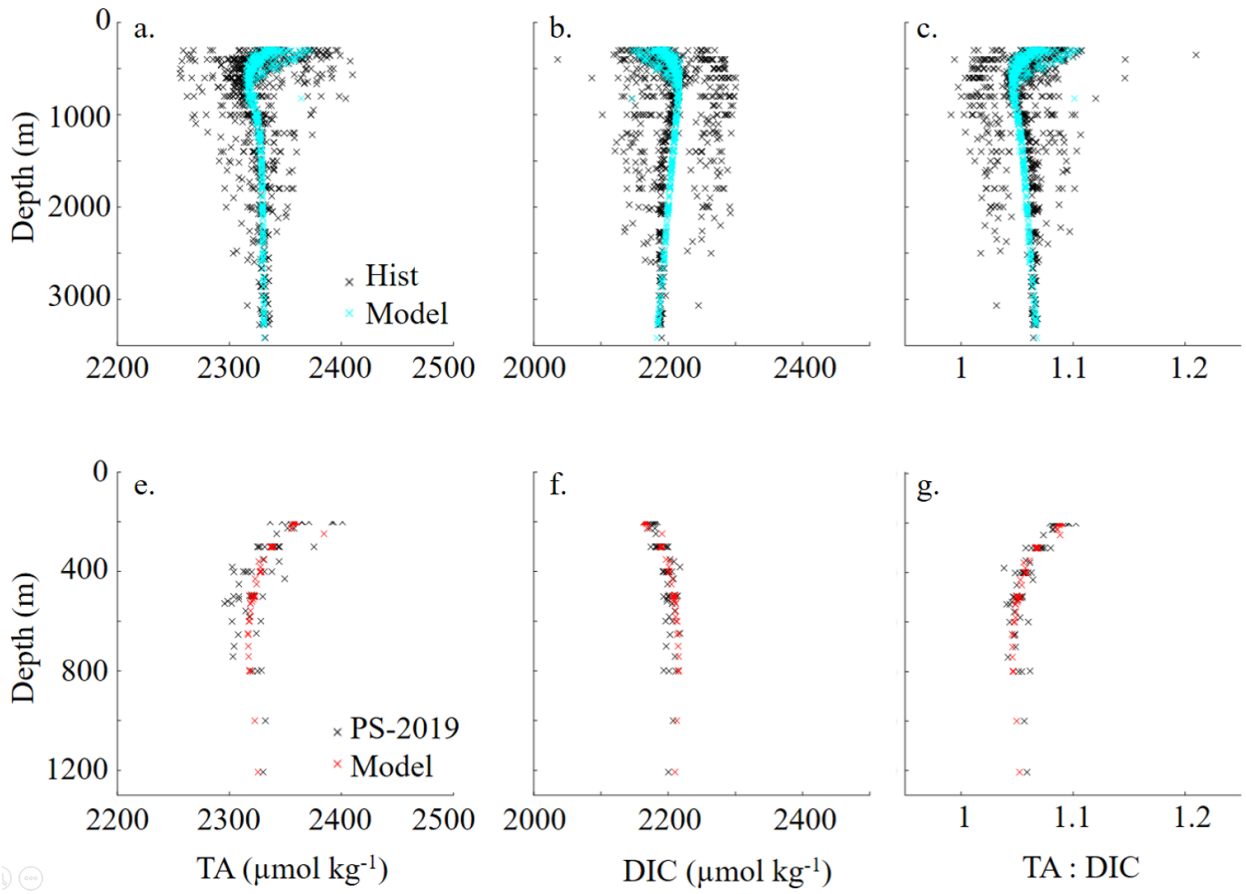

Figure 3.16: Multilinear regression model results for TA (*a*,*e*), DIC (*b*,*f*), and TA:DIC (*c*,*g*), generated by varying depth, temperature, and salinity trained on 893 historical bottle sample data (*top* panels, historical data in black and model outputs in blue), and applied to Point Sur bottle samples (*bottom* panels, samples in black and model outputs in red).

While other variables were considered in these models, including DO and nutrients, the scarcity of samples including additional variables limited the ability of these models to predict the *Point Sur* and *Hogarth* CTD data, for which nutrient data was not available. Temperature, depth, and salinity were determined to be the best set of predictors for the water column model, with R^2 calculated between model and historical values of 0.73, 0.55, and 0.82, respectively, for TA, DIC, and TA:DIC when applied to CTD casts in our study area. Coefficients for these models are provided in Table 3.5.

Similarly, we trained a multilinear regression on CHANOS II DIC to estimate seafloor DIC values in this region given depth, temperature, and salinity, with an R^2 value of 0.87. Coefficients for these models are provided in Table 3.5. We can then compare model outputs to existing CHANOS II data as well as estimate seafloor DIC where CHANOS II data is not available (Figures 3.17 – 3.20, panel *a*).

Table 3.5: Coefficients for water column TA:DIC and seafloor DIC multiple linear regression models

Coefficients	Water column TA:DIC * $TA:DIC \approx b_1 + b_2 \cdot z + b_3 \cdot T + b_4 \cdot S$	Seafloor DIC * $DIC \approx b_1 + b_2 \cdot z + b_3 \cdot T + b_4 \cdot S$
b_1	-0.4513	-413.8492
b_2	$6.1671 \cdot 10^{-6}$	2.0786
b_3	$-7.1782 \cdot 10^{-4}$	41.5175
b_4	$4.2918 \cdot 10^{-4}$	34.8178
*where *z* represents pressure (db), *T* is temperature (°C), and S is salinity		

Using the water column TA:DIC model and CHANOS II seafloor DIC, we conservatively estimated seafloor TA during the ROV dives and compared it to the few bottle samples collected for TA (Figures 3.17 – 3.20, panel *b*). CO2SYS was then used to estimate pH (total scale) and Ω_{Ar} throughout each dive (Figures 3.17 – 3.20, panel *c*) (Pierrot et al., 2006).

The seafloor DIC and TA models were most heavily influenced by depth, as can be seen in the Many Mounds dive where the ROV depth fluctuated while moving upslope over a series of deep coral mounds. This model may over rely on the depth parameter, but tuning is limited due to the lack of data available at these sites. The seafloor DIC model for the Many Mounds dive closely followed CHANOS II DIC, as expected since the model was trained on the CHANOS II ROV dataset from all 4 dives. The model was used to fill in the gaps in the CHANOS II record when the sensor was measuring CRM instead of ambient seawater. TA estimated using the water column TA:DIC and seafloor DIC regression models was closely correlated with the DIC model. The estimated TA was similar to that of the bottle samples taken during the dive. The range of CO2SYS-calculated pH values for this dive (7.0 – 8.8, mean 7.8 ± 0.3) is reasonable for these depths, but is wider than has been observed in bottle samples (Lauvset, 2021). Modeled Ω_{Ar} varied widely during this dive, ranging from 0.2 – 2.5 (mean 1.1 ± 0.6). Ω_{Ar} was less than 1 (undersaturated) for 45% of the recorded measurements in the dive, primarily in the deeper portion of the dive. However, the majority of these low Ω_{Ar} values appear where modeled DIC most poorly approximates seafloor CHANOS II values. While these models are meant to provide a conservative estimate of potential variability in carbonate parameters at depth, we acknowledge that it is difficult to evaluate the modeled pH and Ω_{Ar} values, without sufficient samples for comparison.

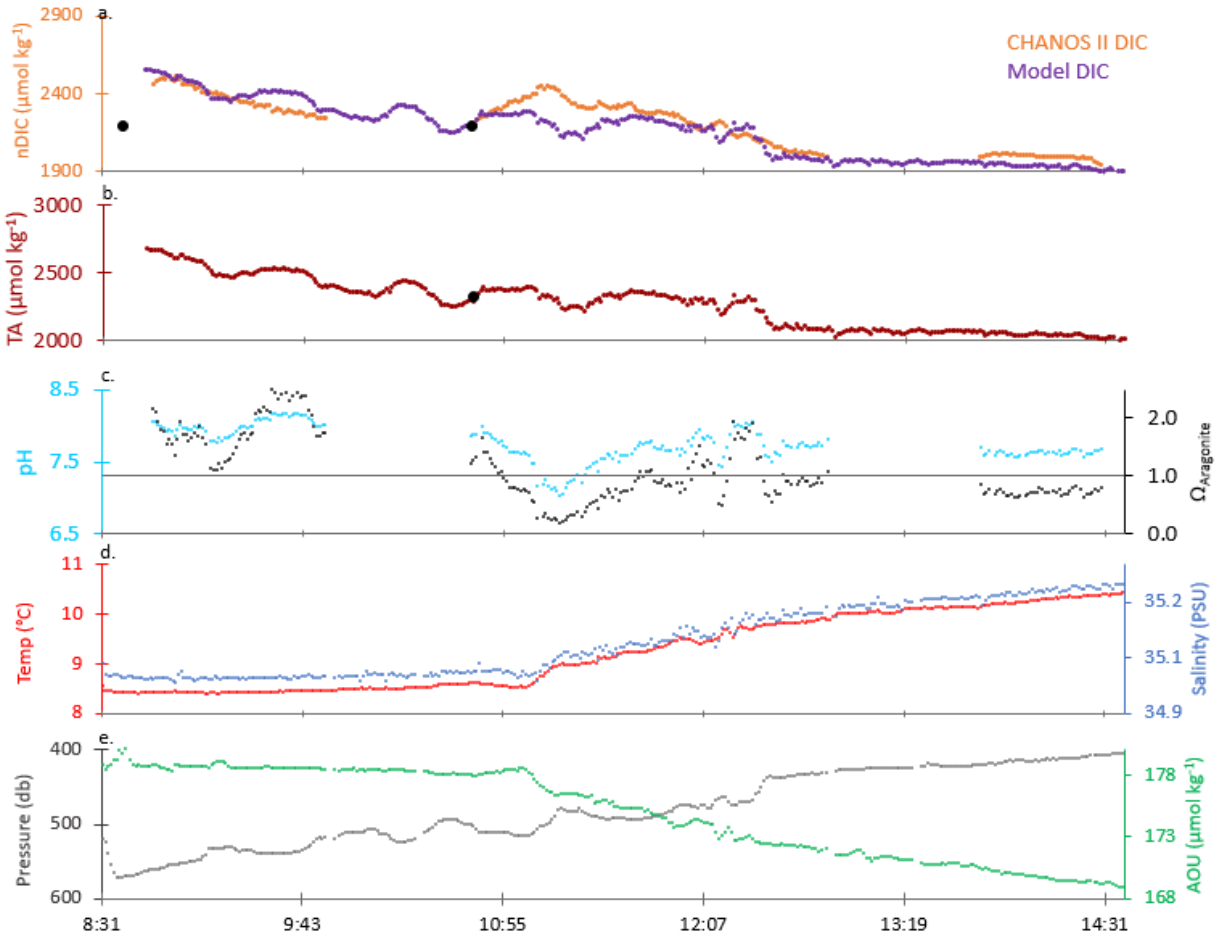

Figure 3.17: Salinity-normalized CHANOS II DIC (*orange*) and seafloor modeled DIC (*purple*) (*a*), seafloor modeled TA (*red*) (*b*), CO2sys calculated pH (*blue*) and saturation state of aragonite (Ω_{Ar}) (*black*) (*c*), ROV temperature (*red*) and salinity (*blue*) (*d*), and pressure (*grey*) and AOU (*green*) (*e*) during the Many Mounds dive, including one ROV bottle sample (black). The horizontal blue line on panel *e* indicates an aragonite saturation state of 1, below which the undersaturated conditions favor carbonate dissolution. The gaps in pH and Ω_{Ar} in panel *c* are present because these values are calculated using CO2Sys with CTD, modeled seafloor TA, and CHANOS II DIC, which saw interruptions in seafloor measurements due to in-situ CRM calibrations.

Model outputs from the remaining dives follow similar patterns. In each case, the seafloor DIC model closely followed that of the CHANOS II DIC, and the correlated TA estimate matched that of the few bottle samples collected.

There was a smaller range of CO2SYS-calculated pH values for the Okeanos Ridge dive (7.0 – 8.84 mean 7.8 ± 0.2). Ω_{Ar} varied widely during this dive, ranging from 0.2 – 3.4 (mean 1.3 ± 0.5). Ω_{Ar} was greater than 1 for 75% of the recorded measurements in the dive, primarily in the shallower portion of this dive.

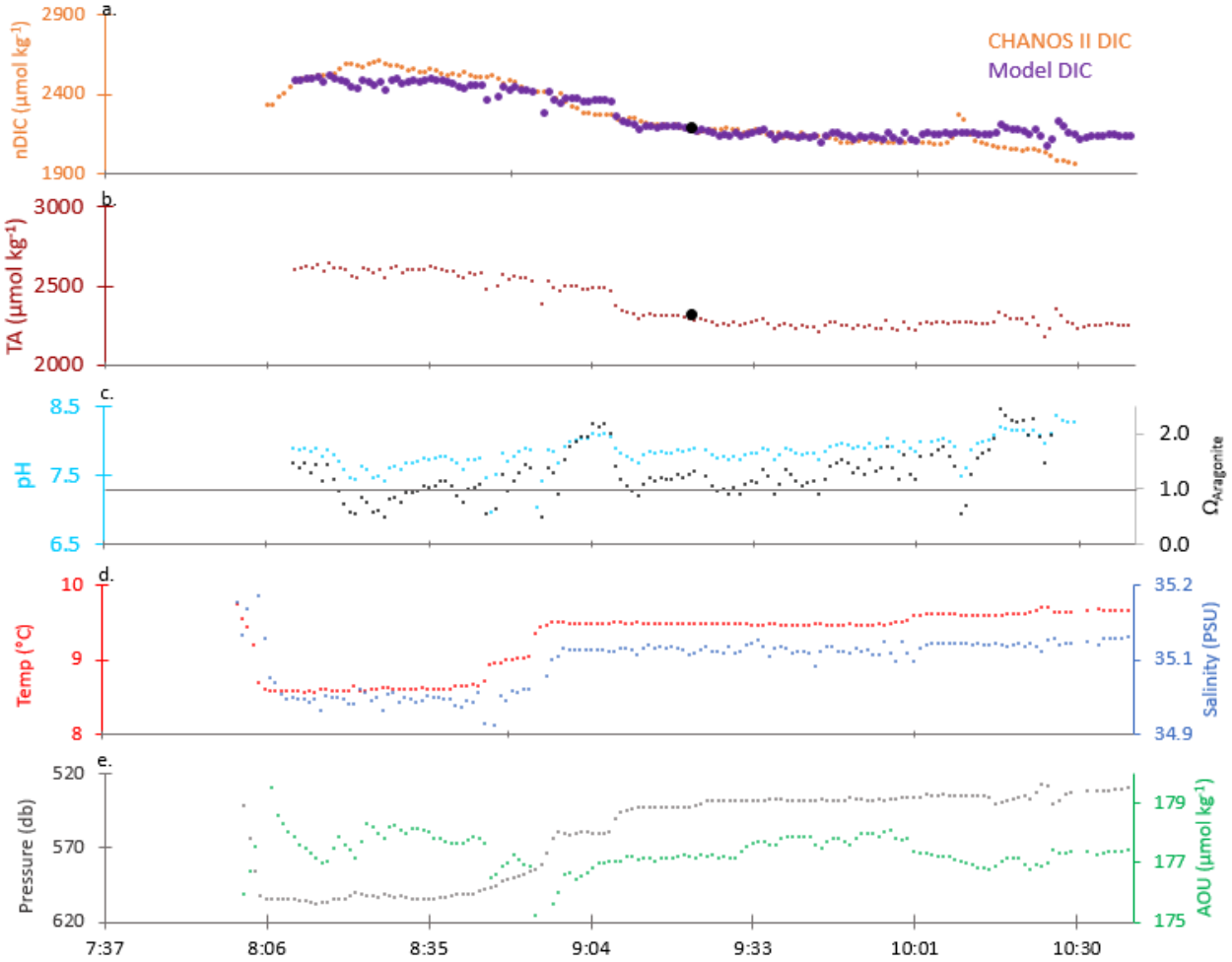

Figure 3.18: Salinity-normalized CHANOS II DIC (*orange*) and seafloor modeled DIC (*purple*) (*a*), seafloor modeled TA (*red*) (*b*), CO2sys calculated pH (*blue*) and saturation state of aragonite (Ω_{Ar}) (*black*) (*c*), ROV temperature (*red*) and salinity (*blue*) (*d*), and pressure (*grey*) and AOU (*green*) (*e*) during the Okeanos Ridge dive, including one ROV bottle sample (*black*). The horizontal blue line on panel *e* indicates an aragonite saturation state of 1, below which the undersaturated conditions favor carbonate dissolution.

There was a smaller range of CO2SYS-calculated pH values for the North Wall dive (7.4 – 8.2 mean 7.8 ± 0.2). Ω_{Ar} varied less widely during this dive, ranging from 0.5 – 2.6 (mean 1.4 ± 0.5). Ω_{Ar} was greater than 1 for 73% of the recorded measurements in the dive, again primarily in the shallower portion of this dive.

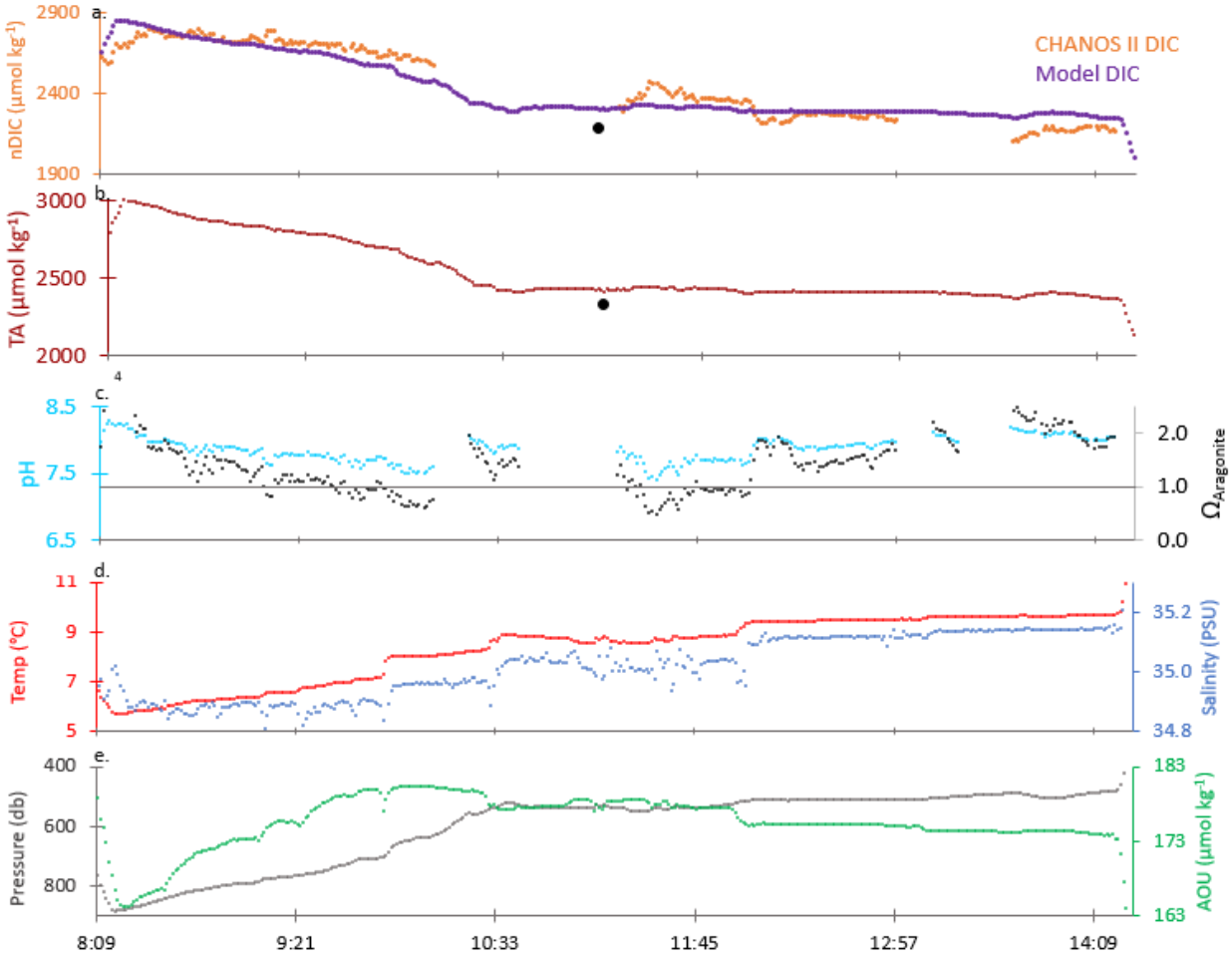

Figure 3.19: Salinity-normalized CHANOS II DIC (*orange*) and seafloor modeled DIC (*purple*) (*a*), seafloor modeled TA (*red*) (*b*), CO2sys calculated pH (*blue*) and saturation state of aragonite (Ω_{Ar}) (black) (*c*), ROV temperature (*red*) and salinity (*blue*) (*d*), and pressure (*grey*) and AOU (*green*) (*e*) during the North Wall dive, including one ROV bottle sample (*black*). The horizontal blue line on panel *e* indicates an aragonite saturation state of 1, below which the undersaturated conditions favor carbonate dissolution. The gaps in pH and Ω_{Ar} in panel *c* are present because these values are calculated using CO2SYS with CTD, modeled seafloor TA, and CHANOS II DIC, which saw interruptions in seafloor measurements due to in-situ CRM calibrations.

Finally, the smallest range in CO2SYS-calculated pH values occurred during the Long Mound dive (7.5 – 8.2 mean 7.8 ± 0.2). Ω_{Ar} varied the least during this dive, ranging from 0.6 – 2.4 (mean 1.3 ± 0.4). Ω_{Ar} was greater than 1 for 75% of the recorded measurements in the dive.

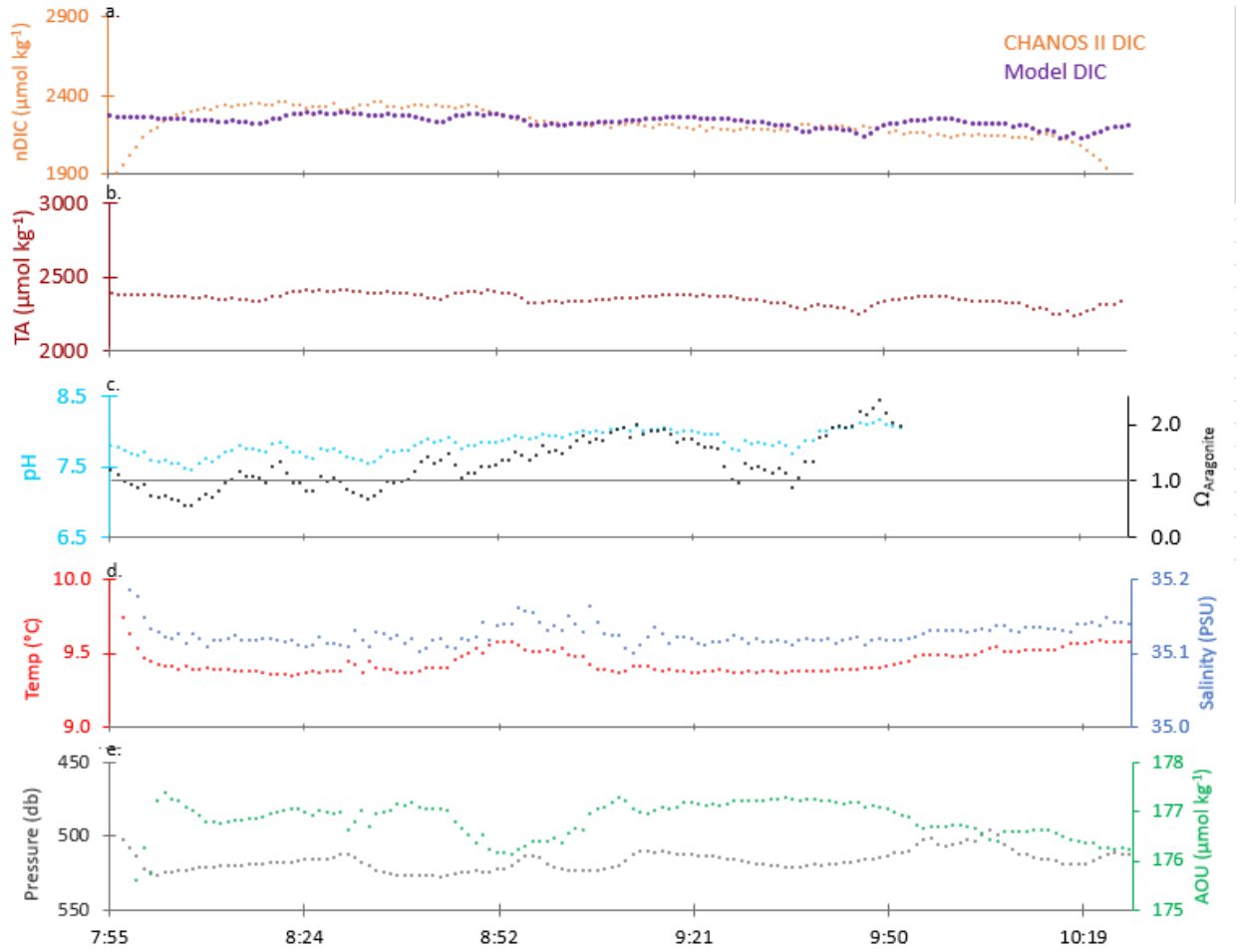

Figure 3.20: Salinity-normalized CHANOS II DIC (*orange*) and seafloor modeled DIC (*purple*) (*a*), seafloor modeled TA (*red*) (*b*), CO2sys calculated pH (*blue*) and saturation state of aragonite (Ω_{Ar}) (*black*) (*c*), ROV temperature (*red*) and salinity (*blue*) (*d*), and pressure (*grey*) and AOU (*green*) (*e*) during the Long Mound dive. The horizontal blue line on panel *e* indicates an aragonite saturation state of 1, below which the undersaturated conditions favor carbonate dissolution.

3.4 Discussion

3.4.1 Addressing large variations in CHANOS II DIC data relative to bottle samples

CHANOS II DIC and bottle samples were plotted against salinity and AOU for all dives (Figure 3.21, top panels *a* and *b*). While sensor measurements were in close agreement with bottle measurements at the time of sampling, this comparison highlights the wide discrepancy in seafloor DIC variability between bottle

samples and CHANOS II measurements, despite the small range of salinity and AOU values encountered across these sites. It may be that the agreement between CHANOS II and these bottle samples is a coincidence, and that the large variations in CHANOS II DIC between bottle sampling periods are exaggerated. However, in two dives, Okeanos Ridge and North Wall, we show that the sensor acceptably measured both secondary standard seawater and ambient seawater simultaneous to bottle samples with large (150+ µmol kg^{-1}) variations in DIC observed between these time points. There are no differences between ambient seawater and standard measurement procedures, except that the standards are pumped from storage in 2 L Calibond bags rather than from the surrounding seawater. It is unlikely that the sensor measured acceptably at each of these time points but failed in between, unless temperature, pressure, or other unknown factors impacted sensor performance between these times as the ROV flew upslope.

First, we note that the sensor was temperature calibrated in the laboratory after ROV deployments via immersion in a controlled water bath while measuring seawater of known DIC. It is more likely that pressure changes could account for the large variability in sensor DIC. CHANOS II compensates for pressure in two ways: first, the electronics housing containing the controlling boards, LED, and spectrometer is a custom cylindrical titanium pressure vessel filled with air and rated to 3000 m depth. It is unlikely that these components are impacted by pressure, but the fiber optic cables connecting the sensor's optical cell to the LED and spectrometer through the bulkhead of the electronics housing are exposed to seawater and may be jostled if the ROV moves rapidly during ascents or descents in the water column. This behavior was seen as a decrease in light signal during repeated measurements of onboard standard seawater during the initial descent (~30 m min^{-1}) to Okeanos Ridge (see section 3.3.4), but was not apparent as the ROV flew much more slowly (~6.5 m min^{-1}) over coral mounds, scarps, and wall features on the seafloor.

Second, the peristaltic pump housings on the CHANOS II are cylindrical acrylic and Delrin cylinders filled with electronic liquid (FC-770, 3M, St. Paul, MN, USA) with a custom membrane to compensate for pressure changes, with an individual housing for each pump. These housings were tested to 1500 m depth and did not develop leaks or show visible damage during pressure tests or after ROV dives. In theory, if the peristaltic pumps are appropriately pressure compensated, there should be no change in pump behavior (i.e. flow speed) with depth, however it is difficult to ascertain this behavior in laboratory or field settings. We expect the peristaltic pumps would slow under increasing pressures if they were not adequately compensated, such that seawater, acid, indicator, and reference flow rates would decrease. The flow rate of the reference pump is unimportant as long as the pump fully flushes the optical cell with reference fluid, as was evident in all reference spectra during the ROV dives. A decreased indicator flow rate may not be problematic to sensor operation: indicator flows through the equilibration and optical cells can be identified

by tracking changes in the acid and base intensities relative to the reference spectra. A decreased indicator flow rate would provide a longer time for CO_2 equilibration between the acidified sample and indicator reagent before passing through the optical cell. This behavior could require a longer running average procedure to estimate DIC as the ROV flew across the seafloor, but the relative spatial trends in DIC changes would likely be similar to those reported in Section 3.3. A decrease in seawater and acid flow rates would be more difficult to diagnose. If the acid pump slowed sufficiently that seawater was not fully acidified (pH ~3), we would likely see an increase in intensity at the acid peak at 432 nm, which did not occur during any of the dives. However, if pressure impacts on the pumps allowed for full acidification but caused the seawater and acid mixing ratio to deviate significantly from the ~200:1 expected, there could be dilution impacts that would be difficult to predict.

Aside from the electronics and pump housings, several other sensor components are subject to changing pressure with depth. Reagent bags were exposed to ambient pressure but should not be adversely impacted unless they contained air bubbles, which were not identified. Similarly, the optical cell should not experience adverse impacts from pressure unless it contained air bubbles, which we did not identify as occurring through the dive spectra. The tube-in-tube PEEK and Teflon AF 2400 equilibration cell was also exposed to pressure changes at depth, and could potentially experience pressure dependent changes in CO_2 diffusion across the Teflon barrier. This factor, as well as the potential for changes in flow rates through this cell due to pressure impacts on the pumps, merits further investigation.

Available pressure test facilities around the timing of this ROV deployment were limited to closed freshwater vessels without simultaneous temperature control (i.e. Hydrostatic Pressure Test Facility, WHOI, Woods Hole, MA, USA). A full investigation of sensor performance in the seafloor depth ranges experienced during these dives (~400 – 900 m) would involve measurement of onboard secondary standards of known DIC in the ranges measured during this deployment (~1900 – 2800 μmol kg^{-1}) conducted in a pressure test vessel, coupled with the post-cruise temperature calibration applied to sensor measurements in this study.

To further investigate potential pressure impacts on the available data, we focus on the shallowest portions of each dive, where the ROV flew upslope across minimal temperature, pressure, salinity, and AOU ranges. Figure 3.21 (top panels *a* and *b*) shows all CHANOS II DIC and bottle sample data plotted against salinity and AOU for the full depth range of all dives. The bottom panels (*c* and *d*) focus on a subset of this data in a narrowed and shallow depth range, which is indicated for each dive in Figure 3.22 and Table 3.6.

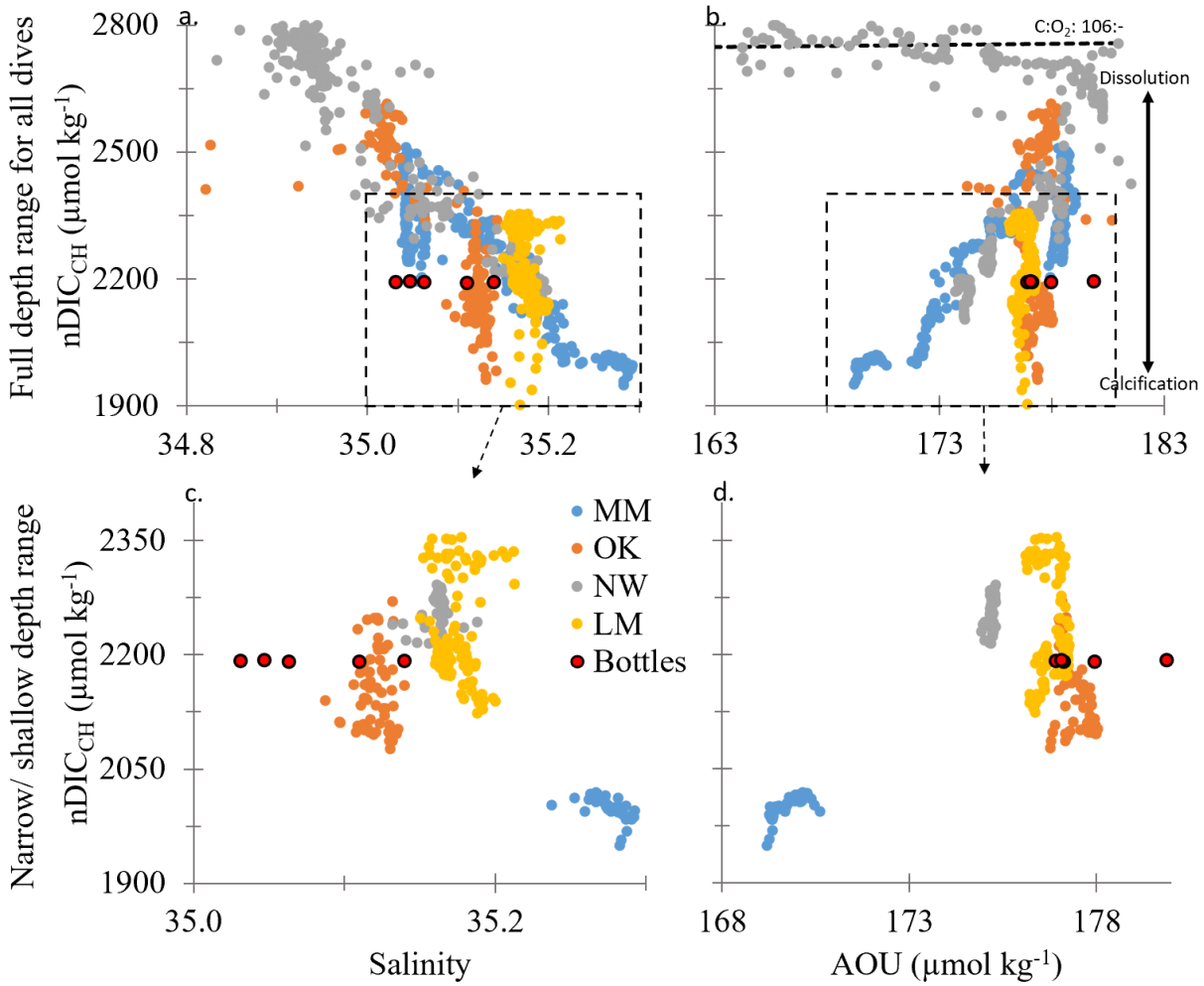

Figure 3.21: *Top*: All CHANOS II DIC measurements and bottle samples (*red*) compared to in-situ temperature salinity (*a*) and AOU (*b*) for Many Mounds (*blue*), Okeanos Ridge (*orange*), North Wall (*grey*), Long Mound (*gold*) dives. The Redfield Ratio for C:O of 106:-138 is plotted as a dashed line in panel *b*. The direction of ΔDIC for dissolution and calcification processes are indicated with the vertical black arrow. *Bottom*: Panels *c* and *d* focus on a subset of CHANOS II DIC measurements recorded only during the narrowest depth range of each dive as shown in Figure 3.22.

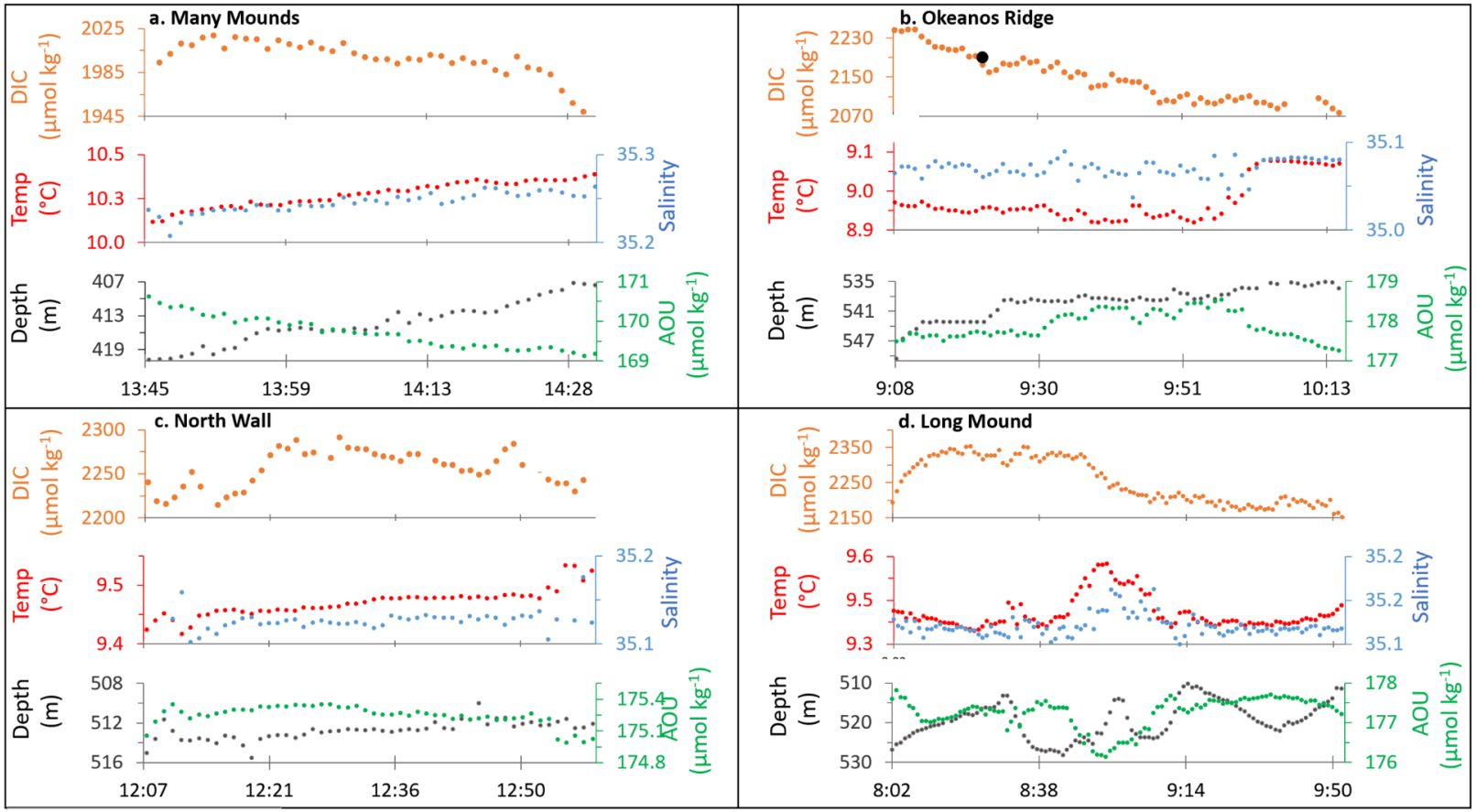

Figure 3.22 Subsets of sensor records for CHANOS II DIC (*orange*), bottle samples (*black*), temperature (*red*), salinity (*blue*), pressure (*grey*), and AOU (*green*), for Many Mounds (*a*), Okeanos Ridge (*b*), North Wall (*c*), Long Mound (*d*) dives. These data are the same as those presented in Figures 3.10-3.13, focusing only on the shallower portions of each dive where pressure changes were minimal, and the absolute range of measured parameters are as follows in Table 3.6:

Table 3.6: Absolute change in environmental parameters in narrowed dive depth range

Site:	Time:	Δ DIC (µmol kg^{-1})	Δ T (°C)	Δ S	Δ Depth (m)	Δ AOU (µmol kg^{-1})
Many Mounds	13:45 – 14:28	70	0.3	0.05	13.5	1.5
Okeanos Ridge	9:08 - 10:13	181	0.2	0.05	15.5	0.1
North Wall	12:07 – 12:58	77	0.1	0.04	5.5	0.4
Long Mound	8:02- 9:50	201	0.2	0.06	18.0	1.3

Even in this narrowed range, with variations of 5.5 – 18.0 m in depth instead of the dozens or hundreds of meters of depth experienced across the earlier portion of each dive, the CHANOS II still records DIC variations ranging from 70 – 201 μmol kg^{-1}. While it will be important to fully establish the potential impacts of changing pressure on CHANOS II measurements, it appears that removing some amount of the pressure factor by focusing on a much narrower range of depths still shows a much higher variability in seafloor CHANOS II DIC than is observed in bottle samples.

A major challenge with seafloor sensing is that the problem that the CHANOS II is meant to address in these deployments, e.g., the difficulty of collecting seafloor bottle samples from ROVs or submersibles, itself limits the amount of data available for ground-truthing in-situ sensor measurements. We note that the CHANOS II has performed acceptably (precision and accuracy ~2.9 μmol kg^{-1} and ± 5.5 μmol kg^{-1}) in other mobile deployments with more available bottle samples for laboratory comparison with sensor measurements, as shown in Chapter 2. The sensor measured onboard standards well and the residuals between sensor and bottle samples are small. This lends confidence in CHANOS II seafloor measurements, which, to the best of our knowledge, are the first of their kind in mapping DIC conditions across deep sea coral communities.

3.4.2 Placing CHANOS II data in context of benthic DIC flux estimates

Outside of potential complications when deploying the sensor at depth, there are some factors that may contribute to the larger variation in DIC as measured by the CHANOS II relative to bottle samples. The only data that followed the typical carbon to oxygen Redfield Ratio of 106:-138 was the deepest portion of the North Wall dive, which had high dissolved oxygen, relatively constant DIC, and variable AOU (Figure 3.21). This region was likely dominated by aerobic benthic respiration. DIC for the shallower portion of the North Wall dive and all other sites was much more variable, where DO was low and AOU remained mostly constant. Calcium carbonate dissolution, calcification, and anaerobic sediment processes, including denitrification and sulfate reduction or nonbiological redox reactions, likely dominated in these regions, altering DIC but not DO or AOU. Unfortunately, while some previous ROV surveys and CTD casts have been conducted at our sites, to our knowledge, there have been no sediment studies in the area. Disregarding studies from very shallow coastal seagrass beds and mangrove sites in the northern Gulf of Mexico, the nearest published benthic DIC fluxes come from a series of benthic lander sediment incubation studies in hypoxic waters ~680 km northwest of North Wall (~27-30 °N and 88-94 °W) (e.g., Rowe et al., 2002, Berelson et al., 2019; Wang et al., 2020). We are not aware of more analogous benthic flux studies at similar depths or near coral mounds. Of these studies, samples from a relatively warm, shallow site at 50 m depth

are not representative of our coral sites, but provide the most similar environmental conditions at sampled sites within the Gulf. Benthic flux studies at this site identified a large DIC flux of 84 ± 10 mmol m^2 day^{-1} and determined that manganese and iron-oxide reduction were the dominant anaerobic processes in the upper 10 cm of sediment cores, followed by denitrification (Wang et al., 2020; Devereux et al., 2019). If we define the bottom layer as 2 m off bottom, we expect a change in DIC concentration of ~41 µmol kg^{-1} day^{-1} at the seafloor.

We place our measurements in context with estimated DIC seafloor fluxes in order to evaluate the degree to which we expect variation in DIC across deep coral mounds. A benthic lander equipped with an ADCP was placed at the Many Mounds sites during the R/V *Point Sur* cruise. We note that between observations during ROV dives and lander data, the currents at Many Mounds were typically weak (<10 cm s^{-1}) and largely stagnant near the bottom, with the exception of a few events recorded during a ~7-month lander deployment. The residence time of waters over the Many Mounds site may be considered on order of several days to a week (M. Jiang, personal communication, February 2022). Unfortunately, further investigation of the benthic currents is outside of the scope of this chapter and will require future investigation into benthic lander results, though it is likely that the movement of water masses will play a significant role in evaluation of benthic carbonate chemistry.

Given flux data from Wang et al. (2020) and assuming a bottom water residence time of ~4 – 7 days at Many Mounds, we expect that sediment processes could generate a change in DIC of ~163 – 286 µmol kg^{-1} at this site. CHANOS II DIC measurements ranged between 2000 – 2454 µmol kg^{-1} across the entire Many Mounds dive, including a relatively steep portion of the dive with a ~130 m ascent. To limit the impact of depth on DIC, we focus only on the last 2 hours of the dive within a depth range of 410 – 440 m. The range of DIC observed in this portion of the dive (~2000 – 2213 µmol kg^{-1}) is on the same order of magnitude of the expected DIC flux, lending some further confidence to the DIC measurements presented.

A closer examination of sediment processes potentially impacting DIC across our coral sites is beyond the scope of this study, but a combination of $CaCO_3$ calcification and dissolution and sediment processes are all likely important contributors to the variation in DIC observed during our ROV deployments.

3.4.3 Comparing bottle samples, water column and seafloor data and model outputs

The difference between water column data and seafloor model outputs for DIC and TA is significant, with similar water column and seafloor values only between depths of ~450 - 575 m (DIC) and ~460 – 500 m

(TA) (Figure 3.22). pH and Ω_{Ar} estimates from CO2SYS calculations on water column and modeled seafloor data are both in relative agreement for a larger range of depths (~450 - 600 m and 700 – 800 m). Seafloor ROV bottle samples and CTD rosette data are similar at all depths for which ROV samples were available. According to our model outputs, Ω_{Ar} may vary widely at the seafloor, frequently approaching or dipping into conditions of undersaturation in regions where deep coral communities live. CO2SYS calculations using DIC and TA from historical West Florida slope water column CTD samples produced a limited range in pH (7.79 - 7.95) and Ω_{Ar} (1.07 – 1.55) at depths of 400 - 800 m where corals, particularly *L. pertusa*, were observed.

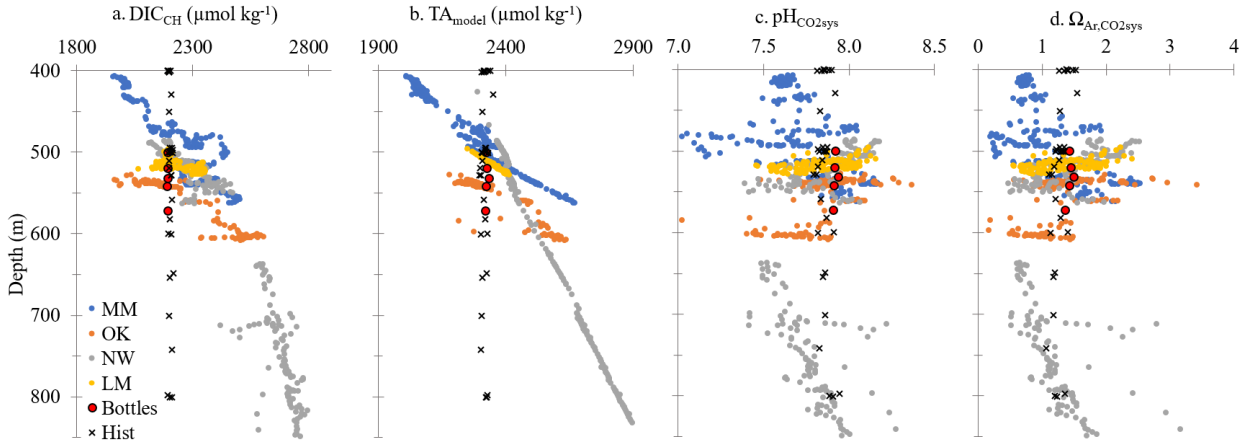

Figure 3.23: CHANOS II DIC (*a*) and conservative TA (*b*), pH (*c*), and Ω_{Ar} (*d*) model estimates plotted against depth for each ROV site, compared to ROV bottle samples (red) and historical water column bottle samples (x) collected via CTD rosette above all sites for Many Mounds (*blue*), Okeanos Ridge (*orange*), North Wall (*grey*), and Long Mound (*gold*) dives.

When comparing sensor data and model estimates to historical CTD cast data at various depths, we note that two biases in sampling may impact our range of observations at the seafloor. The first is that with a maximum of two Niskin bottles available per dive, there was a clear bias in sampling locations. Each sample was taken next to a live, dense *L. pertusa*. These sites were chosen to best represent the environmental conditions experienced by these live corals, some of which were collected for a complementary growth study. It seems unlikely that seafloor DIC is as uniform as the few bottle samples collected might lead us to believe, given that the samples are taken above active coral communities just above the sediment-water interface, where pore water is frequently elevated in DIC compared to that of the water column above. It is possible that the bias in sampling locations may help to explain some of the uniformity in bottle samples collected during the dives, representing healthy coral locations while missing skeletal coral rubble or regions of the seafloor uninhabited by corals.

The second sampling bias comes from CTD rosette casts, which may not accurately represent conditions at the seafloor. For the safety of both instrumentation and seafloor habitats, CTD casts generally stop ~2 m off bottom at best and are often terminated 10 m or more off bottom. For this reason, the historical water column data and regression models should be viewed as a conservative estimate of potential variability in seafloor conditions. Of the 893 historical samples used to train water column TA:DIC models, 168 samples were identified as the deepest sample from a CTD cast. 42% of these samples did not report a bottom depth, but of the remainder, only 12% of samples were collected within 2 m of the seafloor. 35% of samples were collected 10 m of the seafloor, and the remainder ranged to 200+ m off bottom (see Figure 3.24). Clearly, even the deepest CTD samples do not always represent seafloor conditions. While the sample size of the deepest historical CTD samples in this region is low and DIC profiles appear to converge at depth, it appears that there may be some additional variability in DIC nearest the seafloor. By contrast, CHANOS II DIC measurements taken from the bottom of the ROV were always within 1.5 m of the bottom, averaged 1.2 m off bottom, and were closer to the seafloor whenever the ROV settled for coral or water sampling.

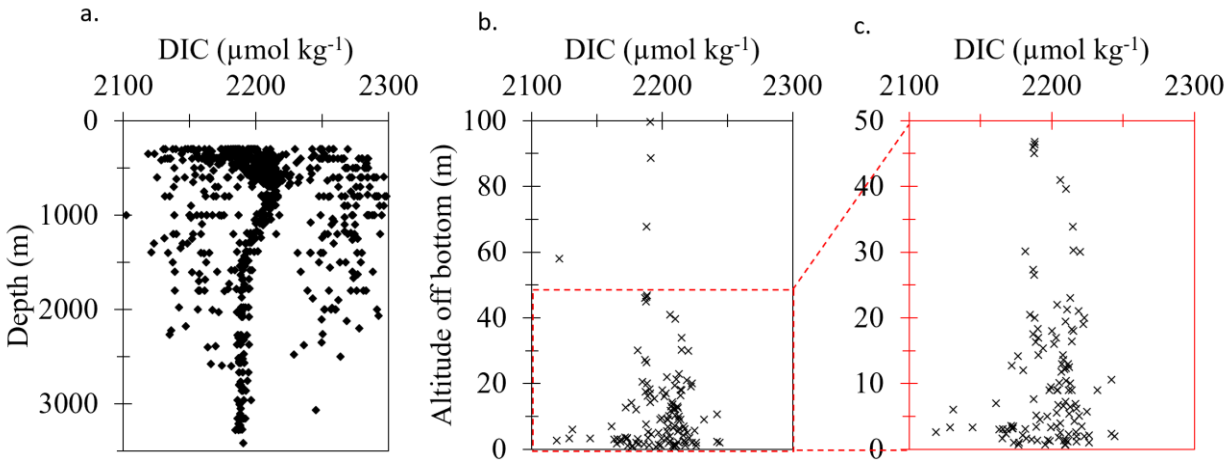

Figure 3.24: *Left*: DIC of historical CTD bottle samples plotted versus depth (*a*). *Middle*: DIC of the single deepest sample from each historical CTD cast versus the altitude off-bottom for samples with known bottom depth (*b*). *Right*: DIC versus altitude off-bottom in middle panel *b*, zoomed into the bottom 50 m off-bottom (*c*).

3.4.4 Implications of seafloor inorganic carbon conditions on coral habitats

The range of DIC values for shallow sloped portions of the other ROV dives are shown in Table 3.7, along with the average coral abundance for all taxa, grouped by minute. We observe that for similar portions of the four ROV dives, i.e., in shallow sloped regions of similar depth ranges with a similar range of DIC, DIC is increasingly variable for sites with increasing coral abundance, as shown in Figure 3.25. It is therefore possible that the DIC variation in these regions is partially driven by calcification at live coral mounds, which would cause a decrease in DIC for sites with higher coral abundance, such as Okeanos Ridge, relative

to sites with a low coral abundance, such as North Wall. Similarly, dissolution of dead coral skeletons could result in an increase in DIC, as hypothesized by Lunden et al., (2013) and Georgian et al., (2016).

Table 3.7: Summary of DIC variation during shallow portions of ROV dives

Location	Depth range (m)	Observed range in DIC (µmol kg^{-1})	Δ DIC (µmol kg^{-1})	Average coral taxa abundance (min^{-1})
Many Mounds	410 – 440	2000 - 2213	213	7.9
Okeanos Ridge	530 – 543	1962 - 2233	271	14.9
North Wall	496 – 512	2117 - 2229	112	2.3
Long Mound	506 – 520	2123 - 2352	229	9.3

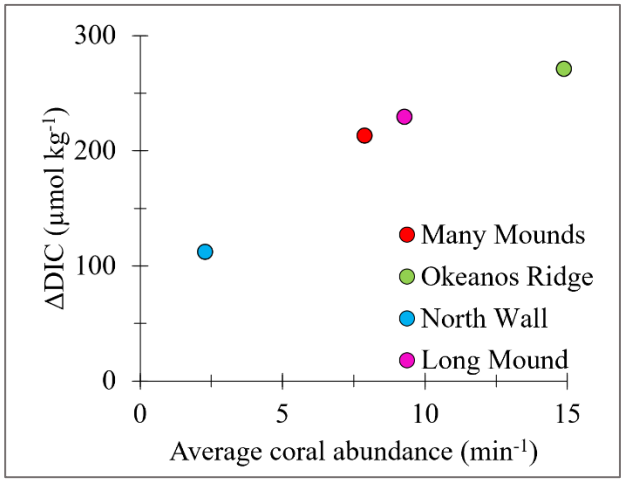

Figure 3.25: Change in CHANOS II DIC observed during shallow sloped regions of similar depth ranges across all dives versus average coral abundance observed in the ROV field of view.

The relationship between coral distribution and conditions of low pH and Ω_{Ar} may have important implications to the health of deep coral communities in the changing oceans. The sensor data and model outputs presented here show a snapshot of conditions at the seafloor during several short dives. We show that Ω_{Ar} is frequently estimated at or below a value of 1, representing undersaturated conditions corrosive to aragonite structures. However, while the currents noted during the Many Mounds dive were small, it is possible that as the Loop Current and associated eddies meander through the region, environmental conditions may shift rapidly. If the conditions reported here are common to this region, these deep coral communities may be relatively resilient to chemical changes resulting from ocean acidification. It is important to establish the occurrence of conditions as recorded during this time to determine whether this study provides baseline measurements for this region. Efforts to understand the potential temporal variation in inorganic carbon chemistry at these sites may be best addressed by repeated ROV dives equipped with inorganic carbon sensors and multiple Niskin bottles, complemented by the deployment of benthic landers fully instrumented with CTD, inorganic carbon, and current sensors to capture both short term and seasonal variation in inorganic carbon chemistry, taking into account water mass movement, internal tide forcing, advection, and other physical factors. It is likely that inorganic carbon chemistry is also dependent on factors

including benthic metabolism and reef morphology; in-situ coral growth and dissolution studies would help to clarify the importance of these factors. Benthic flux experiments and sediment core collection would help to clarify sediment-water interface dynamics at these sites.

3.5 Summary

DIC variation in the deep sea may be driven by a variety of factors, including changes due to depth, water mass movement, calcification and dissolution, and sediment-water fluxes. Our understanding of seafloor inorganic carbon chemistry across deep coral communities has been limited by the scarcity of bottle samples from ROVs or other submersibles and the operating limit of CTD rosette casts to 2+ m above the seafloor. In this chapter, we demonstrated the use of the CHANOS II sensor in mapping DIC across deep coral mounds on small spatial scales (<100 m). While few bottle samples are available to ground-truth sensor data at depth, the bottle sample and in-situ standard measurement data that are available suggest that the CHANOS II operated acceptably during the dives presented. While ROV bottle samples analyzed for DIC and TA did not vary significantly between dives or depths, the CHANOS II sensor measured significant (hundreds of μmol kg^{-1}) variations in DIC across ROV dives. These data suggest that sampling location bias and scarcity prevent us from capturing seafloor ROV variability through discrete bottle samples, such as is measured by the CHANOS II sensor. Given the proximity to the sediment-water interface and complicated coral community structure and dynamics at these sites, it is reasonable to expect some variability in seafloor DIC above that of the bottle samples collected.

Multiple linear regression models trained on historical water column data and seafloor DIC provide a conservative estimate of seafloor TA, pH, and Ω_{Ar}, which all vary significantly at the seafloor. Ω_{Ar} in particular fluctuates between conditions of under and oversaturation, which may be important to the ability of deep corals to flourish under ocean acidification, warming, and other changing oceans.

A priority in future work on this subject is to confirm the range in seafloor DIC variability by increasing the number of Niskin bottles carried onboard ROVs or submersibles and repeating dives at individual deep coral sites to avoid the sampling bias experienced during our dives. Seafloor models can be improved by the addition of separate commercial sensors or CHANOS II channels to simultaneously capture pH or pCO_2 along with DIC. This would allow for full resolution of the inorganic carbon system during any given dive, rather than relying on calculation of TA from models partially trained on CHANOS II DIC data. In-situ data collected can be fed back into models as described above, which may be improved by collection of

additional parameters, particularly by standard oceanographic nutrient analysis on Niskin samples collected in both the water column and seafloor. Such models will allow for estimation of seafloor inorganic carbon conditions given ROV CTD measurements in this region regardless of sensors carried onboard, allowing for increased seafloor studies at decreased cost. Furthermore, after improving these models with additional training data, they could be applied to CTD data collected from past ROV transects at these locations, providing conservative estimates in seafloor inorganic carbon chemistry at discrete periods of time over the past several years. Data collected by these dives and the models generated may be further used in regional oceanographic models to improve our understanding of carbon cycling in this region. They may also be useful in resource management, as a link between variability in inorganic carbon chemistry and distributions of corals may help to identify priority areas for protection from bottom fishing impacts.

3.6 Acknowledgements

We are grateful to the crew of the R/V *Point Sur* and Oceaneering's ROV *Global Explorer* team, who helped us to seamlessly integrate the CHANOS II into CTD Rosette and ROV systems. We thank the WHOI machine shop for a speedy frame job to support the CHANOS II. We thank Sandra Brooke for coral and benthic community expertise, Gabby Fulton for additional ROV video analysis, and Mingshun Jiang for physical oceanography assistance. This work was supported by a NOAA OER grant (Award No. NA18OAR0110352), as well as CHANOS II funds as stated in Chapter 2, and an internal WHOI Grassle fund.

3.7 References

Andersson, A.J., Kuffner, I.B., Mackenzie, F.T., Jokiel, P.L., Rodgers, K.S., and Tan, A., 2009. Net loss of $CaCO_3$ from a subtropical calcifying community due to seawater acidification: mesocosm-scale experimental evidence. Biogeosciences, v. 6, pp. 1811-1823.

Bates, N.R., Amat, A., Andersson, A.J., 2010. Feedbacks and responses of coral calcification on the Bermuda reef system to seasonal changes in biological processes and ocean acidification. Biogeosciences, v. 7, pp. 2509-2530.

Berelson, W.M., McManus, J., Severmann, S., and Rollins, N., 2019. Benthic fluxes from hypoxia-influenced Gulf of Mexico sediments: Impact on bottom water acidification. Marine Chemistry, v. 209, pp. 94-106.

Brooke, S., and Schroeder, W.W., 2007. Chapter 7: State of deep coral ecosystems in the Gulf of Mexico region: Texas to the Florida Straits In: The State of Deep Coral Ecosystems of the United States (Eds. Lumsden, S.E., Hourigan, T.F., and Bruckner, A.W.). NOAA Technical Memorandum NOS-CRCP-3, Silver Spring MD: p 271-306

Brooke, S., and Young, C.M., 2009. Direct measurements of *in-situ* survival and growth of *Lophelia pertusa* in the northern Gulf of Mexico. Marine Ecology Progress Series, v. 397, pp.153-161

Brooke, S., Ross, S.W., Bane, J.M., Seim, H.E., and Young, C.M., 2013. Temperature tolerance of the deep-sea coral *Lophelia pertusa* from the southeastern United States. Deep Sea Research II, v. 92, pp. 240-248.

Brooks, J.M., Fisher, C., Roberts, H., Cordes, E., Baums, I., Bernard, B., Church, R., Etnoyer, P., German, C., Goehring, E., McDonald, I., Roberts, H., Shank, T., Warren, D., Welsh, S., Wolff, G., and Weaver, D., 2015. Exploration and research of northern Gulf of Mexico deep-water natural and artificial hard-bottom habitats with emphasis on coral communities: Reefs, rigs, and wrecks "*Lophelia* II" Final report. OCS Study BOEM 2016-021. p. 628.

Carpenter, K., Abrar, M., Aeby, G., Aronson, R.B., Banks, S., Bruckner, A., …, and Wood, E., 2008. One third of reef-building corals face elevated extinction risk from climate change and local impacts. Science, v. 321, pp. 560-563.

Chassignet, E.P., Hurlburt, H.E., Metzger, E.J., Smedstad, O.M., Cummings, J.A., Halliwell, G.R., …, and Wilkkin, J., 2009. US GODAE: global ocean prediction with the HYbrid Coordinate Ocean Model (HYCOM). Oceanography, v. 22, pp. 64-75.

Cherubin, L.M., Morel, Y., and Chassignet, E.P., 2006. , Loop current ring shedding: The formation of cyclones and the effect of topography. Journal of Physical Oceanography, v. 36, pp.569-591.

CSA International, Inc. 2007. Characterization of northern Gulf of Mexico deep-water hard bottom communities with emphasis on *Lophelia* coral. U.S. Department of the Interior, Minerals Management Service, Gulf of Mexico OCS Region, New Orleans, LA. OCS Study MMS 2007-044. 169 pp. + app.

Davies, A.J., Duineveld, G.C.A., van Weering, T.C.E., Mienis, F., Quattrini, A.M., Seim, H.E., Bane, J.M., and Ross, S.W., 2010. Short-term environmental variability in cold-water coral habitat at Viosca Knoll, Gulf of Mexico. Deep Sea Research Part I: Oceanographic Research Papers, v. 57, pp. 199-212.

Devereux, R., Lehrter, J.C., Cicchetti, G., Beddick, D.L., Yates, D.F., Jarvis, B.M., et al., 2019. Spatially variable bioturbation and physical mixing drive the sedimentary biogeochemical seascape in the Louisiana continental shelf hypoxic zone. Biogeochemistry, v. 143, pp. 151-169.

Dodds, L. A., Roberts, J.M., Taylor, A.C., and Marubini, F., 2007. Metabolic tolerance of the cold-water coral *Lophelia pertusa* (Schleractinia) to temperature and dissolved oxygen change. Journal of Experimental Marine Biology and Ecology, v. 249, pp. 205-214.

Dickson, A.G., and Riley, J., 1978. The effect of analytical error on the evaluation of the components of the aquatic carbon-dioxide system. Marine Chemistry, v. 6, pp. 77-85.

Dickson, A.G., Sabine, C.L., and Christian, J.R., 2007. Guide to best practices for ocean CO_2 measurements. North Pacific Marine Science Organization.

Fassbender, A.J., Sabine, C.L., Lawrence-Slavas, N., De Carlo, E.H., Meinig, C., and Jones, S.M., 2015. Robust sensor for extended autonomous measurements of surface ocean dissolved inorganic carbon. Environmental Science and Technology, v. 49, pp. 3628-3635.

Findlay, H.S., Hennige, S.J., Wicks, L.C., Navas, J.M., Woodward, E.M.S., and Roberts, J.M., 2014. Fine-scale nutrient and carbonate system dynamics around cold-water coral reefs in the northeast Atlantic. Scientific Reports, v. 4, pp. 1-10.

Georgian, S.E., Dupont, S., Kurman, M., Butler, A., Strömberg, S.M., Larsson, A.I., and Cordes, E.E., 2016. Biogeographic variability in the physiological response of the cold-water coral *Lophelia pertusa* to ocean acidification. Marine Ecology, doi: 10.111/maec.12373

Gómez, C.E., Wices, L., Deega, D., Etnoyer, P.J., and Cordes, E.E., 2018. Growth and feeding of deep-sea coral *Lophelia pertusa* from the California margin under simulated ocean acidification conditions. PeerJ,, v. 6, p. e5671.

GMFMC, 2017. Coral Habitat Areas Considered for Management in the Gulf of Mexico. Public hearing draft for Amendment 9 to the Fishery Management Plan for Coral and Coral Reefs of the Gulf of Mexico, US Waters. Gulf of Mexico Fishery Management Council, November 2017, Tab N, No.5 pp.19

Gula, J., Molemaker, M.J., and McWilliams, J.C., 2015. Gulf Stream Dynamics along the Southeastern U.S. Seaboard. Journal of Physical Oceanography, v. 45, pp. 690-715.

Hebbeln, D., Weinberg, C., Dullo, W.C., Freiwald, A., Mienis, F., Orejas, C., and Titschack, J., 2020. Cold-water coral reefs thriving under hypoxia. Coral Reefs, v. 39, pp. 853-859.

Hennige, S.J., Wicks, L.C., Kamenos, N.A., Bakker, D.C.E., Findlay, H.S., Dumousseaud, C., and Roberts, J.M., 2014. Short-term metabolic and growth responses of the cold-water coral *Lophelia pertusa* to ocean acidification. Deep Sea Research Part II: Topical Studies in Oceanography. v. 99, pp. 27-35.

Hennige, S.J., Wicks, L.C., Kamenos, N.A., Perna, G., Findlay, H.S., and Roberts, J.M., 2015. Hidden impacts of ocean acidificationi to live and dead coral framework. Proceedings of the Royal Society B: Biological Sciences. v. 282, 20150990.

Hoegh-Guldberg, O., Mumby, P.J., Hooten, A.J, Steneck, R.S., Greenfield, P., Gomez, E., …, and Hatziolos, M.E., 2007. Coral Reefs under rapid climate change and ocean acidification. Science, v. 318, pp. 1737-1742

Jiang, M.S., Pan, C., Barbero, L., Reed, J., Salisbury, J., VanZwieten, J., and Wanninkhof, R., 2020. Variability of bottom carbonate chemistry over the deep coral reefs in the Florida Straits and the impacts of meso-scale processes. Ocean Modeling, v. 147, 101555.

Jiang, M., Salisbury, J., and VanZwieten, J., H., *in revision.* Eddies and frontal processes drive phytoplankton blooms in the Florida Straits and carbon export to the deep coral reefs. Journal of Geophysical Research: Oceans.

Kourafalou, V.H., and Kang, H., 2012. Florida Current meandering and evolution of cyclonic eddies along the Florida Keys Reef Tract: Are they interconnected? Journal of Geophysical Research, v. 117, C5.

Kurman, M.D., Gómez, C.E., Georgian, S.E., Lunden, J.J., and Cordes, E.E., 2017. Intra-specific variation reveals potential for adaptation to ocean acidification in a cold-water coral from the Gulf of Mexico. Frontiers in Marine Science, v. 4, pp. 111.

Lauvset, S.K., Lange, N., Tanhua, T., et al., 2021. Global Ocean Data Analysis Project version 2.2021 (GLODAPv2.2021). NCEI Accession 0237935. NOAA National Centers for Environmental Information. Dataset. https://doi.org/10.25921/ttgq-n825. Accessed January 2022.

Le Hénaff, M., Kourafalou, V. H., Morel, Y., Srinivasan, A., 2012. Simulating the dynamics and intensification of cyclonic Loop Current Frontal Eddies in the Gulf of Mexico, Journal of Geophysical Research, v. 117, C2.

Leichter, J.J., Stokes, M.D., and Genovese, S.J., 2008. Deep water macroalgal communities adjacent to the Florida Keeys reef tract. Marine Ecology Progress Series, v. 356, pp. 123-138.

Lunden, J., Georgian, S.E., and Cordes, E.E., 2013. Aragonite saturation states at cold-water coral reefs structured by *Lophelia pertusa* in the northern Gulf of Mexico. Limnology and Oceanography, v. 58, pp. 354-362.

Lunden, J., McNicholl, C.G., Sears, C.R., Morrison, C., and Cordes, E.E., 2014. Acute survivorship of the deep sea coral *Lophelia pertusa* from the Gulf of Mexico under acidification, warming, and deoxygenation, Frontier in Marine Science, v. 1, pp. 78.

Maier, C., Hegeman, J., Weinbauer, M.G., and Gattuso, J.-P., 2009. Calcification of the cold-water coral *Lophelia pertusa* under ambient and reduced pH. Biogeosciences, v. 6, pp. 1671-1680.

McDougall, T.J., and Barker, P.M., 2011. Getting started with TEOS-10 and the Gibbs Seawater (GSW) oceanographic toolbox. SCOR/IAPSO WG127, ISBN 978-0-646-55621-5.

Mesinger, F., DiMego, G., Kalnay, E., Mitchell, K., Shafran, P.C., Ebisuzaki, W., and Shi, W., 2006. North American regional reanalysis. Bulletin of the American Meteorological Society, v. 87, pp. 343-360.

Millero, F.J., 2007. The Marine Inorganic Carbon Cycle. Chemical Reviews, v. 107, pp. 308-341.

Newton, C.R., Mullins, H.T., Gardulski, A.F., Hine, A.C., and Dix, G.R., 1987. Coral mounds on the West Florida Slope: Unanswered questions regarding the development of deep-water banks. Society for Sedimentary Geology, v. 2, pp. 359-367.

NOAA National Database for Deep-Sea Corals and Sponges, v. 20190117-0. NOAA Deep Sea Coral Research & Technology Program. https://deepseacoraldata.noaa.gov/

Pandolfi, J.M., Connolly, S.R., Marshall, D.J., and Cohen, A.L., 2011. Projecting coral reef futures under global warming and ocean acidification. Science, v. 333, pp. 418-422.

Pierrot, D., Lewis, E., and Wallace, D.W.R., 2006. MS Excel program developed for CO2 system calculations. ORNL/CDIAC-105a. Carbon Dioxide Information Analysis Center, Oak Ridge National Laboratory, U.S. Department of Energy, Oak Ridge, Tennessee.

Portela, E., Tenreiro, M.., Pallàs-Sanz, E., Meunier, T., Ruiz-Angulo, A., Sosa-Gutiérrez, R., and Cusí, S., 2018. Hyddrography of the Central and Western Gulf of Mexico. Journal of Geophysical Research: Oceans, v. 123, pp..5134-5149.

Reed, J.K., Messing, C., Walker, B., Brooke, S., Correa, T., Brouwer, M., Udouj, T., and Farrington, S., 2013. Habitat characterization, distribution, and areal extent of deep-sea coral ecosystem habitat off Florida, southeastern United States. Journal of Caribbean Science, v. 47, pp. 13-30.

Reed, J.K., Weaver, D.C., and Pomponi, S.A., 2006. Habitat and fauna of deep-water *Lophelia pertusa* coral reefs off the southeastern U.S.: Black Plateau, Straits of Florida, and Gulf of Mexico. Bulletin of Marine Science, v. 78, pp. 343-375.

Roberts, J.M., Wheeler, A.W., Freiwald, A., and Cairns, S., (Eds.), 2009. Cold-water corals: the biology and geology of deep-sea habitats. Cambridge University Press. pp 334

Ross, S.W., and Nizinski, M.S., 2007, State of Deep Coral Ecosystems in the U.S. Southeast Region: Cape Hatteras to southeastern Florida. p. 233-270, Ch. 6, In: Lumsden, S.E., T.F. Hourigan, A.W. Bruckner and G. Dorr (eds.). The State of Deep Coral Ecosystems of the United States. NOAA Tech. Memo. CRCP-3. Silver Spring, MD. 365 pp.

Ross, S.W., Brooke, S., Quattrini, A., Rhode, M., and Watterson, J.C., 2015. A deep-sea community at unusually shallow depths in the western North Atlantic Ocean off northeastern Florida. Marine Biology, v.162, pp. 635-648.

Ross, S.W., Rhode, M., and Brooke, S.D., 2017. Deep sea coral and hardbottom habitats on the west Florida slope, eastern Gulf of Mexico. Deep Sea Research II, v. 120, pp. 14-28.

Rowe, G.T., Kaegi, M.E.C., Morse, J.W., Boland, G.S., and Briones, E.G.E., 2002. Sediment community metabolism associated with continental shelf hypoxia, Northern Gulf of Mexico. Estuaries, v. 25, pp. 1097-1106.

Shchepetkin, A.F., and McWilliams, J.C., 2005. The regional oceanic modeling system (ROMS): a split-explicit, free-surface, topography-following-coordinate oceanic model. Ocean Modeling, v. 9, pp. 347-404.

Thresher, R.E., Tilbrook, B., Fallon, S., ,Wilson, N.C., and Adkins, J., 2011. Effects of chronic low carbonate saturation levels on the distribution, growth and skeletal chemistry of deep-sea corals and other seamount megabenthos. Marine Ecology Progress Series, v. 4422, pp. 87-99.

Turley, C.M., Roberts, J.M., and Guinotte, J.M., 2007. Corals in deep-water: will the unseen hand of ocean acidification destroy cold-water ecosystems? Coral Reefs, v. 26, pp. 445-448.

Vukovich, F.M., and Maul, G.A., 1985. Cyclonic eddies in the eastern Gulf of Mexico. Journal of Physical Oceanography, v. 15, pp. 105–117.

Wang, H., Lehrter, J., Maiti, K., Fennel, K., Laurent, A., Rabalais, R., et al., 2020. Benthic respiration in hypoxic waters enhances bottom water acidification in the northern Gulf of Mexico. Journal of Geophysical Research: Oceans, v. 125, e2020JC016152.

Wagner, D., Etnoyer, P., Nizinski, M., Schmahl, G.P., Hickerson, E., Sterne, T., and Nuttall, M., 2018. Southeast Deep Coral Initiative: Exploring Deep-Sea Coral Ecosystems off the Southeast United States. Oceanography, v. 31, pp. 98-99.

Wang, Z.A., Wanninkhof, R., Cai, W.J., Byrne, R.H., Hu, X., P., Peng, T.H., and Huang, W.J., 2013. The marine inorganic carbon system along the Gulf of Mexico and Atlantic coasts of the United States: Insights from a transregional coastal carbon study. Limnology and Oceanography, v.58, pp. 325-342.

Wang, Z.A., Sonnichsen, F.N., Bradley, A.M., Hoering, K.A., Lanagan, T.M., Chu, S.N., Hammar, T.R., and Camilli, R., 2015. In-situ sensor technology for simultaneous spectrophotometric measurements of seawater total dissolved inorganic carbon and pH. Environmental Science & Technology, v. 49, pp. 4441-4449.

Chapter 4
Conclusions

4.1 Summary

While an understanding of the marine CO_2 system is important to a wide variety of studies, including regional and global CO_2 fluxes, ecological research, ocean acidification, and carbon sequestration, our tools for measuring inorganic carbon parameters are limited. pH and pCO_2 systems are commercially available and total alkalinity (TA) systems are arriving on the market, but the best pairings for CO_2 resolution with limited calculation errors or covariance are dissolved inorganic carbon (DIC) or TA with pH or pCO_2. DIC is a particular focus because DIC methods are more readily adaptable to in-situ measurement, and because DIC data may be valuable to many biogeochemical studies even if another paired inorganic carbonate parameter measurement is not available to fully resolve the marine CO_2 system. While there are no commercially available DIC sensors, several methods for DIC measurement have been applied to in-situ research sensors. This thesis has described the development and testing of one such research sensor with applications in time-series and mobile mapping missions in dynamic coastal ecosystems.

Chapter 2 described the development of the CHANnelized Optical System II (CHANOS II), providing a new option for high resolution inorganic carbon sensing from stationary and mobile platforms. This sensor relies on the highly sensitive spectrophotometric method to produce near-continuous DIC measurements. While this wet chemistry method requires the integration of multiple pumps and valves, we reduce the cost of this unit by using inexpensive off-the-shelf components wherever possible. The sensor was designed for deployment at depth (up to 3000 m) and requires minimal modification to measure pCO_2 or pH instead of, or in addition to, DIC alone. The CHANOS II is applicable to weeks-to-months long time-series deployments in dynamic coastal regions, as described during a ground-truthing deployment in the Pocasset River, MA. A comparison between bottle samples and sensor measurements across the 59 deployment days showed a laboratory accuracy and precision of ~2.9 and 5.5 μmol kg^{-1} with a time-series field deployment accuracy of 9.0 μmol kg^{-1}, allowing for 'weather' quality resolution and approaching 'climate' quality measurements of DIC. The time-series DIC results showed two different biogeochemical responses to storm systems where bottle sampling methods could not capture DIC during poor weather. During a tropical storm, high winds disrupted river sediments and released high DIC, low oxygen waters into the river. During a nor'easter, heavy rains diluted the river DIC signal. Some seasonal differences between sensor

measurements in August and November 2021 also showed biogeochemical changes that could be difficult to detect with low-resolution bottle sampling.

The CHANOS II is also effective in mapping DIC from mobile platforms, including small boat tows and ROVs. A series of towed deployments across Waquoit Bay showed significant differences in the DIC signal across the bay during high and low tides. Each sensor-generated surface map was ground-truthed with ~20 bottle samples taken at 5 min intervals. The high-resolution measurements captured between bottle samples illuminated river and bay endmembers as well as tidal marsh export. Taken together, this sensor provides a new option for high resolution inorganic carbon sensing applicable to a variety of missions and objectives.

In Chapter 3, the CHANOS II was used to better understand inorganic carbon chemistry in another potentially dynamic and relatively inaccessible ecosystem. Deep coral reefs provide ecologically and economically important habitats to a wide variety of marine species. They typically live on bathymetric highs within the oxygen minimum zone and are known to live in seawater approaching corrosive aragonite saturation states. These corals may experience acidifying conditions and associated physiological stresses in the near future. However, many of these corals live in dynamic environments like that of the West Florida Slope: corals here may experience rapid and significant physical and chemical changes due to the meandering of the Loop Current and associated eddies, and may therefore already be accustomed to changing environmental conditions. Our understanding of inorganic carbon chemistry across deep coral habitats is limited by site inaccessibility: ROVs and submersibles carry a finite number of Niskin water samplers for long dives, and CTD Rosette casts typically stop at least 2 m off bottom (and frequently 10 m +) to protect onboard equipment. CHANOS II measurements of seafloor DIC over a series of 4 ROV dives at coral mound sites on the West Florida Slope showed good agreement with the few water samples and in-situ calibrations taken during these dives. The CHANOS II also showed surprisingly large (100's $\mu mol\ kg^{-1}$) variations in DIC across deep coral sites over hundreds of meters. To the best of our knowledge, we present the first high resolution seafloor DIC observations across deep coral mounds. Since CHANOS II DIC measurements alone are not enough to fully resolve the inorganic carbon system at these sites, we developed multilinear regressions to conservatively estimate seafloor TA, based on historical water column TA:DIC data and CHANOS II seafloor DIC. These data were fed into CO2SYS to conservatively estimate seafloor pH and $\Omega_{aragonite}$, illuminating frequently corrosive conditions across the reef sites. Our results demonstrate the need for high resolution seafloor inorganic carbon sensing to better understand the conditions currently experienced at deep coral habitats, so that we can better understand the challenges such habitats may face in future changing oceans.

4.2 Future work

This thesis applies the spectrophotometric DIC method to in-situ sensor development and highlights the need for high resolution time-series and profiling inorganic carbon sensors, particularly those that can fully resolve the marine CO_2 system in a single unit. Future work is needed to bring the CHANOS II unit to a 'climate' quality precision of ±2 μmol kg^{-1} DIC, but the current 'weather' quality precision is sufficient to resolve many biogeochemical DIC changes, particularly if the trade-off between sensor cost and precision allows for more frequent deployments (Newton et al., 2014). Many minor modifications are possible to reduce the current sensor size, cost, and volume requirements, including consolidation of pump housings, board and processor updates, improvements to the equilibration cell design, and the adaptation of a recirculating sample scheme to allow for full equilibration of a given sample at lower volume than the current flow-through method requires. The current system can be modified to measure pCO_2 or pH, and a second channel can be added to simultaneously resolve the marine CO_2 system in a single unit. As more high-resolution in-situ inorganic carbon sensors become available, researchers will be better able to customize both the temporal and spatial scales of their deployments to capture the carbon dynamics of interest. As the changing climate impacts ocean temperatures and CO_2 concentrations, it will become increasingly important to tailor biogeochemical research to include both the establishment of current 'baseline' inorganic carbon conditions and to capture OA impacts on longer timescales.

With few samples to work with, it is difficult to understand deep sea inorganic carbon chemistry in general and benthic habitat biogeochemistry. Available ROV and submersible data tends to highlight seafloor conditions during a single dive, and does not account for seasonal or episodic changes, such as may be present under the Loop Current on the West Florida Slope. Current benthic landers may produce valuable current and CTD records, but little inorganic carbon data is available from such systems. A major priority in future work from this thesis should be to validate the range of CHANOS II DIC observations and related seafloor TA and CO2sys models through repeated dives at our coral sites, as well as through fully equipped benthic landers. Such work would lend greater confidence to the seafloor inorganic carbon data presented in this thesis, and would allow us to tackle related questions:

1) *How widespread and persistent are conditions of low pH and* $\Omega_{aragonite}$ *over deep sea coral mounds?*
2) *How does the growth and dissolution of deep sea coral skeletons impact seafloor* CO_2 *chemistry?*
3) *What links exist between marine* CO_2 *chemistry and the distribution of deep sea corals?*

High resolution profiling and long-term monitoring of the inorganic carbon system will help to tease apart the fine-scale biogeochemical links across these ecosystems, and will allow us to better understand and protect benthic communities that may be vulnerable to changing ocean chemistry.

Bibliography

Amornthammarong, N., Ortner, P.B., Hendee, J., and Woosley, R., 2014. A simplified coulometric method for multi-sample measurements of total dissolved inorganic carbon concentration in marine waters. Analyst, v. 139, pp. 5263-5270.

Andersson, A.J., Kuffner, I.B., Mackenzie, F.T., Jokiel, P.L., Rodgers, K.S., and Tan, A., 2009. Net loss of $CaCO_3$ from a subtropical calcifying community due to seawater acidification: mesocosm-scale experimental evidence. Biogeosciences, v. 6, pp. 1811-1823.

Anisfeld, S.C., and Benoit, G., 1997. Impacts of flow restrictions on salt marshes: An instance of acidification. Environmental Science and Technology, v. 31, pp. 1650-1657.

Bandstra, L., Hales, B., and Takahashi, T., 2006. High-frequency measurements of total CO_2: Method development and first oceanographic observations. Marine Chemistry, v. 100, pp. 24-38.

Bates, N.R., Amat, A., Andersson, A.J., 2010. Feedbacks and responses of coral calcification on the Bermuda reef system to seasonal changes in biological processes and ocean acidification. Biogeosciences, v. 7, pp. 2509-2530.

Bauer, J.E., Cai, W.J., Raymond, P.A., Bianchi, T.S., Hopkinson, C.S., and Regnier, P.A.G., 2013. The changing carbon cycle of the coastal ocean. Nature, v. 504, pp. 61-70.

Baumann, H., Wallace, R.B., Tagliaferri, T., and Gobler, C.J., 2014. Large natural pH, CO2 and O2 fluctuations in a temperate tidal salt marsh on diel, seasonal, and interannual time scales. Estuaries and Coasts, v. 38, pp. 220-231.

Bell, R.J., Short, R.T., and Byrne, R.H., 2011. In-situ determination of total dissolved inorganic carbon by underwater membrane introduction mass spectrometry. Limnology and Oceanography: Methods, v. 9, pp. 164-175.

Berelson, W.M., McManus, J., Severmann, S., and Rollins, N., 2019. Benthic fluxes from hypoxia-influenced Gulf of Mexico sediments: Impact on bottom water acidification. Marine Chemistry, v. 209, pp. 94-106.

Bockmon, E.E., and Dickson, A.G., 2016. An inter-laboratory comparison assessing the quality of seawater carbon dioxide measurements. Marine Chemistry, v. 171, pp. 36-43.

Boulais, M., Chenevert, K.J., Demey, A.T., Darrow, E.S., Robison, M.R., Roberts, J.P., and Volety, A., 2017. Oyster reproduction is compromised by acidification experienced seasonally in coastal regions. Nature: Scientific Reports. v. 7., a 13276.

Briggs, E.M., Heinen De Carlo, H., Sabine, C.L., Howins, N., and Martz, T.R., 2020. Autonomous, ion sensitive field effect transistor-based total alkalinity and pH measurements on a barrier reef of Kāne'ohe Bay. AS Earth and Space Chemistry, v. 4, pp. 355-362.

Briggs, E.M., Sandoval, S., Erten, A., Takeshita, Y., Kummel, A.C., and Martz, T.R., 2017. Solid state sensor for simultaneous measurement of total alkalinity and pH of seawater. ACD Sensors, v. 2, pp. 1302-1309.

Brooke, S., and Schroeder, W.W., 2007. Chapter 7: State of deep coral ecosystems in the Gulf of Mexico region: Texas to the Florida Straits In: The State of Deep Coral Ecosystems of the United States (Eds. Lumsden, S.E., Hourigan, T.F., and Bruckner, A.W.). NOAA Technical Memorandum NOS-CRCP-3, Silver Spring MD: p 271-306

Brooke, S., and Young, C.M., 2009. Direct measurements of *in-situ* survival and growth of *Lophelia pertusa* in the northern Gulf of Mexico. Marine Ecology Progress Series, v. 397, pp.153-161

Brooke, S., Ross, S.W., Bane, J.M., Seim, H.E., and Young, C.M., 2013. Temperature tolerance of the deep-sea coral *Lophelia pertusa* from the southeastern United States. Deep Sea Research II, v. 92, pp. 240-248.

Brooks, J.M., Fisher, C., Roberts, H., Cordes, E., Baums, I., Bernard, B., Church, R., Etnoyer, P., German, C., Goehring, E., McDonald, I., Roberts, H., Shank, T., Warren, D., Welsh, S., Wolff, G., and Weaver, D., 2015. Exploration and research of northern Gulf of Mexico deep-water natural and artificial hard-bottom habitats with emphasis on coral communities: Reefs, rigs, and wrecks "*Lophelia* II" Final report. OCS Study BOEM 2016-021. p. 628.

Bushinsky, S.M., Takeshita, Y., and Williams, N.L., 2019. Observing changes in ocean carbonate chemistry: Our autonomous future. Current Climate Change Reports, v. 5, pp. 207-220.

Bryne, R.H., 2014. Measuring ocean acidification: new technology for a new era of ocean chemistry. Environmental Science & Technology, v. 48, pp. 5352-5360.

Byrne, R.H., Liu, X.W., Kaltenbacher, E.A., and Sell, K., 2002. Spectrophotometric measurement of total inorganic carbon in aqueous solutions using a liquid core waveguide. Analytica Chimica Acta, v. 451, pp. 221-229.

Cai, W.J., Wang, Y., and Hodson, R.E., 1998. Acid-base properties of dissolved organic matter in the estuarine waters of Georgia, USA. Geochemica et Cosmochemica Acta, v. 62, pp. 473-483.

Carpenter, K., Abrar, M., Aeby, G., Aronson, R.B., Banks, S., Bruckner, A., …, and Wood, E., 2008. One third of reef-building corals face elevated extinction risk from climate change and local impacts. Science, v. 321, pp. 560-563.

Carter, B.R., Toggweiler, J.R., Key, R.M., and Sarmiento, J.L., 2014. Processes determining the marine alkalinity and calcium carbonate saturation state distributions. Biogeosciences, v. 11, pp. 7349-7362.

Chassignet, E.P., Hurlburt, H.E., Metzger, E.J., Smedstad, O.M., Cummings, J.A., Halliwell, G.R., …, and Wilkkin, J., 2009. US GODAE: global ocean prediction with the HYbrid Coordinate Ocean Model (HYCOM). Oceanography, v. 22, pp. 64-75.

Cherubin, L.M., Morel, Y., and Chassignet, E.P., 2006. , Loop current ring shedding: The formation of cyclones and the effect of topography. Journal of Physical Oceanography, v. 36, pp.569-591.

Choi, Y.S., Lvova, L., Shin, J.H., Oh, S.H., Lee, C.S., Kim, B.H., Cha, G.S., and Nam, H., 2002. Determination of oceanic carbon dioxide using a carbonate-selective electrode. Analytical Chemistry, v. 85, pp. 1332-1336.

Chua, E.J., Savidge, W., Short, R.T., Cardenas-Valencia, A.M., and Fulweiler, R.W., 2016. A review of the emerging field of underwater mass spectrometry. Marine Science, DOI: 10.3389/fmars.2016.00209

Chu, S.N., Wang, Z.A., Gonneea, M.E., Kroeger, K.D., and Ganji, N.K., 2018. Deciphering the dynamics of inorganic carbon export from intertidal salt marshes using high-frequency measurements. Marine Chemistry, v. 206, pp. 7-18.

Clarke, J.S., Achterberg, E.P., Connelly, D.P., Schuster, U., and Mowlem, M., 2017. Developments in marine pCO_2 measurement technology; towards sustained *in situ* observations. Trends in Analytical Chemistry, v. 88, pp. 53-61.

Clayton, T.D., and Byrne, R.H., 1993. Spectrophotometric seawater pH measurement: Total hydrogen ion concentration scale calibration of m-cresol purple and at sea results. Deep-Sea Research, v. 40, pp. 2115-2129.

Colson, B., and Michel, A., 2022. C-SPEC: A deep sea laser spectrometer for measuring the carbon system (DIC and pCO_2). Poster, Ocean Sciences Meeting, virtual, February 24-March 4, 2022.

CSA International, Inc. 2007. Characterization of northern Gulf of Mexico deep-water hard bottom communities with emphasis on *Lophelia* coral. U.S. Department of the Interior, Minerals Management Service, Gulf of Mexico OCS Region, New Orleans, LA. OCS Study MMS 2007-044. 169 pp. + app.

Davies, A.J., Duineveld, G.C.A., van Weering, T.C.E., Mienis, F., Quattrini, A.M., Seim, H.E., Bane, J.M., and Ross, S.W., 2010. Short-term environmental variability in cold-water coral habitat at Viosca Knoll, Gulf of Mexico. Deep Sea Research Part I: Oceanographic Research Papers, v. 57, pp. 199-212.

DeGrandpre, M.D., Spaulding, R.S., Newton, J.O., Jaqueth, E.J., Hamblock, S.E., Umansky, A.A., and Harris, K.E., 2014. Considerations for the measurement of spectrophotometric pH for ocean acidification and other studies. Limnology and Oceanography: Methods, v. 12, pp. 830-839.

Devereux, R., Lehrter, J.C., Cicchetti, G., Beddick, D.L., Yates, D.F., Jarvis, B.M., et al., 2019. Spatially variable bioturbation and physical mixing drive the sedimentary biogeochemical seascape in the Louisiana continental shelf hypoxic zone. Biogeochemistry, v. 143, pp. 151-169.

Dickson, A.G., 2010. "The carbon dioxide system in seawater: equilibrium chemistry and measurements." *Guide to best practices for ocean acidification research and data reporting*, v. 1, pp. 17-40.

Dickson, A.G., and Riley, J., 1978. The effect of analytical error on the evaluation of the components of the aquatic carbon-dioxide system. Marine Chemistry, v. 6, pp. 77-85.

Dickson, A.G., Sabine, C.L., and Christian, J.R., 2007. Guide to best practices for ocean CO_2 measurements. North Pacific Marine Science Organization.

Dodds, L. A., Roberts, J.M., Taylor, A.C., and Marubini, F., 2007. Metabolic tolerance of the cold-water coral *Lophelia pertusa* (Schleractinia) to temperature and dissolved oxygen change. Journal of Experimental Marine Biology and Ecology, v. 249, pp. 205-214.

Doney, S.C., Balch, W.M., Fabry, V.J., and Feely, R.A., 2009. Ocean Acidification: A critical emerging problem for the ocean sciences. Oceanography, v. 22.

Fassbender, A.J., Sabine, C.L., Lawrence-Slavas, N., De Carlo, E.H., Meinig, C., and Jones, S.M., 2015. Robust sensor for extended autonomous measurements of surface ocean dissolved inorganic carbon. Environmental Science and Technology, v. 49, pp. 3628-3635.

Feely, R.A., Doney, S.C., and Cooley, S.R., 2009. Ocean acidification: Present conditions and future changes in a high-CO_2 world. Oceanography, v. 22, pp. 36-47.

Findlay, H.S., Hennige, S.J., Wicks, L.C., Navas, J.M., Woodward, E.M.S., and Roberts, J.M., 2014. Fine-scale nutrient and carbonate system dynamics around cold-water coral reefs in the northeast Atlantic. Scientific Reports, v. 4, pp. 1-10.

Georgian, S.E., Dupont, S., Kurman, M., Butler, A., Strömberg, S.M., Larsson, A.I., and Cordes, E.E., 2016. Biogeographic variability in the physiological response of the cold-water coral *Lophelia pertusa* to ocean acidification. Marine Ecology, doi: 10.111/maec.12373

Gledhill, D.K., White, M.M., Salisbury, J., Thomas, H., Mlsna, I., Liebman, M., Mook, B., Grear, J., Candelmo, A.C., Chambers, R.C., Gobler, C.J., Hunt, C.W., King, A.L., Price, N.N., Signorini, S.R., Stancioff, E., Stymiest, C., Wahle, R.A., Waller, J.D., Rebuck, N.D., Wang, Z.A., Capson, T.L., Morrison, J.R., Cooley, S.R., and Doney, S.C., 2015. Ocean and coastal acidification off New England and Nova Scotia. Oceanography, v. 28, pp. 182-197.

GMFMC, 2017. Coral Habitat Areas Considered for Management in the Gulf of Mexico. Public hearing draft for Amendment 9 to the Fishery Management Plan for Coral and Coral Reefs of the Gulf of Mexico, US Waters. Gulf of Mexico Fishery Management Council, November 2017, Tab N, No.5 pp.19

Gómez, C.E., Wices, L., Deega, D., Etnoyer, P.J., and Cordes, E.E., 2018. Growth and feeding of deep-sea coral *Lophelia pertusa* from the California margin under simulated ocean acidification conditions. PeerJ,, v. 6, p. e5671.

Gula, J., Molemaker, M.J., and McWilliams, J.C., 2015. Gulf Stream Dynamics along the Southeastern U.S. Seaboard. Journal of Physical Oceanography, v. 45, pp. 690-715.

Hales, B., Chipman, D., and Takahashi, T., 2004. High-frequency measurement of partial pressure and total concentration of carbon dioxide in seawater using microporous hydrophobic membrane contactors. Limnology and Oceanography: Methods, v. 2, pp. 356-364.

Hebbeln, D., Weinberg, C., Dullo, W.C., Freiwald, A., Mienis, F., Orejas, C., and Titschack, J., 2020. Cold-water coral reefs thriving under hypoxia. Coral Reefs, v. 39, pp. 853-859.

Hennige, S.J., Wicks, L.C., Kamenos, N.A., Bakker, D.C.E., Findlay, H.S., Dumousseaud, C., and Roberts, J.M., 2014. Short-term metabolic and growth responses of the cold-water coral *Lophelia pertusa* to ocean acidification. Deep Sea Research Part II: Topical Studies in Oceanography. v. 99, pp. 27-35.

Hennige, S.J., Wicks, L.C., Kamenos, N.A., Perna, G., Findlay, H.S., and Roberts, J.M., 2015. Hidden impacts of ocean acidificationi to live and dead coral framework. Proceedings of the Royal Society B: Biological Sciences. v. 282, 20150990.

Hoegh-Guldberg, O., Mumby, P.J., Hooten, A.J, Steneck, R.S., Greenfield, P., Gomez, E., …, and Hatziolos, M.E., 2007. Coral Reefs under rapid climate change and ocean acidification. Science, v. 318, pp. 1737-1742

Huang, K., Cassar, N., Jönsson, B., Cai, W.J., and Bender, M.L., 2015. An ultrahigh precision, high-frequency dissolved inorganic carbon analyzer based on dual isotope dilution and cavity ring-down spectroscopy. Environmental Science & Technology, v. 49.

Hunt, C., 2021. Alkalinity and buffering in estuarine, coastal and shelf waters. PhD thesis, University of New Hampshire.

IPCC, 2013. Climate change 2013: They physical science basis. Contribution of working group I to the Fifth Assessment Report of the Intergovernmental Panel on Climate Change. Stocker, T.F., Qin, D., Plattner, G.K., Tignor, M., Allen, S.K., Boschung, J., Nauels, A., Xia, Y., Bex, V., and Midgley, PM. (eds.) Cambridge University Press, Cambridge, United Kingdom and New York, NY, USA. 1595 pp.

Jiang, M.S., Pan, C., Barbero, L., Reed, J., Salisbury, J., VanZwieten, J., and Wanninkhof, R., 2020. Variability of bottom carbonate chemistry over the deep coral reefs in the Florida Straits and the impacts of meso-scale processes. Ocean Modeling, v. 147, 101555.

Jiang, M., Salisbury, J., and VanZwieten, J., H., *in revision.* Eddies and frontal processes drive phytoplankton blooms in the Florida Straits and carbon export to the deep coral reefs. Journal of Geophysical Research: Oceans.

Johnson, K.M., Wills, K.D., Butler, D.B., Johnson, W.K., and Wong, C.S., 1993. Coulometric total carbon-dioxide analysis for marine studies: Maximizing the performance of an automated gas extraction system and coulometric detector. Marine Chemistry, v. 44, pp. 167-187.

Kaltin, S., Haraldsson, C., and Anderson, L.G., 2005. A rapid method for determination of total dissolved inorganic carbon in seawater with high accuracy and precision. Marine Chemistry, v. 96, pp. 53-60.

Kourafalou, V.H., and Kang, H., 2012. Florida Current meandering and evolution of cyclonic eddies along the Florida Keys Reef Tract: Are they interconnected? Journal of Geophysical Research, v. 117, C5.

Kurman, M.D., Gómez, C.E., Georgian, S.E., Lunden, J.J., and Cordes, E.E., 2017. Intra-specific variation reveals potential for adaptation to ocean acidification in a cold-water coral from the Gulf of Mexico. Frontiers in Marine Science, v. 4, pp. 111.

Lauvset, S.K., Lange, N., Tanhua, T., et al., 2021. Global Ocean Data Analysis Project version 2.2021 (GLODAPv2.2021). NCEI Accession 0237935. NOAA National Centers for Environmental Information. Dataset. https://doi.org/10.25921/ttgq-n825. Accessed January 2022.

Le Hénaff, M., Kourafalou, V. H., Morel, Y., Srinivasan, A., 2012. Simulating the dynamics and intensification of cyclonic Loop Current Frontal Eddies in the Gulf of Mexico, Journal of Geophysical Research, v. 117, C2.

Leichter, J.J., Stokes, M.D., and Genovese, S.J., 2008. Deep water macroalgal communities adjacent to the Florida Keeys reef tract. Marine Ecology Progress Series, v. 356, pp. 123-138.

Liu, X., Byrne, R.H., Adornato, L., Yates ,K.K., Kaltenbacher, E., Ding, X., and Yang, B., 2013. In situ spectrophotometric measurement of dissolved inorganic carbon in seawater. Environmental Science & Technology, v. 27, pp. 11106-11114.

Lunden, J., Georgian, S.E., and Cordes, E.E., 2013. Aragonite saturation states at cold-water coral reefs structured by *Lophelia pertusa* in the northern Gulf of Mexico. Limnology and Oceanography, v. 58, pp. 354-362.

Lunden, J., McNicholl, C.G., Sears, C.R., Morrison, C., and Cordes, E.E., 2014. Acute survivorship of the deep sea coral *Lophelia pertusa* from the Gulf of Mexico under acidification, warming, and deoxygenation, Frontier in Marine Science, v. 1, pp. 78.

Maier, C., Hegeman, J., Weinbauer, M.G., and Gattuso, J.-P., 2009. Calcification of the cold-water coral *Lophelia pertusa* under ambient and reduced pH. Biogeosciences, v. 6, pp. 1671-1680.

Martz, T.R., Daly, K.L., Byrne, R.H., Stillman, J.H., and Turk, D., 2015. Technology for ocean acidification research: Needs and availability. Oceanography, v. 28, pp. 40-47.

Martin, W.R., Sayles, F.L., McCorkle, D.C., and Weidman, C., 2013. Continuous, autonomous measurement of the CO_2 system in Waquoit Bay, MA. AGU Fall Meeting Abstracts, OS53D-07.

McDougall, T.J., and Barker, P.M., 2011. Getting started with TEOS-10 and the Gibbs Seawater (GSW) oceanographic toolbox. SCOR/IAPSO WG127, ISBN 978-0-646-55621-5.

Mesinger, F., DiMego, G., Kalnay, E., Mitchell, K., Shafran, P.C., Ebisuzaki, W., and Shi, W., 2006. North American regional reanalysis. Bulletin of the American Meteorological Society, v. 87, pp. 343-360.

Millero, F.J., 1986. The pH of estuarine waters. Limnology & Oceanography, v. 31, pp. 839-847.

Millero, F.J., 2007. The Marine Inorganic Carbon Cycle. Chemical Reviews, v. 107, pp. 308-341.

Moseman-Valtierra, S., Abdul-Aziz, O.I., Tang, J., Ishtiaq, K.S., Morkeski, K., Mora, J., Quinn, R.K., Martin, R.M., Egan, K., Brannon, E.Q., Carey, J., and Kroeger, K.D., 2016. Carbon dioxide fluxes reflect plant zonation and belowground biomass in a coastal marsh. Ecosphere, v. 7, article e01560.

Newton, C.R., Mullins, H.T., Gardulski, A.F., Hine, A.C., and Dix, G.R., 1987. Coral mounds on the West Florida Slope: Unanswered questions regarding the development of deep-water banks. Society for Sedimentary Geology, v. 2, pp. 359-367.

Newton, J.A., Feely, R.A., Jewett, E.B., Williamson, P., and Mathis, J., 2014. Global ocean acidification observing network: Requirements and governance plan. GOA-ON, 57.

Nightingale, A.M., Beaton, A.D., Mowlem, M.C., 2015. Trends in microfluidic systems for in situ chemical analysis of natural waters. Sensors and Actuators, B: Chemical. v.221, pp. 1398-1405.

NOAA National Database for Deep-Sea Corals and Sponges, v. 20190117-0. NOAA Deep Sea Coral Research & Technology Program. https://deepseacoraldata.noaa.gov/

Orr, J.C., Fabry, V.J., Aumont, O., Bopp, L., Doney, S.C., Feely, R.A., Gnanadesikan, A., Gruber, N., Ishida, A., Joos, F., Key, R.M., Lindsay, K., Maier-Reimer, E., Matear, R., Monfray, P., Mouchet, A., Najjar, R.G., Plattner, G.K., Rodgers, K.B., Sabine, C.L., Sarmiento, J.L., Schlitzer, R., Slater, R.D., Totterdell, I.J., Weirig, M.F., Yamanaka, Y., and Yool., A., 2005. Anthropogenic ocean acidification over the twenty-first century and its impact on calcifying organisms. Nature, v. 437, pp. 681-686.

Orr, J.C., Najjar, R.G., Aumont, O., et al., 2017. Biogeochemical protocols and diagnostics for the CMIP6 Ocean Model Intercomparison Project (OMIP). Geoscientific Model Development, v. 10, pp. 2169-2199.

Pandolfi, J.M., Connolly, S.R., Marshall, D.J., and Cohen, A.L., 2011. Projecting coral reef futures under global warming and ocean acidification. Science, v. 333, pp. 418-422.

Pierrot, D., Lewis, E., and Wallace, D.W.R., 2006. MS Excel program developed for CO2 system calculations. ORNL/CDIAC-105a. Carbon Dioxide Information Analysis Center, Oak Ridge National Laboratory, U.S. Department of Energy, Oak Ridge, Tennessee.

Portela, E., Tenreiro, M.., Pallàs-Sanz, E., Meunier, T., Ruiz-Angulo, A., Sosa-Gutiérrez, R., and Cusí, S., 2018. Hyddrography of the Central and Western Gulf of Mexico. Journal of Geophysical Research: Oceans, v. 123, pp..5134-5149.

Reed, J.K., Messing, C., Walker, B., Brooke, S., Correa, T., Brouwer, M., Udouj, T., and Farrington, S., 2013. Habitat characterization, distribution, and areal extent of deep-sea coral ecosystem habitat off Florida, southeastern United States. Journal of Caribbean Science, v. 47, pp. 13-30.

Reed, J.K., Weaver, D.C., and Pomponi, S.A., 2006. Habitat and fauna of deep-water *Lophelia pertusa* coral reefs off the southeastern U.S.: Black Plateau, Straits of Florida, and Gulf of Mexico. Bulletin of Marine Science, v. 78, pp. 343-375.

Roberts, J.M., Wheeler, A.W., Freiwald, A., and Cairns, S., (Eds.), 2009. Cold-water corals: the biology and geology of deep-sea habitats. Cambridge University Press. pp 334

Ross, S.W., and Nizinski, M.S., 2007, State of Deep Coral Ecosystems in the U.S. Southeast Region: Cape Hatteras to southeastern Florida. p. 233-270, Ch. 6, In: Lumsden, S.E., T.F. Hourigan, A.W. Bruckner and G. Dorr (eds.). The State of Deep Coral Ecosystems of the United States. NOAA Tech. Memo. CRCP-3. Silver Spring, MD. 365 pp.

Ross, S.W., Brooke, S., Quattrini, A., Rhode, M., and Watterson, J.C., 2015. A deep-sea community at unusually shallow depths in the western North Atlantic Ocean off northeastern Florida. Marine Biology, v.162, pp. 635-648.

Ross, S.W., Rhode, M., and Brooke, S.D., 2017. Deep sea coral and hardbottom habitats on the west Florida slope, eastern Gulf of Mexico. Deep Sea Research II, v. 120, pp. 14-28.

Rowe, G.T., Kaegi, M.E.C., Morse, J.W., Boland, G.S., and Briones, E.G.E., 2002. Sediment community metabolism associated with continental shelf hypoxia, Northern Gulf of Mexico. Estuaries, v. 25, pp. 1097-1106.

Sayles, F.L., and Eck, C., 2009. An autonomous instrument for time series analysis of TCO_2 from oceanographic moorings. Deep Sea Research, Part I, v. 56, pp. 1590-1603.

Schuster, U., Hannides, A., Mintrop, L., and Körtzinger, A., 2009. Sensors and instruments for oceanic dissolved carbon measurements. Ocean Science, v. 5, pp. 547-558.

Shangguan, Q., Lai, C., Beatty, C.M., Young, F.L., Spaulding, R.S., and DeGrandpre, M.D., 2021. Autonomous in situ measurements of freshwater alkalinity. Limnology and Oceanography: Methods, v. 19, pp.51-66.

Shchepetkin, A.F., and McWilliams, J.C., 2005. The regional oceanic modeling system (ROMS): a split-explicit, free-surface, topography-following-coordinate oceanic model. Ocean Modeling, v. 9, pp. 347-404.

Song, S., Wang, Z.A., Gonneea, M.E., Jroeger, K.D., Chu, S.N., Li, D., and Liang, H., 2020. An important biogeochemical link between organic and inorganic carbon cycling: Effects of organic alkalinity on carbonate chemistry in coastal waters influenced by intertidal salt marshes. Geochimica et Cosmochimica Acta, v. 275, pp. 123-139.

Spivak, A.C., Gosselin, K., Howard, E., Mariotti, G., Forbrich, I., Stanley, R., and Sylva, S.P., 2017. Shallow ponds are heterogenous habitats within a temperate salt marsh ecosystem. Journal of Geophysical Research: Biogeosciences, v. 122, pp. 1371-1384.

Takahashi and Sutherland, 2017. Global ocean surface water partial pressure of CO_2 database: Measurements performed during 1957-2016. NOAA/NCEI/ OCADS NDP-088 (V2016).

Thresher, R.E., Tilbrook, B., Fallon, S., ,Wilson, N.C., and Adkins, J., 2011. Effects of chronic low carbonate saturation levels on the distribution, growth and skeletal chemistry of deep-sea corals and other seamount megabenthos. Marine Ecology Progress Series, v. 4422, pp. 87-99.

Tue-Ngeun, O., Sandford, R.C., Jakmunee, J., Grudpan, K., McKelvie, I.D., Worsfold, P.J., 2005. Determination of dissolved inorganic carbon (DIC) and dissolved organic carbon (DOC) in freshwaters by sequential injection spectrophotometry with on-line UV photo-oxidation. Analytica Chimica Acta, v. 554, pp. 17-24.

Turley, C.M., Roberts, J.M., and Guinotte, J.M., 2007. Corals in deep-water: will the unseen hand of ocean acidification destroy cold-water ecosystems? Coral Reefs, v. 26, pp. 445-448.

Van Heuven, S., Pierrot, D., Rae, J.W.B., Lewis, E., and Wallace, D.W.R., 2011. MATLAB program developed for CO2 system calculations.ORNL/CDIAC-105b.

Vukovich, F.M., and Maul, G.A., 1985. Cyclonic eddies in the eastern Gulf of Mexico. Journal of Physical Oceanography, v. 15, pp. 105–117.

Wagner, D., Etnoyer, P., Nizinski, M., Schmahl, G.P., Hickerson, E., Sterne, T., and Nuttall, M., 2018. Southeast Deep Coral Initiative: Exploring Deep-Sea Coral Ecosystems off the Southeast United States. Oceanography, v. 31, pp. 98-99.

Waldbusser, G.G., and Salisbury, J.E., 2014. Ocean acidification in the coastal zone from an organism's perspective: Multiple system parameters, frequency domains, and habitats. Annual Review of Marine Science, v. 6, pp. 221-247.

Waldbusser, G.G., Hales, B., Langdon, C.J., et al., 2015. Saturation-state sensitivity of marine bivalve larvae to ocean acidification. Nature Climate Change, v. 5, pp. 273-280.

Wallace, R.B., Baumann, H., Grear, J.S., Aller, R.C., and Gobler, C.J., 2014. Coastal ocean acidification: The other eutrophication problem. Estuarine, Coastal and Shelf Science, v. 148, pp. 1-13.

Wang, H., Lehrter, J., Maiti, K., Fennel, K., Laurent, A., Rabalais, R., et al., 2020. Benthic respiration in hypoxic waters enhances bottom water acidification in the northern Gulf of Mexico. Journal of Geophysical Research: Oceans, v. 125, e2020JC016152.

Wang, Z.A., Cai, W.J., Wang, Y., and Upchurch, B.L., 2003. A long pathlength liquid-core waveguide sensor for real-time pCO_2 measurements at sea. Marine Chemistry, v. 84, pp. 73-84.

Wang, Z.A., Chu, S.N., and Hoering, K.A., 2013. High-frequency spectrophotometric measurements of total dissolved inorganic carbon in seawater. Environmental Science & Technology, v. 47, pp. 7840-7847.

Wang, A.Z., Kroeger, K.D., Ganju, N.K., Gonneea, M.E., and Chu, S.N., 2017. Intertidal salt marshes as an important source of inorganic carbon to the coastal ocean. Limnology and Oceanography, v. 61, pp. 1916-1931.

Wang, Z.A., Lawson, G.L., Pilskaln, C.H., and Maas, A.E., 2017. Seasonal controls of aragonite saturation states in the Gulf of Maine. Journal of Geophysical Research: Oceans. v. 122, pp. 372-389.

Wang, Z.H.A., Liu, X.W., Byrne, R.H., Wanninkhof, R., Bernstein, R.E., Kaltenbacher, E.A., and Patten, J., 2007. Simultaneous spectrophotometric flow-through measurements of pH, carbon dioxide, fugacity, and total inorganic carbon in seawater. Analytica Chimica Acta, v. 596, pp. 23-36.

Wang, Z.A., Sonnichsen, F.N., Bradley, A.M., Hoering, K.A., Lanagan, T.M., Chu, S.N., Hammar, T.R., and Camilli, R., 2015. In-situ sensor technology for simultaneous spectrophotometric measurements of seawater total dissolved inorganic carbon and pH. Environmental Science & Technology, v. 49, pp. 4441-4449.

Wolf-Gladrow, D.A., Zeebe, R.E., Klaas, C., Körtzinger, A., and Dickson, A.G., 2007. Total Alkalinity: The explicit conservative expression and its application to biogeochemical processes. Marine Chemistry, v. 106, pp. 287-300.

Xie, X.J., and Bakker, E., 2013. Non-Severinghaus potentiometric dissolved CO_2 sensor with improved characteristics. Analytical Chemistry, v. 85, pp. 1332-1336.